



universität
wien

DIPLOMARBEIT

Titel der Diplomarbeit

Interpretation of temporal gravity variations in
Obergurgl – effect of glacial ablation

Verfasser

Patrick Arneitz

angestrebter akademischer Grad

Magister der Naturwissenschaften (Mag. rer.nat.)

Wien, 2012

Studienkennzahl lt. Studienblatt: A 416

Studienrichtung lt. Studienblatt: Geophysik

Betreuer: Ao. Univ. Prof. Dr. Bruno Meurers, Universität Wien

Abstract

In Obergurgl, located at an elevation of about 1930 m in the Austrian Eastern Alps, absolute gravity measurements have been regularly performed by BEV operating JILAg-6 (1987-2009). In this period a gravity increase in the order of 300 nm/s^2 has been observed. As main approach to interpret this trend the ablation of the surrounding glaciers is contemplated in this thesis.

To model the caused mass deficit, ice thickness changes are determined within the Ötztal Alps using high resolution digital elevation models (DEM) for the years 1969, 1997, and 2006 (ABERMANN ET AL., 2009). The affected ice volume is approximated by rectangular prisms with small basis areas (5 m x 5 m and 8 m x 8 m respectively). In this way gravity effects of 122 nm/s^2 (1969-1997) and 81 nm/s^2 (1997-2006) respectively are computed. For other glaciers (Stubai Alps, South Tyrol), which were not contained in the DEMs, an effect of 22 nm/s^2 is estimated (1969-2006).

Local topographic changes due to man-made mass displacements close to the measuring site are modeled by polyhedrons. Their total contribution is -27 nm/s^2 . The impact of geodynamical processes like the uplift of the Alps or postglacial deformation, which show a decreasing gravity effect, as well as of snow mass causing seasonal gravity variations cannot be quantified due to limited data.

After the correction of the gravity time series concerning ablation and man-made effects a positive trend of about 100 nm/s^2 remains. This means that about 2/3 of the observed gravity increase can be explained by quantitative modeling of glacial ablation. The origin of the residual trend remains open.

Zusammenfassung

In Obergurgl, auf einer Höhe von ca. 1930 m in den österreichischen Ostalpen gelegen, wurden vom BEV regelmäßig Absolutschweremessungen mit dem Instrument JILAg-6 durchgeführt (1987-2009). In diesem Zeitraum wurde eine Schwerezunahme in der Größenordnung von 300 nm/s^2 beobachtet. Als Hauptansatz zur Interpretation dieses Trends wird in der Arbeit die Ablation der umliegenden Gletscher ins Auge gefasst.

Um die hervorgerufenen Massendefizite zu modellieren, werden unter Verwendung von hochauflösenden digitalen Geländemodellen (DGM), die für die Jahre 1969, 1997 und 2006 gegeben sind, die Änderungen der Eismächtigkeit in den Ötztaler Alpen bestimmt (ABERMANN ET AL., 2009). Das betroffene Eisvolumen wird durch Quader mit kleinen Grundflächen approximiert (5 m x 5 m beziehungsweise 8 m x 8 m). Auf diese Weise werden Schwerewirkungen von 122 nm/s^2 (1969-1997) bzw. 81 nm/s^2 (1997-2006) berechnet. Für andere Gletscher (Stubai Alpen, Südtirol), die nicht in den DGM enthalten waren, wird eine Wirkung von 22 nm/s^2 abgeschätzt (1969-2006).

Lokale Änderungen der Topographie nahe der Messstation, welche durch anthropogene Massenverlagerungen verursacht wurden, werden mittels Polyedern modelliert. Sie tragen -27 nm/s^2 bei. Der Einfluss geodynamischer Prozesse wie die Alpenhebung oder postglaziale Deformation, welche eine verringernde Schwerewirkung aufweisen, sowie jener von Schneemassen, die jahreszeitliche Schwerevariationen verursachen, kann aufgrund begrenzten Datenmaterials nicht quantifiziert werden.

Nach der Korrektur der Schwerezeitreihe bezüglich der Ablation und anthropogener Effekte bleibt ein positiver Trend von ungefähr 100 nm/s^2 übrig. Dies bedeutet, dass ca. 2/3 der beobachteten Schwerezunahme durch die quantitative Modellierung der Gletscherablation erklärt werden können. Woher der verbleibende Trend stammt, bleibt offen.

CONTENTS

1. INTRODUCTION	1
2. GRAVITY DATA	5
2.1 JILAg-6	5
2.2 CORRECTIONS OF RAW DATA	6
2.3 MEASUREMENT RESULTS	7
3. GLACIER INVENTORIES AND DATA	15
3.1 ÖTZTAL ALPS	15
3.2 STUBAI ALPS AND ÜBELTALFERNER	18
4. GRAVIMETRIC MODELS AND DATA PROCESSING	21
4.1 GRAVIMETRIC MODELS.....	21
4.2 GRAVITY PROGRAMS.....	23
4.3 DATA PROCESSING	26
4.3.1 <i>Sensitivity study</i>	26
4.3.2 <i>Man-made gravity effects</i>	26
4.3.2.1 DEM modifications.....	27
4.3.2.2 Point sources.....	29
4.3.3 <i>Seasonal gravity variations</i>	30
4.3.4 <i>Glacier data</i>	31
4.3.4.1 Ötztal Alps	31
4.3.4.2 Stubai Alps and Übeltalferner	34
4.3.4.3 Missing glaciers	35
5. RESULTS	37
5.1 SENSITIVITY STUDY	37
5.2. MAN-MADE GRAVITY EFFECTS	38
5.2.1 <i>DEM modifications</i>	38
5.2.2 <i>Point sources</i>	39
5.2.3 <i>Corrections of the gravity time series</i>	40
5.3 SEASONAL GRAVITY VARIATIONS.....	41
5.4 UPLIFT OF THE ALPS AND POSTGLACIAL DEFORMATION	45
5.5 GLACIERS	47
5.5.1 <i>Ötztal Alps</i>	47
5.5.2 <i>Stubai Alps and Übeltalferner</i>	49
5.5.3 <i>Missing glaciers</i>	51
5.5.5 <i>Corrections of the gravity time series</i>	51
5.6 ANALYSIS.....	53
6. CONCLUSIONS	61
APPENDIX	65
ACKNOWLEDGEMENTS	69
REFERENCES	71
CURRICULUM VITAE	75

1. Introduction

In gravimetry there are two types of measurements. Relative measurements are used to determine the difference in gravity of two different points in space or at different times, whereas absolute gravity delivers g , which is the norm of the gravity acceleration vector \mathbf{g} . The measurement of this absolute value is appropriate to ensure a stable gravity network as well as to detect temporal gravity changes. The latter ones can be caused by geodynamical processes like active crustal movements, variations of earth rotation, mass displacements on surface or in near-surface regions and also atmospheric processes. Repeated determination of g at one location is an effective tool to examine these temporal variations, while in comparison relative measurements show the disadvantage of concatenation with other measuring points, which leads to error propagation and so to a lack of conceptual clarity (e.g. STEINHAUSER & SEIBERL, 1984).

The following paragraph refers to lecture notes by RUESS. The generation of a national gravity network and gravity data archive in Austria, as well as the localization and monitoring of recent gravity variations is performed by the Federal Office for Metrology and Surveying (BEV). Between 1949 and 1980 relative instruments (Norgaard, Worden) were used for these purposes and the gravity network was tied to the *European Calibration Line* (ECL). In 1980 absolute values were measured with the instrument IMGIC at four stations (Altenburg, Kremsmünster, Graz and Penk). Since 1981 these newly constructed stations have formed the basis of the Austrian gravity network (ÖSGN). The purchase of the absolute gravimeter JLAG-6 in 1987 by BEV in corporation with other scientific institutions in Austria allowed to increase the number of absolute stations (so called zero order gravity stations) up to 40 in Austria and 39 abroad (May 2004). Repeated absolute measurements guarantee control of stability of gravity, whereby conditions of accuracy of 10^{-8} m/s^2 have to be met. Since autumn 1987 absolute gravity measurements have been regularly performed in Obergurgl (Tyrol), a small village in the Austrian Eastern Alps. Fig. 1.1 illustrates the surrounding, which is dominated by glacier capped mountains. Beside the validation of repeatability of absolute gravity measurements in general, the original aim of the measurement series was the examination of gravity variations at a stable station in the Alps. To create good conditions for these measurements a room in the cellar of the Alpine Research Site Obergurgl of the University of Innsbruck was chosen, because it guarantees stability of temperature. The coordinates in Gauss-Krueger-System of the measurement point are given by Tab. 1.1. A solid subsoil was reached by constructing a socket, which is planted directly on the underlying rock to reduce floor recoil effects. Fig. 1.2 tries to convey an impression of these circumstances. Furthermore, parasitic errors due to for example traffic or industries are not expected in this area (cf. RUESS, lecture notes).

Zone	Northing [m]	Easting [m]	Elevation [m]
M28	192242	52748,7	1936,21

Tab. 1.1: Coordinates (Gauss-Krueger-System) of the reference point in Obergurgl.

1. Introduction



Fig. 1.1: A Google Earth image, in which Obergurgl is highlighted by the red square (© 2011 Google). Latitude and longitude of the village are approximately $46,9^{\circ}$ N respectively $11,0^{\circ}$ E. In the south and west of the illustration glaciers of the Ötztal Alps are visible, whereas in the northeast one can find the ice masses of the Stubai Alps.

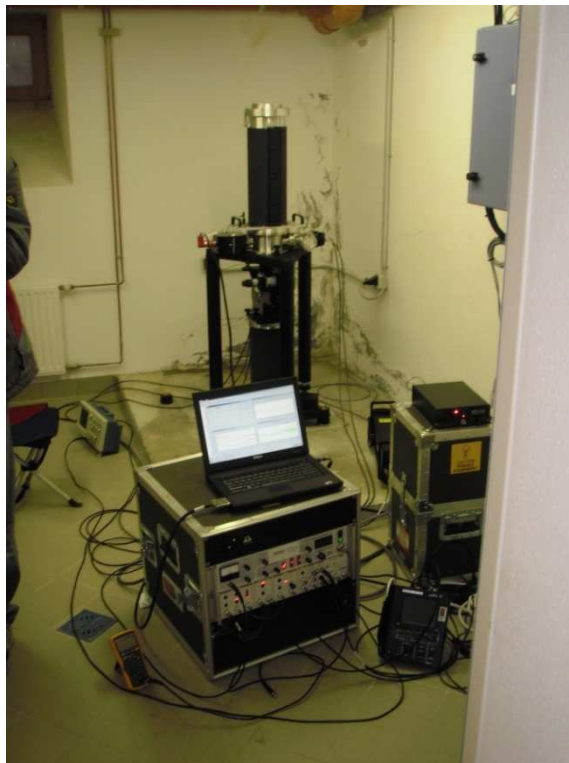


Fig. 1.2: Room in the Alpine Research Site Obergurgl with the new instrument FG5, used for measurements since autumn 2010.

1. Introduction

The BEV tried to perform measurements in cycles of half a year to investigate seasonal gravity variations due to the snow cover (RUESS, 1993). A specific campaign consists of a few independent experiments (hereinafter referred to as single measurements), after which the instrument setup is controlled and re-adjustments are made when required. Ruess (pers. comm., 2010) provides results of all single absolute gravity measurements (index sm) for the whole series from 1987 to 2009 in Obergurgl, whereby measurements performed in spring (index sp) and autumn (index au) are presented in different colors (blue and red respectively) in Fig. 1.3. Over the whole period an increase in gravity of a few tens of μGal^1 can be assumed. This is a quite surprising fact, because one would have rather expected the contrary due to the uplift of the Alps (e.g. HASLINGER ET AL., 2007). Hence, there is a need to find reasonable explanations for the observed gravity variations, which constitutes the aim of this thesis.

As main approach glacial ablation is contemplated. Ice mass losses in the region of the Ötztal Alps have been evaluated by ABERMANN ET AL. (2009) analyzing Digital Elevation Models (DEMs) for different points in time (1969, 1997 and 2006). In this thesis temporal mean ice thickness changes are determined and used to quantify the associated gravity effect, which has to contribute to the observed gravity increase due to the disappearance of ice masses above the measuring site in Obergurgl. Further glaciers within South Tyrol and Stubai Alps, for which no digital elevation changes are available, are considered too. Gravity effects due to postglacial rebound can be estimated by comparison with e.g. MEMIN ET AL. (2009), who have dealt with the modeling of gravity variations due to glacial ablation and resulting deformation in the Mont Blanc massif. However, in this thesis a gravity time series of more than 20 years affords the opportunity to compare computed gravity effects for glacier regions around Obergurgl.

Depending on their dimension and distance to the measuring point, mass displacements due to human interference can cause considerable temporal gravity changes. In this context several construction works during the measurement series in and around Obergurgl are presented and their gravity effects are evaluated.

The comparison of measurement results for spring and autumn in Fig. 1.3 hints at seasonal gravity variations. The snow cover on the mostly higher situated topography around Obergurgl normally shows its maximum and minimum respectively for these seasons. A first assumption for the effect of a constant snow cover has been made by RUESS & HÖGGERL (2002) varying the altitudes of the snowline. Their results suggest an effect in the order of $-10 \mu\text{Gal}$ of snow mass. In contrast here the evaluation of the gravity effect of a snow cover dependent on topographic elevation is intended.

In this thesis all required steps for an appropriate interpretation of the observed gravity variations are discussed. First of all a representation of the measured gravity data is given. In this context it is important to deal with the measurement uncertainty of the gravimeter JILAg-6 as well as with its history concerning technical modifications. The applied corrections of gravity raw data also have to be commented on. The used information of all regarded glaciers as well as available accuracies are discussed afterwards as observed gravity variations are mainly interpreted in respect thereof. The next step is the introduction of used computer programs for the computation of gravity effects and the associated mathematical basis. Therefore, the preparation of data as adequate input for all above mentioned problems is required and described. Then the computation results are presented, from which effects of serious magnitude are selected for the correction of the gravity time series.

¹ $1 \mu\text{Gal} = 10^{-8} \text{ m/s}^2$

1. Introduction

Finally a statistical analysis supports the interpretation of the observed and residual gravity variations.

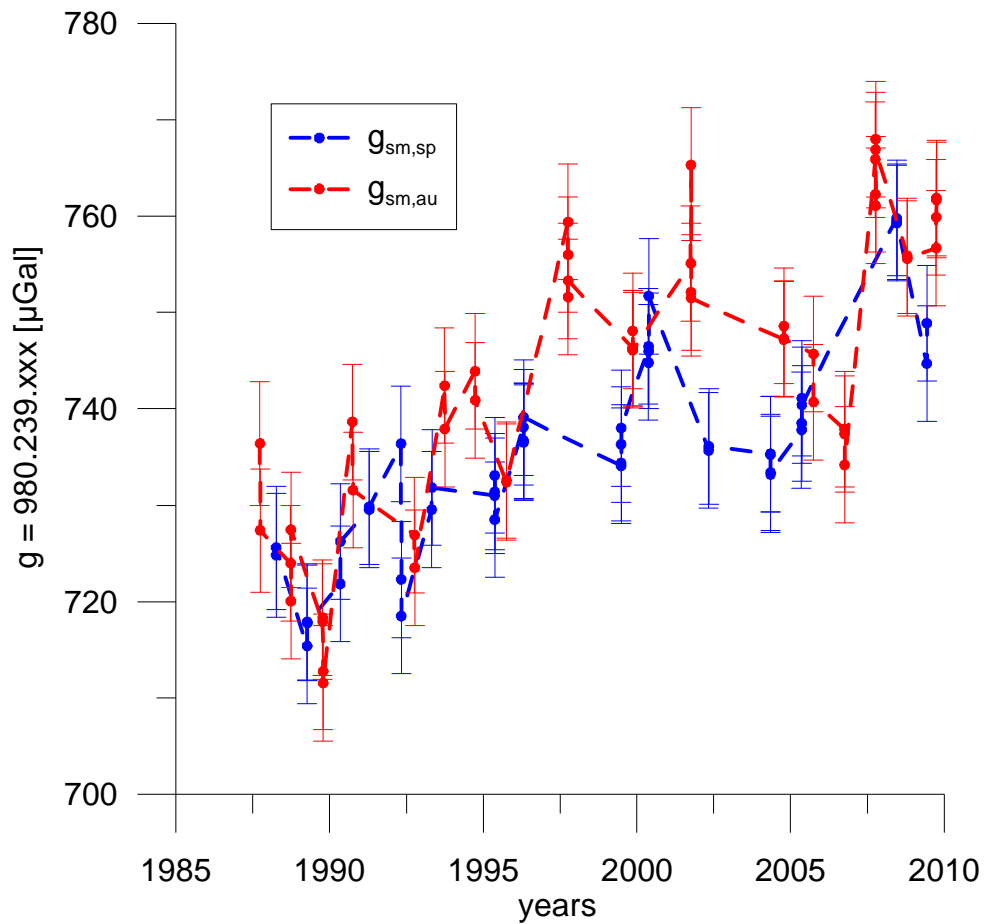


Fig. 1.3: Illustration of results of all single absolute gravity measurements (index sm) for the whole series from 1987 to 2009 in Obergurgl. Symbols and dashed lines in blue refer to gravity observed in spring (index sp), the color red is used for autumn values (index au). In general a gravity increase can be derived for this time period. Overall, gravity values determined in autumn tend to be greater than values determined in spring.

2. Gravity data

2.1 JILAg-6

The instrument used for data acquisition is JILAg-6, which is a transportable absolute gravimeter based on the free-fall method produced by the Joint Institute for Laboratory Astrophysics (JILA). General information of the functionality of this gravimeter type can be found e.g. in TORGE (1989). To determine its measurement uncertainty, comparison with other absolute gravimeters is necessary. Therefore, the International Comparison of Absolute Gravimeters (ICAG) at the Bureau International des Poids et Mesures (BIPM) afforded an opportunity between 1981 and 2009. In this meeting the Comparison Reference Value (CRV), which is a set of adjusted gravity values defined at a height of 0,9 m above the benchmark, is derived in the data processing of absolute and relative gravity measurements of all participants performed at designated BIPM stations (JIANG ET AL., 2011). RUESS & ULLRICH (2011) have discussed six participations of the Austrian JILAg-6 at the ICAGs since 1989 and their results are briefly presented below in this paragraph. Fig. 2.1 shows the deviation of JILAg-6 from the CRV. It has to be mentioned that in the campaign 1994 a systematic error at the comparator circuit was detected and results were corrected accordingly, which underlines the importance of these campaigns. The deviations from the CRV are in the order of 5 μGal , except for the year 2001, when more than 10 μGal appeared. For the ICAG in 2009 the CRV was interpolated, because the final report is not given yet. The standard deviation of the deviation from CRV is $\pm 6 \mu\text{Gal}$. From the technical protocol 2009 a combined uncertainty estimation, which includes the instrumental uncertainty, the site-dependent uncertainty and the experimental standard deviation, is given for JILAg-6 with $\pm 7,9 \mu\text{Gal}$ for the location in Paris (cf. RUESS & ULLRICH, 2011).

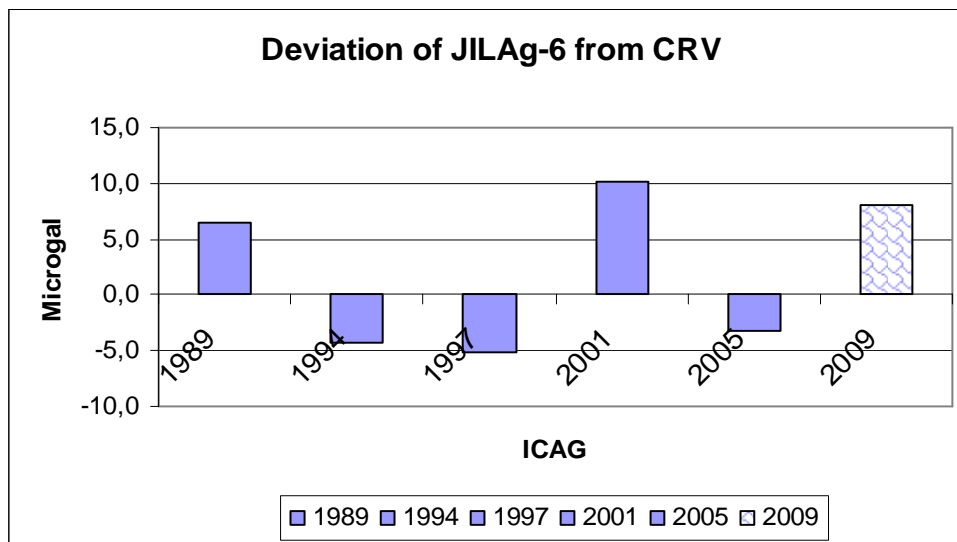


Fig. 2.1: Deviations of JILAg-6 results from then CRV for the six participations at the ICAG (RUESS & ULLRICH, 2011). The value of the CRV for 2009 was interpolated.

A brief summary of instrumental upgrades and technical services concerning JILAg-6 is listed below (Ruess, pers. comm., 2011):

- 1987-1993: Original condition
- 1994: Electronic improvement (with new scaler/counter, start/stop digitizer, computer)
- 1996: Complete technical service (dropper, superspring), new electronics, new laser

2. Gravity Data

- 1999: New BSI-workstation (with scaler and start/stop digitizer onboard)

The iodine stabilized He-Ne laser purchased in 1996 has guaranteed more stability to external influences. Since the electronic improvement in 1994 the trigger point height of the dropper has remained stable (before there had been a variation of about 2-3 mm during a measurement run of several hours). That gives accordingly a stable effective height for gravity of the JILAg-6 instrument. The reference height is defined by 84 cm above the floor for the most JILAg-6 observations in Obergurgl. This height corresponds to the position at about one third of the falling distance (ZUMBERGE, 1981). The effective height depends on the setup and the used fringe-number and its determination is still under debate (e.g. NIEBAUER, 1989; TIMMEN, 2003). However, as the observed absolute gravity values are compared relatively in this study, a constant height offset does not carry weight.

2.2 Corrections of raw data

Beside appropriate measuring instruments knowledge and modeling of all sources, which contribute to gravity changes, are required in order to compare absolute gravity values and in further consequence to analyze small temporal gravity variations. Concerning the issue a distinction is made between desired signal and noise. The gravity effects of tides, pole motion and atmospheric pressure variations have been removed by the BEV from raw data of the measurement series in Obergurgl. These corrections are presented below.

Since internal JILAg-6 codes were not satisfying, all observed gravity data have been reprocessed using ETGTAB, Fortran 77 version 3.0, (WENZEL, 1994) to correct the influence of tidal forces. By this way model body tides are computed using different tidal potential developments (DOODSEN, 1921; CARTWRIGHT & EDDEN, 1973; TAMURA, 1987; BÜLLESFELD, 1985). For including the ocean loading effect at the location of the measuring point main tidal parameters are interpolated by the program WPAREX, Fortran 90 version 1996.09.07, (TIMMEN & WENZEL, 1994) which is based on an 1 by 1 degree grid and SCHWIDERSKI's (1980) ocean tide model. Pole correction has been derived using the software package ETERNA 3.3 (WENZEL, 1996) based on the method of WAHR (1985) (Ruess, pers. comm., 2011).

To perform atmospheric pressure corrections, a single admittance factor of 0,3 $\mu\text{Gal}/\text{hPa}$ has been used by BEV. This value is multiplied with the difference of measured atmospheric pressure and the standard atmosphere determined in accordance with DIN 5450 for the measuring point, which describes a linear relation of gravity changes and local atmospheric pressure variations. However, a single admittance factor does not consider the frequency dependency of the local pressure effect (e.g. WARBURTON & GOODKIND, 1977). The atmospheric pressure admittance varies between 0,2 and 0,4 μGal in the amplitude spectrum (e.g. NEUMEYER & PFLUG, 1997). Regarding this range as well as the maximum of determined pressure deviations from the standard atmosphere in Obergurgl, a maximum error of $\pm 2\mu\text{Gal}$ can appear using the single admittance factor. However, without the information of global or regional pressure models an exact determination of the admittance function for Obergurgl is not possible and an error smaller than 1 μGal can be assumed as most pressure deviations remain smaller than 10 hPa for the measurement series. In chapter 2.1 mentioned comparator corrections were only necessary until 1996.

2.3 Measurement results

In Tab. 2.1 results of absolute gravity measurements in Obergurgl from 1987 until 2009 provided by Ruess (pers. comm., 2010) are compiled. The first column shows the date of measurement, the second the point identification number in the ÖSGN representing the site. It has to be noticed that the first two observations had been performed before the construction of the socket at 0-173-000 instead of 0-173-001, where all further measurements took place. The value of gravity g in column 4 is valid for the corresponding reference height. It already comprises all listed and above described corrections, only the pole correction has to be added to g until 1994. σ_{set} and σ_{drop} represent the standard deviations of sets and drops. Using the reference height and the vertical gradient, which is determined by relative measurements, all values are reduced to a height of 84 cm above ground level at ÖSGN-point 0-173-001 listed in the second last column (g_{sm}). Weighted means of all values of one campaign (g_{wm}) considering the according standard deviations of sets are printed in bold below the dashed lines. For a more convenient representation 980239000 μGal are subtracted. An estimated error of $\pm 6 \mu\text{Gal}$ is presented in the last column, which matches with the result of the standard deviation of the deviations of JILAg-6 from CRV at the ICAGs. The two measurement series at ÖSGN-point 0-173-000 were assigned to point 0-173-001 by subtracting 32 μGal , whereby therefore an additional error of $\sqrt{5} \mu\text{Gal}$ is assumed in error propagation. An illustration of all single measurement results was already presented in Fig. 1.3, where high scatter within a specific campaign is revealed. Fig. 2.2 presents g_{wm} , whereby the gravity increase and indications of seasonal variations are confirmed. In the succeeding chapters, whenever the gravity time series in Obergurgl is discussed, it is always referred to the results g_{wm} , if not mentioned otherwise.

2. Gravity Data

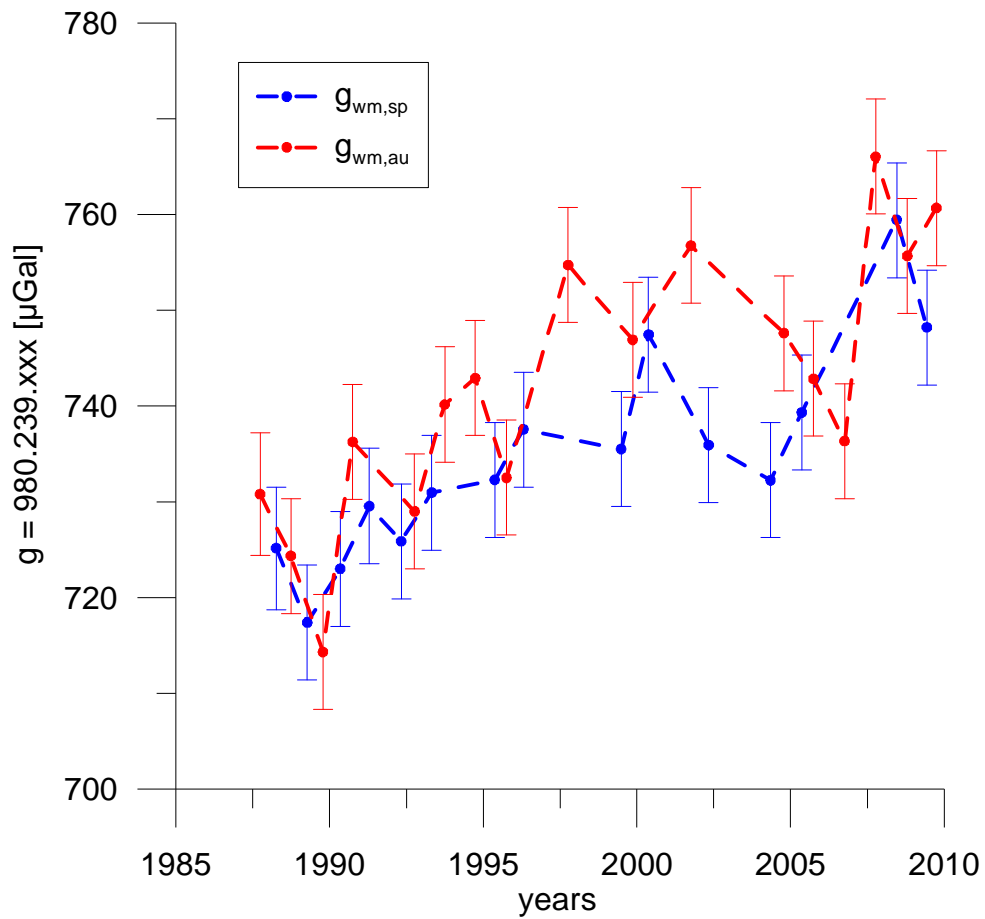


Fig. 2.2: Results of weighted means of gravity concerning one campaign (index wm) for the whole measurement series from 1987 to 2009 in Oberurgl. Symbols and dashed lines in blue refer to gravity observed in spring (index sp), the color red is used for autumn values (index au). In general a gravity increase can be derived for this time period. Overall, gravity values determined in autumn tend to be greater than values determined in spring.

2. Gravity Data

Date	ÖSGN point	Number of	Gravity g [μ Gal]	σ set [μ Gal]	σ drop [μ Gal]	Pressure corr. [μ Gal]	Pole corr. [μ Gal]	Comparator corr. [μ Gal]	Reference height above floor level h [m]	Vertical gradient [μ Gal/m]	\pm [μ Gal/m]	$g_{sm}-980239000$ [μ Gal] at 0-173-01 h=0,84 m	Estimated error \pm [μ Gal]
	number	drops										$g_{wm}-980239000$ [μ Gal]	
870929	0-173-00	450	980.239.766,1	4,2	73,6	2,0	2,1	-11,0	0,841	189,1	3,3	736,4	6,4
870930	0-173-00	990	980.239.757,1	3,3	113,7	2,0	2,1	-11,0	0,841	189,1	3,3	727,4	6,4
												730,8	6,4
880406	0-173-00	1800	980.239.757,6	1,4	34,9	0,0	-1,0	-11,0	0,841	207,8	4,3	724,8	6,4
880407	0-173-00	2160	980.239.758,9	1,6	34,8	-0,5	-1,1	-11,0	0,839	207,8	4,3	725,6	6,4
												725,2	6,4
880929-30	0-173-01	300	980.239.724,7	2,0	17,6	1,9	0,2	-11,0	0,835	189,5	7,0	724,0	6,0
880930	0-173-01	360	980.239.720,7	1,8	14,4	2,4	0,3	-11,0	0,835	189,5	7,0	720,1	6,0
880930-01	0-173-01	1080	980.239.728,1	1,5	16,8	3,0	0,3	-11,0	0,835	189,5	7,0	727,5	6,0
												724,4	6,0
890411	0-173-01	420	980.239.714,6	3,2	21,2	-0,3	0,6	-11,0	0,841	189,6	5,0	715,4	6,0
890411-12	0-173-01	1440	980.239.717,1	1,9	17,1	-0,5	0,6	-11,0	0,841	189,6	5,0	717,9	6,0
890412-13	0-173-01	1800	980.239.717,1	2,7	18,7	-3,6	0,5	-11,0	0,841	189,6	5,0	717,8	6,0
												717,4	6,0
891013	0-173-01	240	980.239.718,6	2,4	15,7	1,6	-2,0	-11,0	0,847	189,6	5,0	717,9	6,0
891013-14	0-173-01	1080	980.239.719,1	1,9	12,7	1,4	-1,9	-11,0	0,846	189,6	5,0	718,3	6,0
891017-18	0-173-01	270	980.239.713,4	1,8	13,1	4,4	-1,6	-11,0	0,845	189,6	5,0	712,7	6,0
891018-19	0-173-01	612	980.239.711,8	1,5	12,8	2,3	-1,6	-11,0	0,847	189,6	5,0	711,5	6,0
												714,3	6,0

Tab. 2.1: Results of absolute gravity measurements in Obergurgl provided by Ruess (pers. comm., 2010). Determined gravity values g valid for a certain reference height above floor level (h) including corrections except the pole correction until 1994 are listed for the given ÖSGN point numbers and dates. In the second last column all values are reduced to h=84 cm (g_{sm}) using the according vertical gradient and a value of 980239000 μ Gal is subtracted for a better representation, whereby for the first two measurement series also a correction of -32 μ Gal was applied due to the transmission to ÖSGN point number 0-173-001. A weighted mean (g_{wm}) using the corresponding standard deviations of sets is calculated and printed in bold under the dashed lines for each measurement campaign. The estimated errors of ± 6 μ Gal suffer an additional assumed uncertainty of $\sqrt{5}$ μ Gal due to transmission for the first two measurement series.

2. Gravity Data

Date	ÖSGN point	Number of	Gravity g [μ Gal]	σ set	σ drop	Pressure corr.	Pole corr.	Comparator corr.	Reference height above floor level h [m]	Vertical gradient [μ Gal/m]	\pm [μ Gal/m]	$g_{sm-980239000}$ [μ Gal] at 0-173-01 h=0,84 m	Estimated error \pm [μ Gal]
	number	drops		[μ Gal]	[μ Gal]	[μ Gal]	[μ Gal]	[μ Gal]				$g_{wm-980239000}$ [μ Gal]	
900507-08	0-173-01	1200	980.239.717,7	1,9	40,0	1,7	3,0	-11,0	0,846	189,7	7,2	721,8	6,0
900509-10	0-173-01	1200	980.239.722,1	3,2	15,4	1,9	2,8	-11,0	0,847	189,7	7,2	726,2	6,0
												723,0	6,0
901001-02	0-173-01	1200	980.239.742,4	2,0	14,8	2,5	-4,5	-11,0	0,844	186,2	3,3	738,6	6,0
901008-09	0-173-01	1200	980.239.735,5	2,8	15,9	2,6	-4,5	-11,0	0,843	189,7	7,2	731,6	6,0
												736,2	6,0
910416-17	0-173-01	1500	980.239.722,2	1,3	14,0	-1,9	5,3	-11,0	0,851	185,6	4,1	729,5	6,0
910417	0-173-01	1500	980.239.722,5	2,7	20,5	-2,6	5,3	-11,0	0,851	185,6	4,1	729,8	6,0
												729,6	6,0
920427-28	0-173-01	1200	980.239.731,7	1,6	13,8	1,4	3,2	-11,0	0,848	185,6	4,1	736,4	6,0
920428-29	0-173-01	1800	980.239.717,5	1,7	13,2	-0,6	3,3	-11,0	0,848	185,6	4,1	722,3	6,0
920429-30	0-173-01	1800	980.239.713,9	1,6	13,6	0,8	3,3	-11,0	0,847	185,6	4,1	718,5	6,0
												725,9	6,0
921006-07	0-173-01	1800	980.239.726,4	1,5	14,3	-0,9	0,5	-11,0	0,840	184,6	3,5	726,9	6,0
921007-08	0-173-01	1800	980.239.723,1	1,7	12,8	2,2	0,4	-11,0	0,840	184,6	3,5	723,5	6,0
												729,0	6,0
930427-28	0-173-01	1800	980.239.727,9	2,0	16,5	1,4	-0,2	-11,0	0,850	184,2	3,3	729,5	6,0
930428-29	0-173-01	1800	980.239.730,1	1,5	52,1	0,7	-0,1	-11,0	0,850	184,2	3,3	731,8	6,0
												731,0	6,0
930928-29	0-173-01	1800	980.239.738,2	1,5	14,3	0,1	3,1	-11,0	0,846	184,0	4,9	742,4	6,0
930929-30	0-173-01	1800	980.239.733,7	1,5	25,2	0,7	3,1	-11,0	0,846	184,0	4,9	737,9	6,0
												740,2	6,0
940927-28	0-173-01	2436	980.239.743,9	1,7	10,5	3,1	1,7	-8,0	0,840	183,9	4,3	743,9	6,0
940928	0-173-01	3480	980.239.740,9	2,4	8,6	3,8	1,8	-8,0	0,840	183,9	4,3	740,9	6,0
												742,9	6,0

Tab. 2.1: Continuation.

2. Gravity Data

Date	ÖSGN	Number	Gravity g	σ	σ	Pressure	Pole	Comparator	Reference height	Vertical	\pm	$g_{sm}-980239000$ [μ Gal]	Estimated
	point	of		set	drop	corr.	corr.	corr.	above floor level h	gradient		at 0-173-01 h=0,84 m	error
	number	drops	[μ Gal]	[μ Gal]	[μ Gal]	[μ Gal]	[μ Gal]	[μ Gal]	[m]	[μ Gal/m]	[μ Gal/m]	$g_{wm}-980239000$ [μ Gal]	\pm [μ Gal]
950515	0-173-01	2088	980.239.731,0	3,3	9,9	1,4	-1,5	-8,0	0,840	183,9	4,3	731,0	6,0
950516	0-173-01	525	980.239.733,1	1,5	7,6	0,6	-1,6	-8,0	0,840	183,9	4,3	733,1	6,0
950516-17	0-173-01	1750	980.239.731,4	2,7	12,3	0,0	-1,6	-8,0	0,840	183,9	4,3	731,4	6,0
950517	0-173-01	2112	980.239.728,5	5,7	12,2	0,1	-1,7	-8,0	0,840	183,9	4,3	728,5	6,0
												732,3	
951003	0-173-01	2136	980.239.732,4	1,5	8,4	4,2	-2,0	-7,3	0,840	182,9	3,0	732,4	6,0
951004	0-173-01	2136	980.239.732,6	1,4	7,8	3,6	-2,0	-5,4	0,840	182,9	3,0	732,6	6,0
												732,5	6,0
960422-23	0-173-01	2492	980.239.738,1	2,0	8,2	2,4	3,7	-5,0	0,840	182,2	3,8	738,1	6,0
960423	0-173-01	2492	980.239.736,5	1,8	8,2	2,1	3,7	-5,0	0,840	182,2	3,8	736,5	6,0
960423-24	0-173-01	2492	980.239.736,7	3,0	9,0	2,0	3,7	-5,2	0,840	182,2	3,8	736,7	6,0
960424	0-173-01	2492	980.239.743,9	2,0	8,2	2,3	3,6	-4,8	0,800	182,2	3,8	736,6	6,0
960424-25	0-173-01	2848	980.239.746,4	1,7	8,4	3,0	3,6	-4,7	0,800	182,2	3,8	739,1	6,0
												737,6	6,0
971006-07	0-173-01	1320	980.239.759,4	3,0	10,5	1,2	-3,3		0,840	184,6	3,3	759,4	6,0
971007	0-173-01	1416	980.239.756,0	1,2	8,1	1,2	-3,0		0,840	184,1	1,6	756,0	6,0
971007-08	0-173-01	2124	980.239.751,6	1,8	9,5	2,0	-2,9		0,840	184,1	1,6	751,6	6,0
971008	0-173-01	1180	980.239.753,3	1,8	10,6	2,4	-2,9		0,840	184,1	1,6	753,3	6,0
												754,7	6,0
990624	0-173-01	175	980.239.734,1	1,4	17,9	3,4	1,7		0,840	185,7	5,4	734,1	6,0
990624	0-173-01	170	980.239.734,4	0,4	5,3	3,3	1,7		0,840	185,7	5,4	734,4	6,0
990624-25	0-173-01	2040	980.239.736,3	0,8	4,3	3,6	1,7		0,840	185,7	5,4	736,3	6,0
990625	0-173-01	2550	980.239.738,0	0,8	4,5	2,7	1,7		0,840	185,7	5,4	738,0	6,0
												735,5	6,0

Tab. 2.1: Continuation.

2. Gravity Data

Date	ÖSGN	Number	Gravity g	σ	σ	Pressure	Pole	Comparator	Reference height	Vertical	\pm	$g_{sm}-980239000$ [μ Gal]	Estimated
	point	of		set	drop	corr.	corr.	corr.	above floor level h	gradient		at 0-173-01 h=0,84 m	error
	number	drops	[μ Gal]	[μ Gal]	[μ Gal]	[μ Gal]	[μ Gal]	[μ Gal]	[m]	[μ Gal/m]	[μ Gal/m]	$g_{wm}-980239000$ [μ Gal]	\pm [μ Gal]
991108-09	0-173-01	1700	980.239.746,3	3,4	6,3	2,5	0,9		0,840	182,2	3,5	746,3	6,0
991109	0-173-01	1360	980.239.746,3	3,2	6,8	2,2	0,9		0,840	182,2	3,5	746,3	6,0
991109-10	0-173-01	2040	980.239.748,1	2,8	5,4	1,3	0,9		0,840	182,2	3,5	748,1	6,0
991110	0-173-01	1700	980.239.746,1	4,6	5,3	1,2	0,9		0,840	182,2	3,5	746,1	6,0
												746,9	6,0
000516	0-173-01	1667	980.239.746,5	1,3	5,3	2,7	-0,3		0,840	185,9	4,2	746,5	6,0
000516-17	0-173-01	2100	980.239.744,8	1,7	4,8	2,4	-0,6		0,840	185,9	4,2	744,8	6,0
000517	0-173-01	1400	980.239.746,0	1,9	5,4	1,4	-0,6		0,840	185,9	4,2	746,0	6,0
000517-18	0-173-01	2100	980.239.751,7	1,5	4,4	0,7	-0,6		0,840	185,9	4,2	751,7	6,0
												747,5	6,0
011001-02	0-173-01	2040	980.239.755,1	1,6	5,4	2,6	-0,7		0,840	186,4	2,6	755,1	6,0
011002	0-173-01	2040	980.239.765,3	0,9	5,1	2,4	-0,7		0,840	186,4	2,6	765,3	6,0
011002-03	0-173-01	2040	980.239.752,1	1,0	5,3	2,1	-0,7		0,840	186,4	2,6	752,1	6,0
011003-04	0-173-01	2040	980.239.751,5	1,0	4,8	1,5	-0,6		0,840	186,4	2,6	751,5	6,0
												756,8	6,0
020430-01	0-173-01	2040	980.239.735,7	2,4	5,5	0,7	-0,3		0,840	185,1	1,3	735,7	6,0
020501-02	0-173-01	4080	980.239.736,1	2,2	5,1	-0,2	-0,3		0,840	185,1	1,3	736,1	6,0
												735,9	6,0
040504-05	0-173-01	850	980.239.735,3	1,4	13,1	-4,3	3,7		0,840	185,1	1,3	735,3	6,0
040505	0-173-01	1360	980.239.735,3	1,0	9,4	-5,7	3,7		0,840	185,1	1,3	735,3	6,0
040505-06	0-173-01	2380	980.239.733,2	1,1	9,1	-6,2	3,7		0,840	185,1	1,3	733,2	6,0
040506	0-173-01	1360	980.239.733,4	1,1	9,7	-5,6	3,7		0,840	185,1	1,3	733,4	6,0
												732,3	6,0

Tab. 2.1: Continuation.

2. Gravity Data

Date	ÖSGN	Number	Gravity g	σ	σ	Pressure	Pole	Comparator	Reference height	Vertical	\pm	$g_{sm}-980239000$ [μ Gal]	Estimated
	point	of		set	drop	corr.	corr.	corr.	above floor level h	gradient		at 0-173-01 h=0,84 m	error
	number	drops	[μ Gal]	[μ Gal]	[μ Gal]	[μ Gal]	[μ Gal]	[μ Gal]	[m]	[μ Gal/m]	[μ Gal/m]	$g_{wm}-980239000$ [μ Gal]	\pm [μ Gal]
041011-12	0-173-01	2040	980.239.747,2	2,0	9,4	1,2	-2,3		0,840	185,1	1,3	747,2	6,0
041012-13	0-173-01	3570	980.239.748,6	2,6	9,5	1,5	-2,3		0,840	185,1	1,3	748,6	6,0
041013-14	0-173-01	4080	980.239.747,3	2,5	8,8	0,4	-2,4		0,840	185,1	1,3	747,3	6,0
												747,6	6,0
050510	0-173-01	678	980.239.737,8	4,4	49,6	-0,6	2,3		0,840	185,1	1,3	737,8	6,0
050510-11	0-173-01	2040	980.239.738,5	1,0	8,4	1,1	2,3		0,840	185,1	1,3	738,5	6,0
050511-12	0-173-01	3740	980.239.741,1	2,1	9,7	0,1	2,3		0,840	185,1	1,3	741,1	6,0
050512	0-173-01	191	980.239.740,4	1,5	10,2	1,0	2,3		0,840	185,1	1,3	740,4	6,0
												739,3	6,0
050928-29	0-173-01	2380	980.239.745,7	1,5	6,9	2,2	0,1		0,840	185,1	1,3	745,7	6,0
050929	0-173-01	1190	980.239.740,7	1,3	7,6	1,6	0,1		0,840	185,1	1,3	740,7	6,0
												742,8	6,0
061002-03	0-173-01	1700	980.239.737,9	1,0	6,8	0,4	0,4		0,840	185,1	1,3	737,9	6,0
061003-04	0-173-01	4080	980.239.737,4	1,0	7,1	-0,8	0,4		0,840	185,1	1,3	737,4	6,0
061004	0-173-01	1360	980.239.734,2	0,9	7,3	-0,1	0,4		0,840	185,1	1,3	734,2	6,0
												736,3	6,0
071001	0-173-01	323	980.239.765,9	6,7	21,3	3,7	-1,7		0,840	185,1	1,3	765,9	6,0
071002	0-173-01	981	980.239.762,3	6,6	11,2	2,9	-1,7		0,840	185,1	1,3	762,3	6,0
071002-03	0-173-01	2840	980.239.761,1	5,5	14,1	3,0	-1,7		0,840	185,1	1,3	761,1	6,0
071003	0-173-01	977	980.239.768,0	2,9	31,0	3,1	-1,6		0,840	185,1	1,3	768,0	6,0
071003-04	0-173-01	944	980.239.766,9	7,2	15,9	3,2	-1,6		0,840	185,1	1,3	766,9	6,0
												766,0	6,0
080609-10	0-173-01	1700	980.239.759,8	3,3	8,1	2,9	-0,8		0,840	185,1	1,3	759,8	6,0
080610-11	0-173-01	4080	980.239.759,4	1,5	7,6	2,4	-0,9		0,840	185,1	1,3	759,4	6,0
080611-12	0-173-01	3570	980.239.759,3	2,7	9,7	1,2	-1,0		0,840	185,1	1,3	759,3	6,0
												759,4	6,0

Tab. 2.1: Continuation.

2. Gravity Data

Date	ÖSGN	Number	Gravity g	σ	σ	Pressure	Pole	Comparator	Reference height	Vertical	\pm	$g_{sm}-980239000$ [μ Gal]	Estimated
	point	of		set	drop	corr.	corr.	corr.	above floor level h	gradient		at 0-173-01 h=0,84 m	error
	number	drops	[μ Gal]	[μ Gal]	[μ Gal]	[μ Gal]	[μ Gal]	[μ Gal]	[m]	[μ Gal/m]	[μ Gal/m]	$g_{wm}-980239000$ [μ Gal]	\pm [μ Gal]
081013-14	0-173-01	2549	980.239.755,9	2,3	9,4	3,4	-3,8		0,840	185,1	1,3	755,9	6,0
081014-15	0-173-01	4078	980.239.755,6	1,3	7,0	2,9	-3,7		0,840	185,1	1,3	755,6	6,0
												755,7	6,0
090602-03	0-173-01	3456	980.239.744,7	4,9	22,1	1,1	1,3		0,840	185,1	1,3	744,7	6,0
090603-04	0-173-01	2335	980.239.748,9	2,2	12,1	0,1	1,2		0,840	185,1	1,3	748,9	6,0
												748,2	6,0
090924	0-173-01	1058	980.239.756,7	3,7	16,7	2,9	-3,8		0,840	185,1	1,3	756,7	6,0
090925	0-173-01	2122	980.239.759,9	3,7	13,8	2,9	-3,8		0,840	185,1	1,3	759,9	6,0
090925-26	0-173-01	3157	980.239.761,9	2,4	12,2	3,2	-3,8		0,840	185,1	1,3	761,9	6,0
090927	0-173-01	1325	980.239.761,7	2,8	12,1	3,6	-3,8		0,840	185,1	1,3	761,7	6,0
												760,7	6,0

Tab. 2.1: Continuation.

3. Glacier inventories and data

3.1 Ötztal Alps

ABERMANN ET AL. (2009) were dealing with methods to derive recent changes of glacial areas and volumes using DEMs of the Ötztal Alps for the years 1969, 1997 and 2006. Their results are presented below in this paragraph. In Austria two complete glacier inventories were established for 1969 (September, October) and 1998, whereby data acquisition for the second one for the Ötztal Alps was at September 11 1997 and presented an area of ice masses of 151 km² for this region. Used methods were analogue and digital airborne photogrammetry. In this process aerial photos were analyzed and the topology was determined. The DEM for the year 2006 was derived by high resolution airborne LIDAR (light detection and ranging) between August 23 and September 11; that makes the dataset closely comparable with the one of 1997 concerning the acquisition date. In their study ABERMANN ET AL. (2009) used about 84% of LIDAR data (81 remeasured glaciers). These glacial areas are illustrated in Fig. 3.1. By analyzing the DEMs results for area, volume and mean thickness changes have been reached, whereby the glaciers are separated into six size classes based on their area in 2006. Tab. 3.1 gives an overview of these results. Volume changes of -1,3 km³ for 1969-1997 and -1 km³ for 1997-2006 have been determined by subtracting DEMs from each other and calculating the product of a plane basis square (5 m x 5 m) with the associated elevation difference. This corresponds to -9,5 m and -8,2 m changes of mean thickness. The minimum altitude of ice cover has moved up to an elevation of 2060 to 2120. This underlines the positive gravity effect of ablation as the absolute gravity station in Obergurgl is situated at about 1935 m. Mass balance measurements on three glaciers (Hintereisferner, Kesselwandferner, Vernagtferner) have demonstrated a mass gain beginning in 1973 (arrow 3 in Fig. 3.2). This gain has been lost in 1985 (arrow 4). These data are encouraged by precipitation observations in Vent, which show positive anomalies for the mid-1970s (cf. ABERMANN ET AL., 2009). One should keep these facts in mind for the interpretation of the upcoming results of gravimetric modeling.

The accuracy of data acquisitions is an important factor, which is treated in the following paragraph based on ABERMANN ET AL. (2010). In Tab. 3.2 specifications of LIDAR used in 2006 are compiled. The values of interest are vertical and horizontal accuracy with $\pm 0,1$ and $\pm 0,3$ m. For the inventory of 1997 $\pm 0,7$ m and ± 1 m for these quantities are given, whereby LAMBRECHT & KUHN (2007) discuss a value of vertical accuracy of $\pm 1,9$ m. PATZELT (1980) suggested an elevation data accuracy of 25 m for the first inventory in 1969. With the law of error propagation (ETZELMÜLLER, 2000)

$$\varepsilon_{\Delta z} = \sqrt{\varepsilon_{DEM1}^2 + \varepsilon_{DEM2}^2} \quad (3.1)$$

the errors of the elevation difference $\varepsilon_{\Delta z}$ of two DEMs using above presented individual vertical accuracies (ε_{DEM1} and ε_{DEM2}) is $\pm 0,7$ m and $\pm 1,9$ m respectively for the period 1997-2006 and ± 25 m for the period 1969-1997. It has to be mentioned that horizontal errors, especially on steep slopes, or fresh snow on acquisition date may lead to larger vertical deviations compared to the given accuracies. Another important aspect is the methodology of glacier boundary delineation, which has been performed by calculating surface elevation differences for two points in time (t_1, t_2) to separate

3. Glacier inventories and data

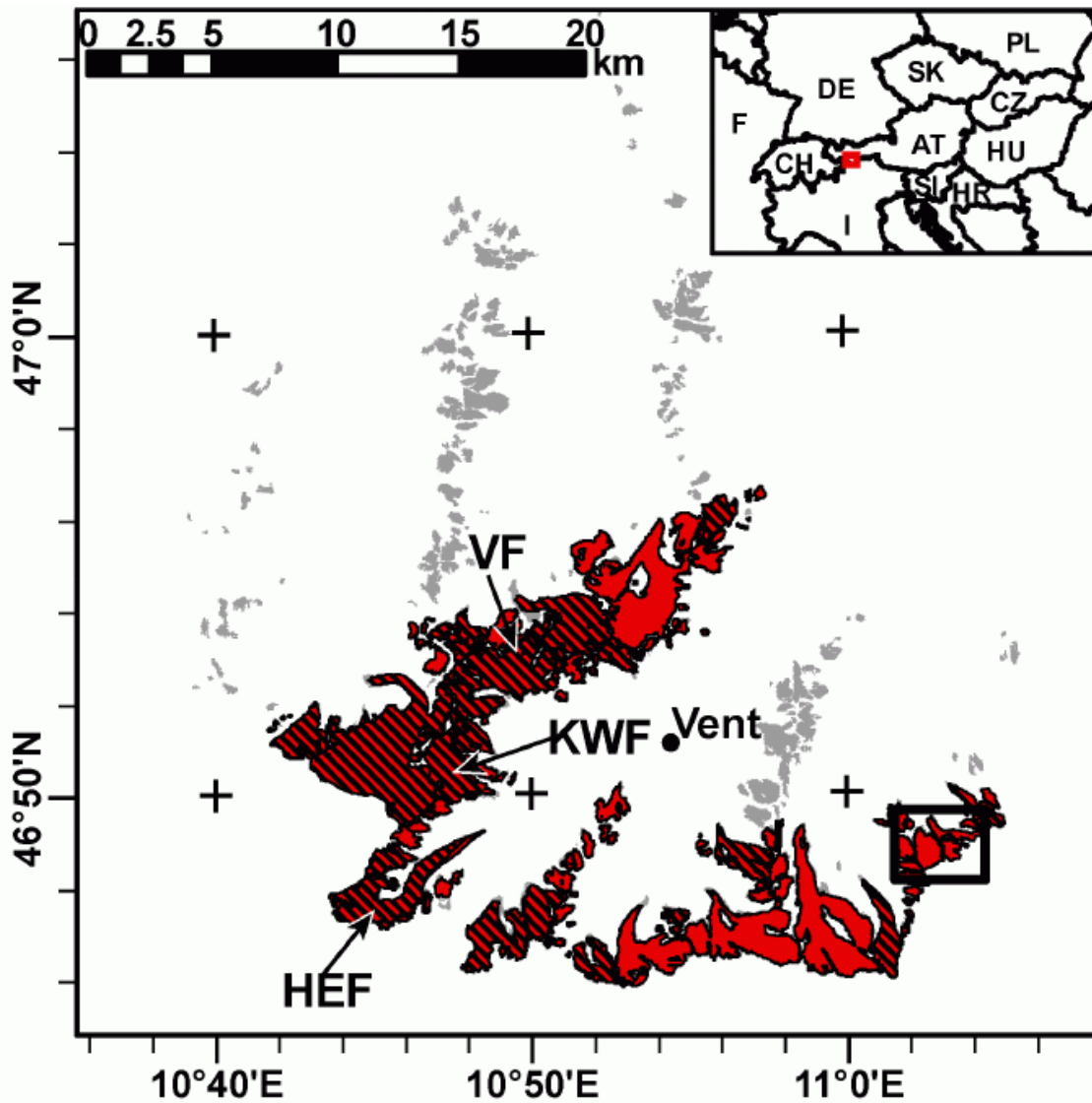


Fig. 3.1: Study area within Ötztal Alps (ABERMANN ET AL., 2009). The red areas (also dashed ones) are considered in their evaluations.

Class	Count 06	A 69	A 97	A 06	ΔA 69–97	ΔA 97–06	ΔV 69–97	ΔV 97–06	$\Delta \bar{z}_{69-97}$	$\Delta \bar{z}_{97-06}$		
[km ²]		[km ²]	[km ²]	[km ²]	[km ²]	%	[*10 ⁶ m ³]	[*10 ⁶ m ³]	[m]	[m]		
10–20	1	18.0	17.2	16.6	–0.8	–4.4	–0.5	–3.1	–129	–78	–7.4	–4.6
5–10	7	64.5	57.8	53.2	–6.7	–10.4	–4.6	–8.0	–688	–554	–11.2	–10.0
1–5	15	38.7	34.3	31.3	–4.4	–11.4	–3.0	–8.7	–331	–239	–9.1	–7.3
0.5–1	11	10.1	8.2	7.3	–1.8	–18.2	–0.9	–10.9	–57	–61	–6.2	–7.8
0.1–0.5	25	10.1	7.8	6.5	–2.4	–23.3	–1.3	–16.5	–63	–52	–7.0	–7.4
0.01–0.1	22	2.8	1.4	1.2	–1.5	–52.2	–0.2	–11.8	–19	–7	–9.3	–5.1
All	81	144.2	126.6	116.1	–17.6	–12.2	–10.5	–8.3	–1286	–990	–9.5	–8.2

Tab. 3.1: Results reached by ABERMANN ET AL. (2009) for Ötztal Alps. For six glacier classes areas (A) for the years 1969, 1997 and 2006, as well as absolute and relative area changes (ΔA), volume changes (ΔV) and mean thickness changes ($\Delta \bar{z}$) are listed for the two periods 1969–1997 and 1997–2006.

3. Glacier inventories and data

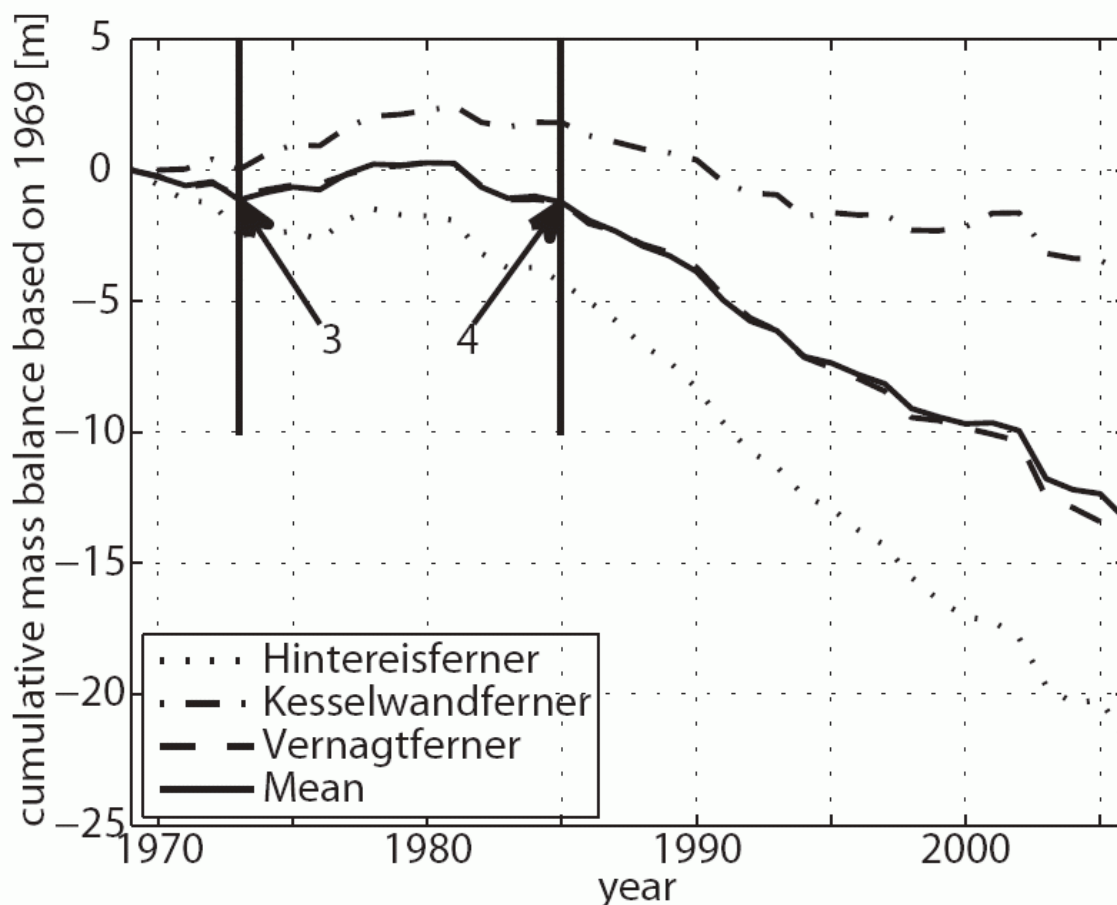


Fig. 3.2.: Cumulative mean specific mass balance of Hintereisferner, Kesselwandferner, Vernagtferner and their mean based on 1969 (ABERMANN ET AL., 2009). A gain in the second half of the 1970s is observed. Arrow 4 indicates that the same state of mass was reached as for arrow 3.

Sensor	Optech ALTM3100
Laser Wavelength	1064 nm
Scan Frequency	33 Hz
Scan angle	+/-20°
Point density	Minimum: 1 point/4 m ²
Measurement frequency	71 kHz
Average flight height	1100 m a.g.l.
Mode	Last Pulse
Interpolation software	SCOP++
Interpolation method	Moving Planes
Horizontal accuracy	+/-0.3 m
Vertical accuracy	+/-0.1 m
Spatial resolution	1 m

Tab. 3.2: Technical specification of LIDAR acquisition campaign in 2006 (ABERMANN ET AL., 2010). In this case the values of interest are horizontal ($\pm 0,3\text{m}$) and vertical ($\pm 0,1\text{m}$) accuracy.

glaciers and their surroundings. The maximum elevation decrease from the margin at t_1 upwards indicates the margin at t_2 , with a successive decrease in between. By the control of relief-shaded representations of a DEM glacial boundaries can be digitized manually according to the strongest roughness changes. Debris cover can complicate this process due to reduced ablation. For accumulation zones, where small elevation changes appear, available aerial photos can be used for

3. Glacier inventories and data

interpretation. Also processes like denudation, rockfall or washout, which change elevation of ice-free terrain, could be wrongly considered as a part of the glacial area. However, 80% of ground-truthed values from geodetic measurements on test sites have shown an absolute deviation below 4m for glacier boundaries derived from LIDAR acquired DEMs. An accuracy estimation of $\pm 1,5\%$ of the total glacial area for glaciers larger than 1 km^2 and $\pm 5\%$ for smaller glaciers has been made (cf. ABERMANN ET AL., 2010).

3.2 Stubai Alps and Übeltalferner

The succeeding information concerning glacial evolution in Stubai Alps in this paragraph is extracted from SEISER (2010). In analogy to Ötztal Alps data acquisitions were performed in 1969 and 1997 by the usage of analogue and digital photogrammetry and in 2006 airborne laserscanning provided the elevation data. The inventories comprise 13 glaciers of size class 4 ($1\text{-}5 \text{ km}^2$), 11 of size class 3 ($0,5\text{-}1 \text{ km}^2$), 52 of size class 2 ($0,1\text{-}0,5 \text{ km}^2$) and 39 of size class 1 ($0,01\text{-}0,1 \text{ km}^2$). The determined total volume loss of all glaciers in the Stubai Alps is about $0,74 \text{ km}^3$ ($0,47 \text{ km}^3$ in the period 1969-1997 and $0,27 \text{ km}^3$ in the period 1997-2006). Class 4 glaciers, which are illustrated in Fig. 3.3, contribute about $0,41 \text{ km}^3$ to the total ice loss from 1969 to 2006. Tab. 3.3 presents detailed results for individual absolute area and volume changes, whereby the numbers of the glaciers associate with those in Fig. 3.3. (cf. SEISER, 2010).

Nr.	Gletschername	Akk.	Abl.	$\Delta A \text{ 69-97}$ [km^2] 10^{-3}	$\Delta V \text{ 69-97}$ [km^3] 10^{-3}	$\Delta A \text{ 97-06}$ [km^2] 10^{-3}	$\Delta V \text{ 97-06}$ [km^3] 10^{-3}
1	Sulzenau Ferner	N	N	-197,91	-39,70	-73,44	-25,84
2	Sulztal Ferner	N	N	-173,84	-26,49	-318,00	-19,96
3	Alpeiner Ferner	N	NE	-305,57	-29,41	-196,33	-20,29
4	Lisenser Ferner	NE	NE	-176,54	-21,97	-114,56	-18,39
5	Bachfallen Ferner	N	N	-264,99	-29,13	-109,34	-14,75
6	Grünau Ferner	N	N	-122,78	-14,08	-67,30	-10,76
7	Triebenkarlas Ferner	W	W	-92,80	-15,49	-72,92	-10,99
8	Fernau Ferner	NW	N	-251,93	-13,92	-176,15	-9,14
9	Schwarzenberg Ferner	SE	SW	-66,20	-10,94	-187,35	-8,76
10	Daunkogel Ferner	NE	NE	-93,92	-12,12	-94,66	-7,22
11	Schaufel Ferner	NE	NE	-295,79	-13,06	-214,28	-7,59
12	Hochmoos Ferner	E	NE	-184,61	-7,22	-53,67	-6,40
13	Wütenkar Ferner	NW	NW	-151,76	-7,34	-112,09	-5,63

Tab. 3.3: Results of analysis for the 13 glaciers of size class 4 within Stubai Alps (SEISER, 2010). Values of absolute area and volume changes (ΔA , ΔV) for the two periods 1969-1997 and 1997-2006, as well as the location concerning cardinal direction of ablation (Abl.) and of accumulation area (Akk.) are presented.

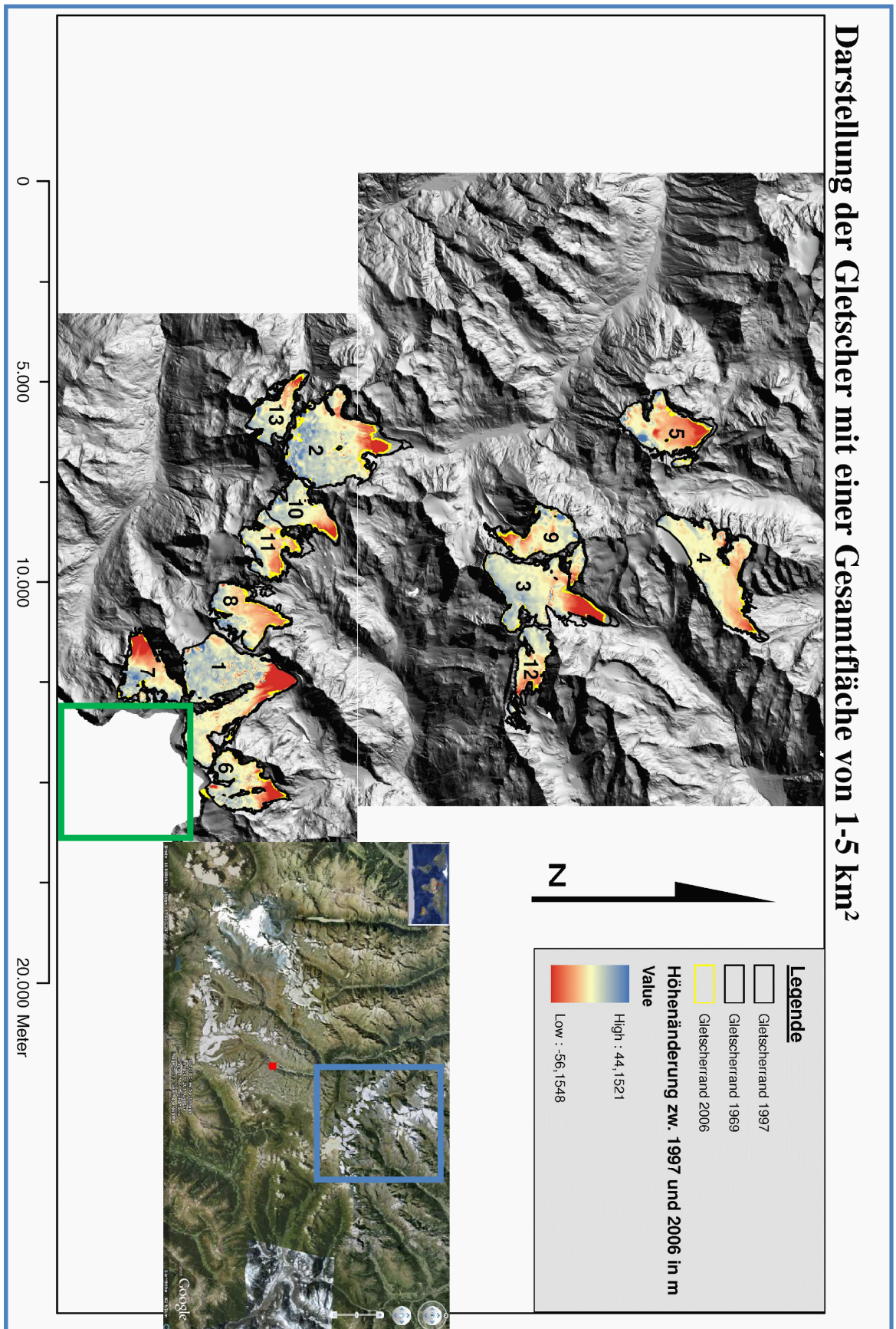


Fig. 3.3: Overview of glaciers of size class 4 in Stubai Alps (SEISER, 2010). Elevation changes between 1997 and 2006 are observable indicated with colors blue or red, as well as glacial boundaries in the colors yellow (2006) and black (1969 respectively 1997). The green rectangle marks the approximate location of Übeltalferner.

3. Glacier inventories and data

The Übeltalferner is situated on the Italian side of the Stubai Alps and so was not considered by SEISER (2010). Roberto Dinale (pers. comm., 2011) from the Hydrographic Department Bozen supports this thesis by a DEM (20 m x 20 m resolution) and digitized glacier boundaries for the year 1996, which are illustrated in Fig. 3.4. At this time glacial masses covered nearly 8 km² with a distance of approximately 15 km to Obergurgl. In the Glacierreport of Übeltalferner for the year 2008/2009 (DI LULLO ET AL., 2010) a cumulative mass balance of -7441 mm water equivalent since 2001/2002 has been presented.

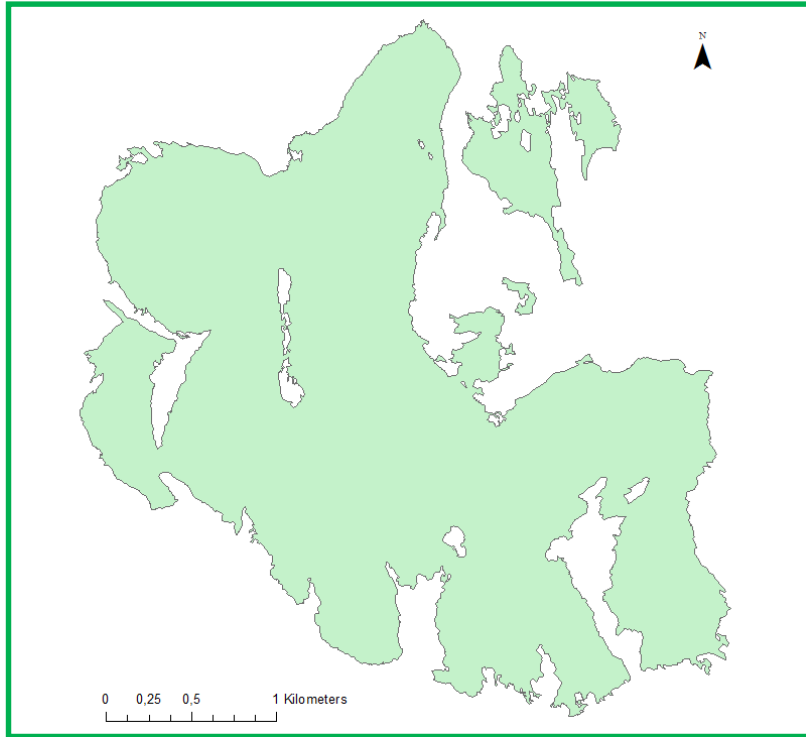


Fig. 3.4: Glacial area of Übeltalferner (green rectangle in Fig. 3.3) in 1996 provided by Roberto Dinale (pers. comm., 2011).

4. Gravimetric models and data processing

4.1 Gravimetric models

In a Cartesian coordinate system, where the z-axis points in the opposite direction of the normal of the ellipsoid, observed gravity \mathbf{g} is composed as a sum of normal gravity $\boldsymbol{\gamma}$ and gravity disturbance $\delta\mathbf{g}$. In general the plumb-line deviation ε , which is the angle between \mathbf{g} and $\boldsymbol{\gamma}$, is very small and thus one can write

$$\delta g_z \cong g - \gamma \quad (4.1)$$

with δg_z as vertical component of vector $\delta\mathbf{g}$ and the absolute values g and γ . Hence, the vertical component of the gravity disturbance is the crucial quantity in gravimetric modeling, because it can be equaled with the gravity effect of sources causing the gravity disturbance and that leads to simplifications in computations. For processing in potential theory it also has the advantage of fulfilling the Laplace equation contrary to the absolute value of $\delta\mathbf{g}$ (e.g. cf. MEURERS, lecture notes).

For the approximation of the shape of disturbing sources several equations are available (e.g. TELFORD ET AL., 1990). If bodies of simple geometry (e.g. point, rectangular prism) are chosen, computation time will be short, but reality is not reflected very precisely. More complicated bodies (e.g. polyhedron) reflect reality more exactly, but make calculations more time consuming. Especially for modeling the near zone of a measuring point the latter type is advisable. Hence, the processor has to consider this to choose the right approximation for a problem. Bodies used for gravimetric modeling in this thesis are discussed below. In most cases it is important to assume a constant density difference $\Delta\rho$ to the surrounding for the source to reach analytical expressions.

The disturbing potential δU at the reference point $P(x, y, z)$ caused by a point source with mass M at location $P'(x', y', z')$ is given by

$$\delta U(P) = \frac{GM}{((x - x')^2 + (y - y')^2 + (z - z')^2)^{\frac{1}{2}}} \quad (4.2),$$

where G denotes the gravitational constant. Differentiating δU with respect to z leads to the vertical component of its gradient

$$\delta g_z = \frac{\partial \delta U}{\partial z} = \frac{GM}{((x - x')^2 + (y - y')^2 + (z - z')^2)^{\frac{3}{2}}} (z - z') \quad (4.3).$$

This is the simplest way to approximate sources and it provides a rough estimation of the gravity effect.

Topography can be fragmented into rectangular prisms. With the relations from Fig. 4.1, the following integration, which can be found e.g. in MILITZER & WEBER (1984) as well as the succeeding formulas, presents the gravity effect at the origin of the coordinate system.

4. Gravimetric models and data processing

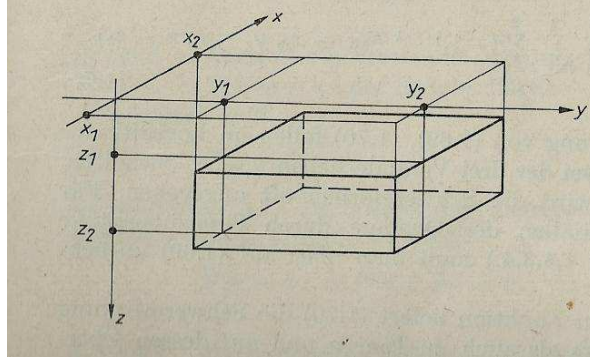


Fig. 4.1: Illustration of the parameter for the rectangular prism used for the further evaluation (MILITZER & WEBER, 1984).

$$\delta g_z(0,0,0) = G\Delta\rho \int_{x'=x_1}^{x_2} \int_{y'=y_1}^{y_2} \int_{z'=z_1}^{z_2} \frac{z' dx' dy' dz'}{R^3} \quad (4.4),$$

with $R^2 = x'^2 + y'^2 + z'^2$. The solution of these integrals with appropriate choice of the constants of integration leads to the function

$$F(u, v, w) = \text{sign}(uv) \left[|u| \ln \frac{(|v| + R_3)R_2}{|u|(|v| + R)} + |v| \ln \frac{(|u| + R_3)R_1}{|v|(|u| + R)} + w \arctan \frac{|uv|}{wR} \right] \quad (4.5)$$

with $R_1^2 = v^2 + w^2$; $R_2^2 = u^2 + w^2$; $R_3^2 = u^2 + v^2$; $R^2 = u^2 + v^2 + w^2$. The effect of gravity at any point (x, y, z) is then given by

$$\delta g_z(x, y, z) = G\Delta\rho \sum_{i=1}^2 \sum_{j=1}^2 \sum_{k=1}^2 (-1)^{i+j+k} F(x - x_i, y - y_j, z - z_k) \quad (4.6)$$

outside, interior and on the edge of the rectangular prism.

Another, more precise approach to represent the topography is the application of homogenous polyhedrons with plane surfaces, whereby the volume integral is transformed into a sum of line integrals. The volume integral that describes the attraction of a homogenous polyhedron in general is given by (e.g. GÖTZE & LAHMEYER, 1988):

$$\delta U(P) = G \iiint_{V(\text{Poly})} \left(\frac{1}{R} \right) dm \quad (4.7),$$

with the disturbing potential δU located at point P and R is the distance between P and dm. dm describes one mass element The derivative with respect to z yields to

$$\delta g_z(P) = \frac{\partial \delta U}{\partial z}(P) = G\Delta\rho \iiint_{V(\text{Poly})} \frac{\partial}{\partial z} \left(\frac{1}{R} \right) dv \quad (4.8).$$

4. Gravimetric models and data processing

With Gauss' theorem one can rewrite the volume integral as

$$\delta g_z(P) = G\Delta\rho \iiint_{Rd(V)} \cos(\mathbf{n}, \mathbf{z}) \frac{1}{R} dS \quad (4.9),$$

with \mathbf{n} as the unit normal vector of the surface element dS and vector $\mathbf{z} = (0, 0, 1)$. The cosine term is constant for each polyhedron surface. Hence, the gravity effect of a polyhedron can be described by the superposition of the effect of each individual surface S_j

$$\delta g_z(P) = G\Delta\rho \sum_{j=1}^m \left[\cos(\mathbf{n}_j, \mathbf{z}) \iint_{S_j} \left(\frac{1}{R}\right) dS_j \right] \quad (4.10).$$

Now a transformation of the coordinate system for each polygon is required in that form, that the new z' -axis is orientated parallel to the respective surface normal \mathbf{n}_j . According to Gauß-Ostrogradski the surface integral can be transformed into a line integral along a polygon P_j bounding surface S_j . The final solution, which is a very complicated expression, can be found e.g. in GÖTZE & LAHMEYER (1988).

For exact evaluations of remote disturbing sources one has to consider the curvature of the earth. The depression d is approximated by

$$d = \frac{R^2}{2R_V} \quad (4.11),$$

with R_V as volumetric radius of the earth. This value has to be subtracted from the respective elevation information.

4.2 Gravity programs

In this chapter computer programs for the computation of gravity effects provided by Meurers (pers. comm.) are discussed.

GQuader:

GQuader is used to compute the gravity effect of bodies approximated by rectangular prisms defined by two different DEMs. Input parameters are station coordinates, the center coordinates of each DEM grid cell together with the two elevations defining the height of the prism and the cell size, which describes the plane square basis area of the body. With this information rectangular prisms are designed and their gravity effect is computed by using Eq. (4.6). The calculation is done for different distance ranges in order to study the influence of far distant zones. Earth's curvature is taken into account. Additionally, there are two options: Height differences exceeding a pre-defined threshold can be excluded from computations, and, for error investigation, random errors can be added, based on the function *gasdev* (PRESS ET AL., 1992), which returns a normally distributed deviate of a predefined value.

4. Gravimetric models and data processing

Gravpolysd:

Gravpolysd is a program to compute the gravity effect of a homogeneous mass extending between the topography and a flat plane as lower boundary based on Eq. (4.10). The topography is defined by irregularly distributed sampling points using a polyhedron approximation, whereby the polyhedral surface is composed by plane triangles. As input one selects the DEM, the location of the reference point and the elevation of the lower boundary. After reading the DEM data and excluding identical coordinates the triangulation is started based on the Delaunay triangulation code by RENKA (1996). The code cannot handle vertex configurations where three or more consecutive vertices are located on a common line. Therefore, it is important to resort the DEM data before this process accordingly. The triangulation result is checked and visualized. Fig. 4.2 gives an example. Each triangle forms the upper boundary of a vertical prism extending infinitely downwards. After sorting the vertices of each triangle clockwise, the gravity effect of each prism is calculated by the algorithm by GÖTZE & LAHMEYER (1988). Earth's curvature is taken into account. This procedure is applied twice, for the triangles representing the topography and for the corresponding triangles of the lower model boundary, and the results are subtracted. Finally, the sum over all prisms yields the total gravity effect of the topography.

Hydromodel2:

In Hydromodel2, which is based on Gravpolysd, the gravity effect of a layer of constant thickness parallel to the topography can be computed. In this case, the vertical prisms are bounded by the upper and lower layer topography. Only triangles with their centroids in a previously defined polygon and within in a circle of selectable radius are considered. The coordinates of the reference point, the DEM and the coordinates of the polygon vertices (clockwise or anti-clockwise sequence) have to be entered. Finally, one has to define the layer thickness, the density and the circle radius. Earth's curvature is taken into account.

Boug7n2a:

It is originally used to compute the mass correction for the Bouguer anomaly within the far distant zone, which is divided into seven ranges with different grid sizes (R1-R7) presented in Fig. 4.3. For considering the near and transition zone by more accurate methods, 1x1, 2x2, 3x3, 5x5 or 7x7 R1 elements can be omitted. In this thesis, Boug7n2a is modified to calculate the gravity effect of a layer with its lower boundary at the topography and thickness defined by a polynomial function of topographic elevation. The layer is approximated by rectangular prisms. Earth's curvature is taken into account. Input parameters are coordinates of the reference point, the DEM representing the topography and the reduction radius, which is conventionally set to 167 km.

Uedgm#dp1_vlt:

This program is originally used to compute the mass correction for the Bouguer anomaly within the near and transition zone based on polyhedron approximation of the topography. The extent of these zones has to be selected according to Boug7n2a. Again, the gravity effect of a layer of variable thickness on the topography is determined. Optionally a certain area defined by a polygon can be excluded from the calculation. The gravity effect of the layer is computed by the algorithm of Gravpolysd.

4. Gravimetric models and data processing

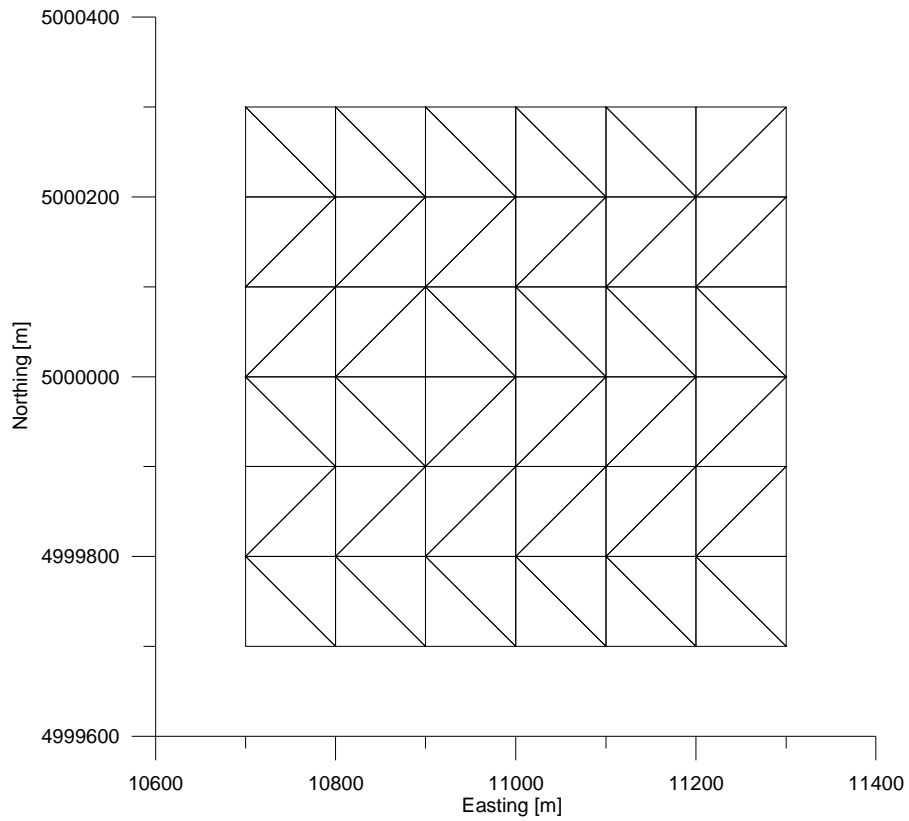


Fig. 4.2: Illustration of the triangulation mesh for an equidistant raster.

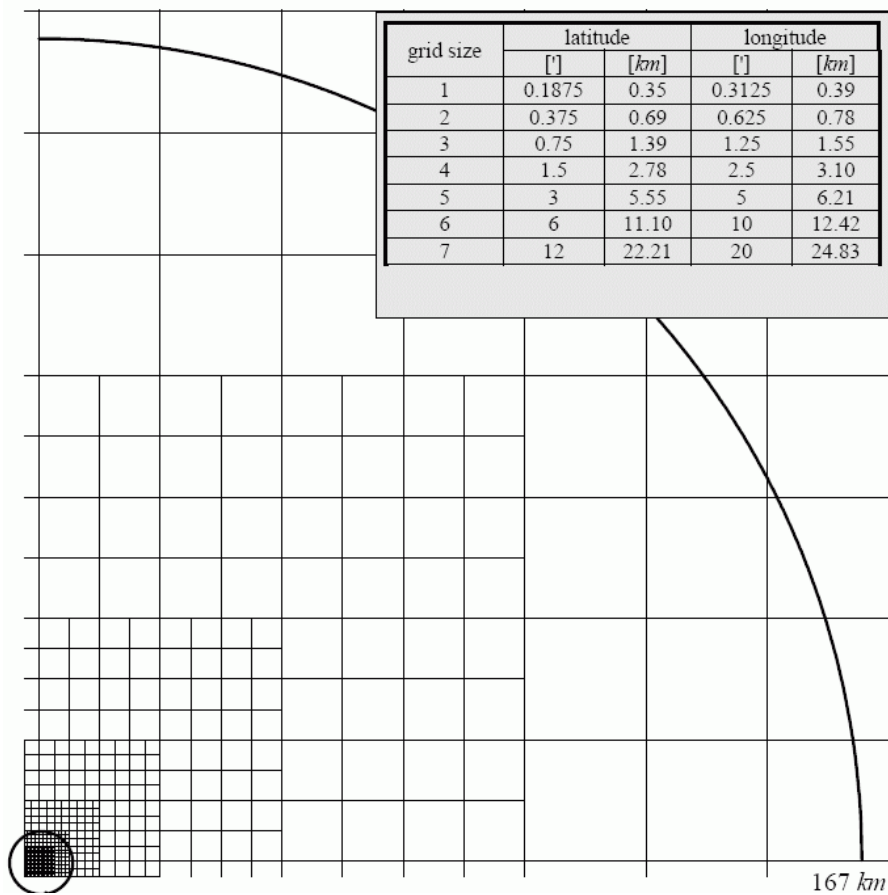


Fig. 4.3: Overview of ranges and grid sizes for the far distant zone (MEURERS, lecture notes). The zone of grid size 1 is marked by the circle.

4.3 Data processing

For the evaluation of gravity effects of different investigated problems adequate preparation of the corresponding available data is necessary. In further consequence the data processing as well as the methods of computation using the gravity programs described above are presented.

4.3.1 Sensitivity study

This study is performed to estimate the gravity effect of ablation at smaller glaciers. The affected volume of one glacier is approximated by one rectangular prism. The basis area and prism height as well as the distance to the reference point are varied. For calculations Hydromodel2 is used, setting a layer of constant thickness on the basis area of the prism. In further consequence results are used to determine the gravity effect of ablation for size class 2 and 3 glaciers within Stubai Alps (ref. to 4.3.4.2).

4.3.2 Man-made gravity effects

From 1987 until 2009 several construction works have been performed in the village and its surrounding. In the close vicinity of the gravity station a parking area and a building have been expanded. A forest road has been broadened and an avalanche gallery has been constructed. The associated locations are illustrated in Fig. 4.4. To evaluate the gravity variation due to these mass displacements a high resolution (10 m x 10 m) DEM of this region is provided by Ruess (pers. comm., 2011). These elevation data are processed based on the information provided by Ruess and Ullrich (pers. comm., 2011) to reflect topographic changes after human interference. The corresponding gravity effects are determined by applying Gravpolysd on the original and changed topography. Further constructions works are approximated by point sources due to far distances compared to their volumetric extent. That regards a water reservoir for artificial snow making and two garages.



Fig. 4.4: tirisMaps image of the village Obergurgl (© 2011, tiris, BEV). The gravity measurement point is marked by the red cross. The building and parking area (yellow rectangle), the forest road (green) and the avalanche gallery (blue) are highlighted.

4. Gravimetric models and data processing

4.3.2.1 DEM modifications

Expansion of the parking area and the building:

In the mid-1990s the parking area of a building in close vicinity of the absolute gravity station has been extended, which is evident looking at Figs. 4.5a-b. The DEM does not show any indication of this area as contour lines of 1 m interval in Fig. 4.5a demonstrate. Hence, it is necessary to modify the topography twice, once for representing the old parking area before enlargement and once for representing the current conditions. Therefore, the boundaries of these areas are picked as polygons using Figs. 4.5a-b and points inside are assigned the actual elevation. The southern edge of the areas is located at an elevation of approximately 1926 m and there is an inclination downwards of 0,5 m towards the north-north-east. The proof that the expansion of the parking area has led to a mass deficit is given by Fig. 4.5c, which illustrates the elevation difference of the two modified DEMs. The black rectangle in Fig. 4.5b marks an addition to the house constructed in the second half of 2005. Scooping earth for the basement caused a mass deficit, which is considered by creating one DEM with a constant elevation of 1929 m and one with a constant elevation of 1926,5 m for only the affected area.

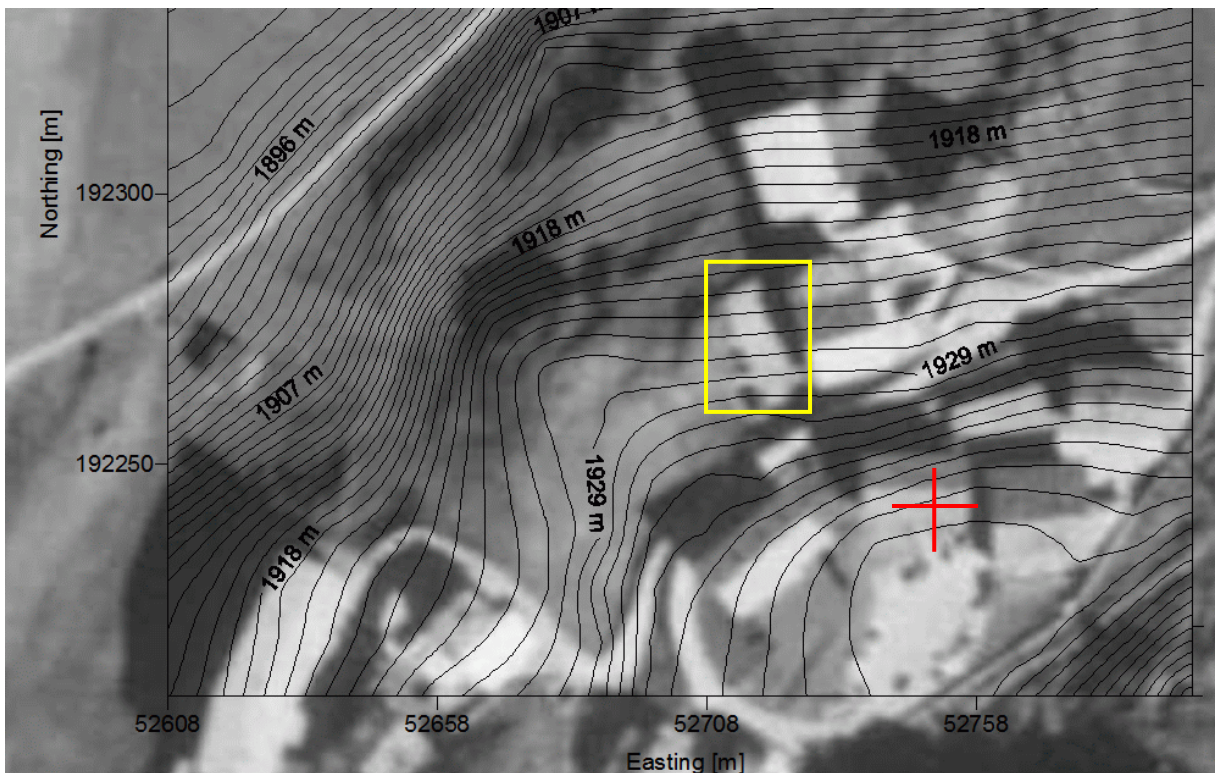


Fig. 4.5a: Illustration of the old parking area, marked by the yellow rectangle. The gravity measuring point is marked by the red cross. Computed contour intervals of 1 m demonstrate that the used DEM does not contain any information about the old parking area, which features only a slope of half a meter according to in-situ determination of elevation (Ullrich, pers. comm., 2011).

4. Gravimetric models and data processing

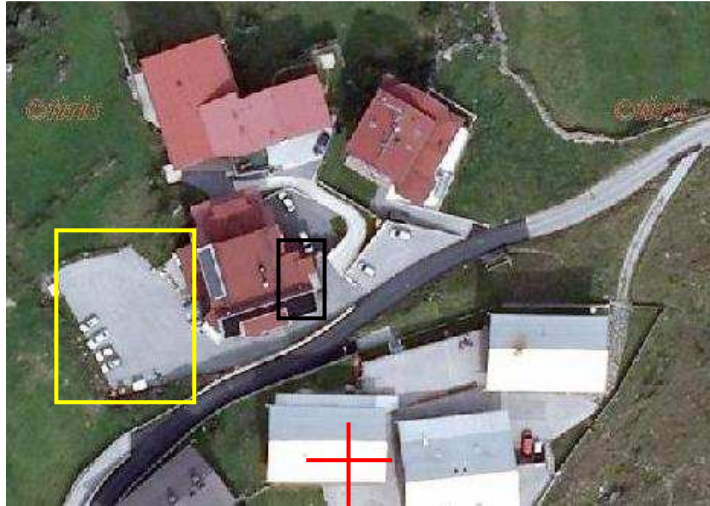


Fig. 4.5b: Illustration of the expanded new parking area marked by the yellow rectangle from tirisMaps(© 2011, tiris, BEV). The gravity measurement point is marked by the red cross. The addition to the building is highlighted by the black rectangle.

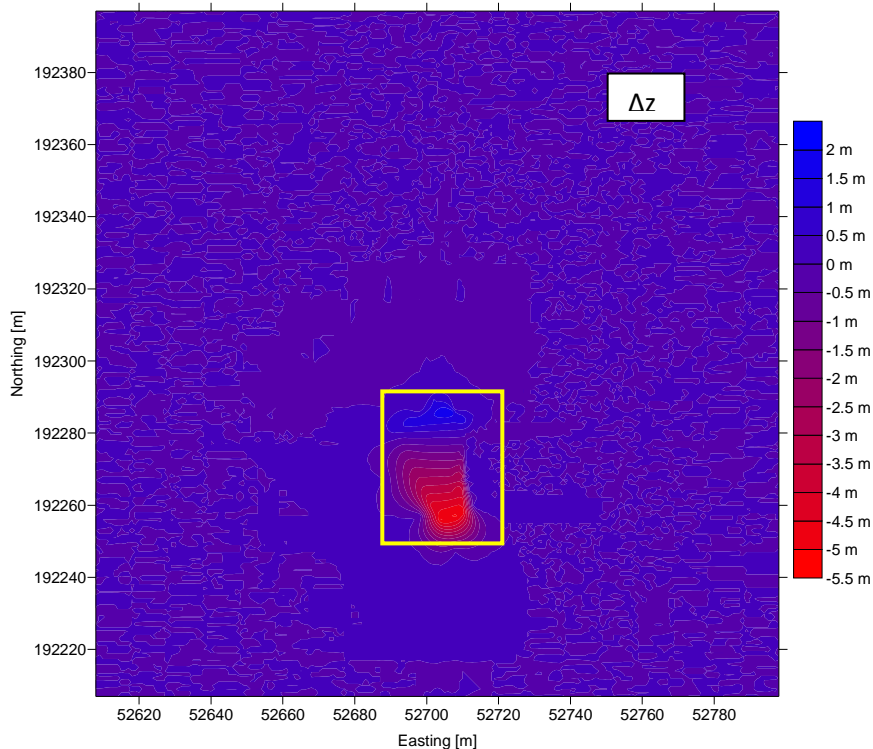


Fig. 4.5c: Elevation differences (interpolated to a 1 m x 1 m grid) of the DEMs including the parking area in current and previous state. The negative values in the southern zone of the expanded parking area (yellow rectangle) indicate a mass deficit.

Forest road reconstruction:

In summer 2008 a broadening of the forest road used as ski trail in winter with associated slope reconstruction was performed. The vertices of the 10 m x 10 m DEM grid along the road are selected based on geo-referenced topographic maps (Austrian Map Fly, version 4.0) provided by BEV (red dots in Fig. 4.6). Then, the elevation of the westerly neighbor of each vertex is set to the same elevation as that of the vertex to realize the road broadening.

4. Gravimetric models and data processing

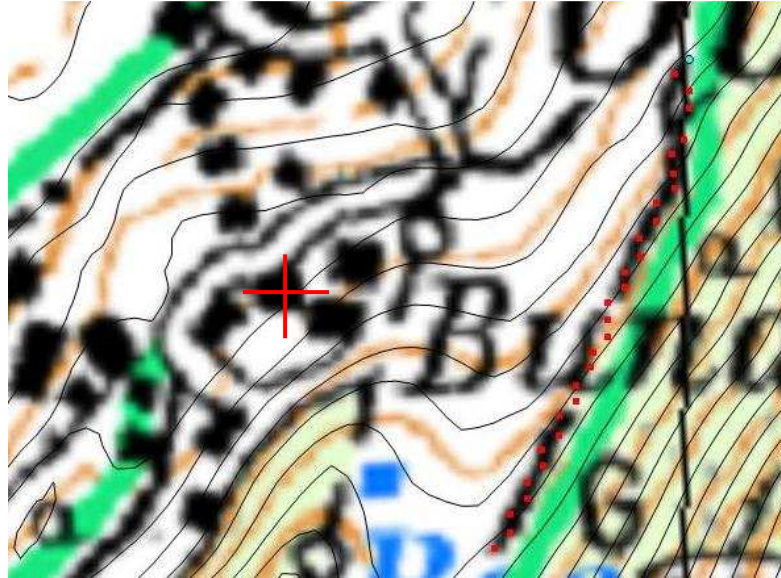


Fig. 4.6: Picks (red dots) of the forest road in Obergurgl (Austrian Map Fly, version 4.0). The red cross marks the gravity measurement site.

Avalanche gallery:

No information concerning the height of the constructed avalanche gallery is available. Therefore, different constant heights are added to the corresponding DEM vertices along the gallery (Fig. 4.7) to consider several scenarios.

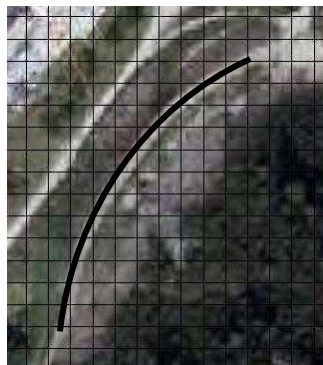


Fig. 4.7: Different constant heights are added to the DEM vertices along the black line representing the avalanche gallery (© 2011, tiris, BEV).

4.3.2.2 Point sources

Eq. (4.3) is used to determine the gravity effect of mass displacements which can be approximated by point sources. Information about location and affected volume is given by Ruesch and Ullrich (pers. comm., 2011) and is summarized in Tab. 4.1.

Mass displacement	Northing [m]	Easting [m]	Elevation [m]	r [m]	V [m ³]
Water reservoir	190054	52307	2270	2257	50000
Garage 1	192654	53087	1934	533	10000
Garage 2	193072	53873	1933	1398	15000

Tab. 4.1: Location (Gauss-Krueger-System), distance r to the measuring site and volume of mass displacements approximated by point sources.

4.3.3 Seasonal gravity variations

To quantify seasonal gravity variations a model of snow depth as a function of elevation is required. The coverage of the investigated area by snow depth observations is extremely scarce and not suitable to derive such a relation. Therefore, information of snow distribution along a north-south profile located approximately two degrees eastwards of Obergurgl for April 20 2001 from STEIN (2006) is used. This snow distribution has been derived by applying VERAXX, a 3-dimensional interpolation algorithm used in meteorological data analysis, which is a purely mathematical procedure. While cross validations have confirmed interpolation results in valleys, they have shown deviations between interpolated and measured values at higher locations (cf. STEIN, 2006). The data provide dense information and the date almost corresponds with the gravity measuring dates in spring. Fig. 4.8 illustrates the data indicating the expected correlation between elevation and snow thickness.

However, the data have to be treated with caution as snow depth varies locally in mountain regions. Therefore, the data, which are obtained by digitizing the snow depth and associated elevation in Fig 4.8, are used to generate a model valid until an elevation of 2000 m, whereby snow-free topography is assumed until 500 m. Above 2000 m, snow depth observed at ZAMG station Pitztal glacier (2850 m) is considered. At this station only snow depths below 4 m have been observed at the time of gravity measurements. Hence, above 2000m, the observed snow depth-elevation relation is scaled accordingly, i.e. the maximum snow depth is fixed to 4 m in the model. Fig. 4.9 presents the polynomial fit of the model. The computation of the gravity effect of this layer is performed with the programs Boug7n2a and Uedgm#dp1_vlt both using the 5th degree polynomial defining the relation between snow depth and elevation. Within the near and transition zone the building of the Alpine Research Site Obergurgl is excluded. The transition zone is extended to 3x3 respectively 7x7 R1 elements. The reduction radius of the far distant zone is set to 167 km.

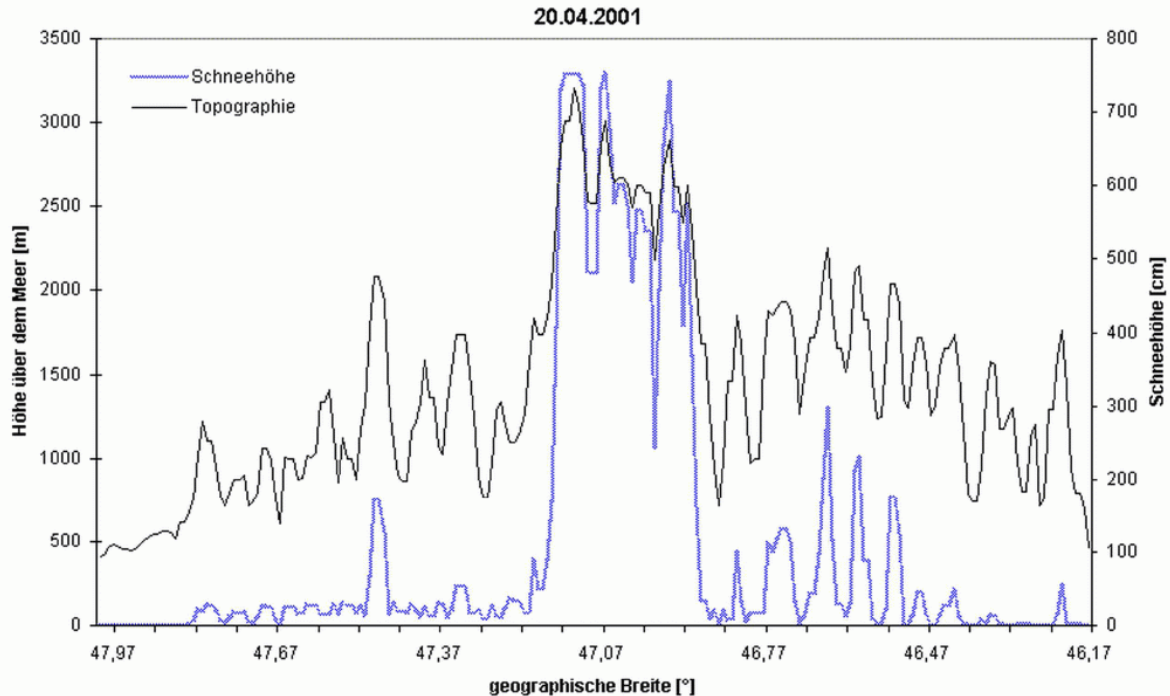


Fig. 4.8: In this diagram snow thickness (blue) and topographic elevations (black) are plotted for a profile across the Alps around a longitude of 12,7° E for the April 20 2001 (STEIN, 2006). Geographical latitude is given at the abscissa, the left ordinate axis represents elevation in m and the right ordinate axis represents snow thickness in cm.

4. Gravimetric models and data processing

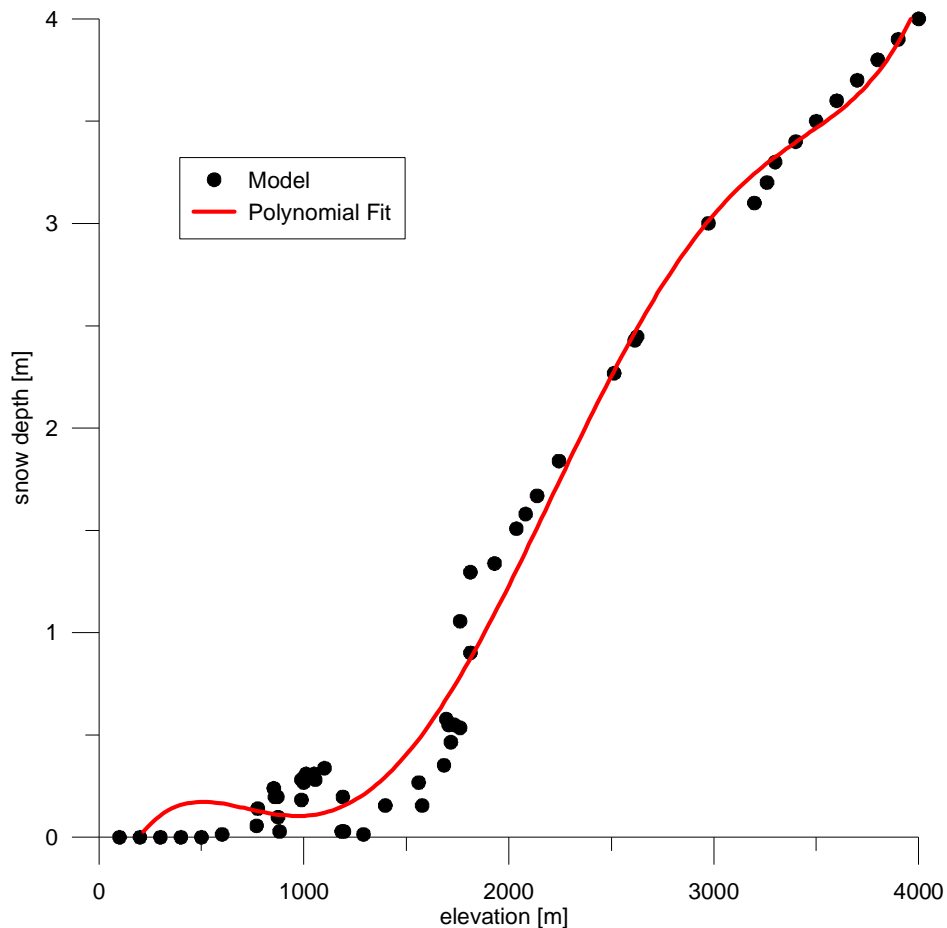


Fig. 4.9: Model of snow depths (black) and corresponding 5th degree polynomial fit (red).

4.3.4 Glacier data

4.3.4.1 Ötztal Alps

The best way to represent the glacier topography is the polyhedron method used in Gravpolygd. However, the large number of DEM vertices would cause a tremendous computational effort. Hence, GQuader is used for the determination of the gravity effect. This method exhibits a sufficient accuracy considering the occurring distances as long as prism basis areas remain small. Since the DEMs of different glacier inventories generally do not coincide, a specific data processing is required to determine the desired elevation changes.

Glacier data of the Ötztal Alps are provided by Abermann (pers. comm., 2010) in a format compatible with the GIS software ArcGIS by ESRI. The software ArcMap 9.3 is used for first data processing. The data consist of so called File System Raster (=DEM) for the years 1969, 1997 and 2006 and Personal Geodatabase Feature Class Files, which define the polygonal glacier areas for the years 1997 and 2006. Tab. 4.2 gives information about the used files. While for 1969 and 1997 always one total DEM exists, for 2006 the inventory is split up into 3 files (named after one specific glacier in the region) due to the high spatial resolution. It is intended to evaluate the gravity effect for the periods 1969-1997 and 1997-2006. The way of creating adequate elevation differences for each time period is described below.

4. Gravimetric models and data processing

Number	Name	Data type	Geometry type	Resolution [m x m]	Time
1	gletscherrand_oetztal69_ed	Personal Geodatabase Feature Class	Polygon	-	1969
2	gletscherrand_oetztal97_neu	Personal Geodatabase Feature Class	Polygon	-	1997
3	alloet69	File System Raster	-	5	1969
4	oetz_97allhm	File System Raster	-	5	1997
5	gurg06neu	File System Raster	-	1	2006
6	hochjf_rast06	File System Raster	-	1	2006
7	vernfo6neu	File System Raster	-	1	2006

Tab. 4.2: Overview of data provided by Abermann (pers. comm., 2010).

In order to decrease computation effort the amount of DEM vertices is reduced by resampling. For this purpose, the ArcGIS tool Resample with resampling technique “bilinear” is used. Of course interpolation leads to smoothing effects, which is acceptable as long as the cell size remains small. Then from both DEMs to be compared, only those data points which are located in the glacial regions of the older inventory are extracted. Hence, for example, the raster 5 to 7 from 2006 and raster 4 from 1997 (ref. to Tab. 4.2) are reduced to the areas which were covered by ice in 1997. The tool Extract by Mask executes this task. For both inventories, the tool Sample with resampling technique “nearest” finally creates ZXY-tables, which are exported for further processing. As this process is restricted to less than about 1 million vertices, the tool Clip is previously used to create subsets of the grids. All processing steps in ArcMap are summarized in Tab. 4.3 for the example of raster oetz_97allhm for the time period 1997-2006. As grids of both DEMs generally do not coincide, the next step is to find for each point of the younger grid the corresponding point of the older one. This is done by program GHDiff, which assumes that the cell size of the younger DEM is smaller than that of the older one. Under this assumption a specific grid element either is entirely contained in one grid cell of the older DEM or overlaps partially with up to four cells. GHDiff calculates a weighted mean of the height differences at each corner point of a specific cell of the younger grid. The weight is proportional to the overlapping areas. The weighted mean is then assigned to the midpoint of the cell of the newer grid and the elevation of the older inventory is calculated at these horizontal coordinates. Hence, the resulting files contain x-, y- and two z-values as well as their differences, the basis for computations using rectangular prisms. Prism basis areas of 5 m x 5 m and 8 m x 8 m result for the periods 1969-1997 and 1997-2006 respectively. Fig. 4.10a illustrates the computed elevation differences for the period 1997-2006, where mass loss is dominating. By closer inspection, also positive elevation changes can be detected. This is shown, for example, by Fig. 4.10b. These positive values can be realistic in specific areas (ABERMANN et al. 2009). In areas where glaciers have completely retreated during one period, ice-free terrain showing far larger acquisition uncertainties has to be considered. Hence, glacial elevation can be distorted and positive elevations changes can result at glacier edges.

4. Gravimetric models and data processing

Name	Type	Resolution [m x m]	Number of vertices	Tool	Technique or mask
oetz_97allhm	Grid	5	56251273	-	-
oetz_97allhm_10x10	Grid	10	14066577	Resample	bilinear
oetz97_gl97	Grid	10	14066577	Extract by Mask	gletscherrand_oetzta197_neu
oetz97_gl97_west	Grid	10	7031283	Clip	-
oetz97_OstII	Grid	10	7035294		
oetz97_west_processed	Table	10	845011	Sample	Nearest
oetz97_ostII_processed	Table	10	666496		

Tab. 4.3: Example for the processing steps in ArcMap for the grid oetz_97allhm for the period 1997-2006. Because of elimination of flagged values by the tool Sample the number of vertices is decreased significantly.

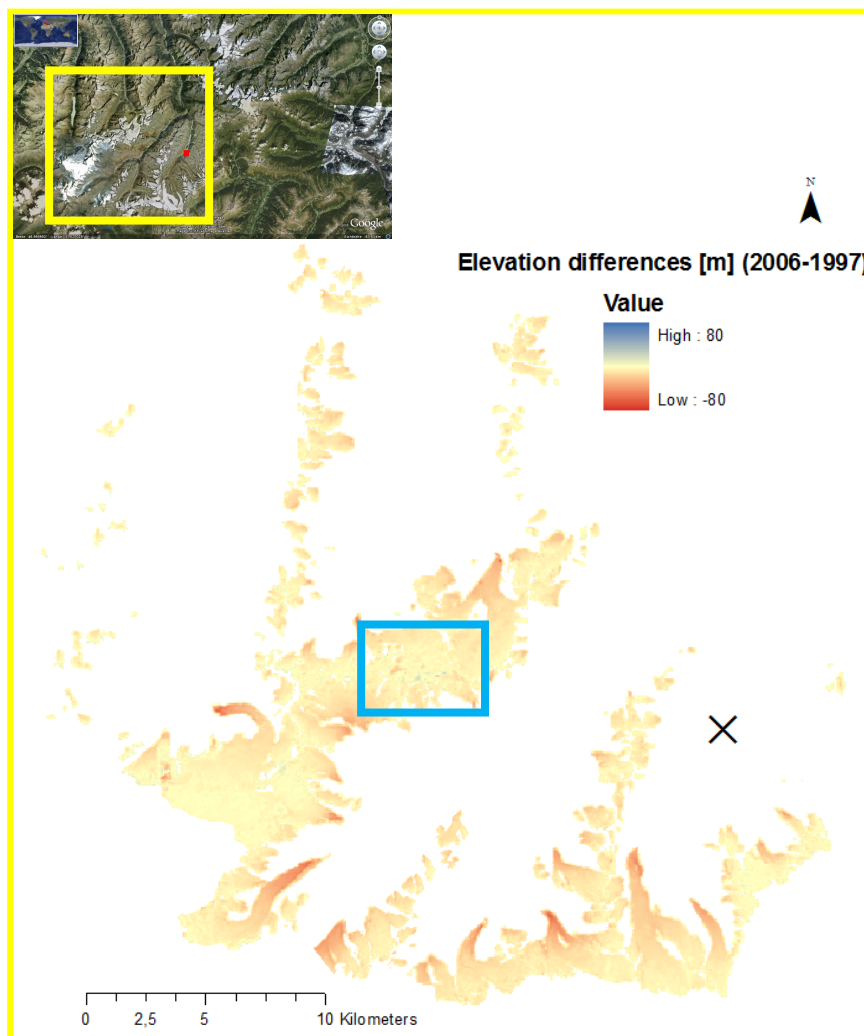


Fig. 4.10a: Illustration of elevation changes of glacial areas in Ötztal Alps between 1997 and 2006. As the red color is dominating, mainly ice mass loss occurred. The black cross highlights the location of Obergurgl, whereas the region marked by the blue rectangle and is presented more detailed in Fig. 4.10b.

4. Gravimetric models and data processing

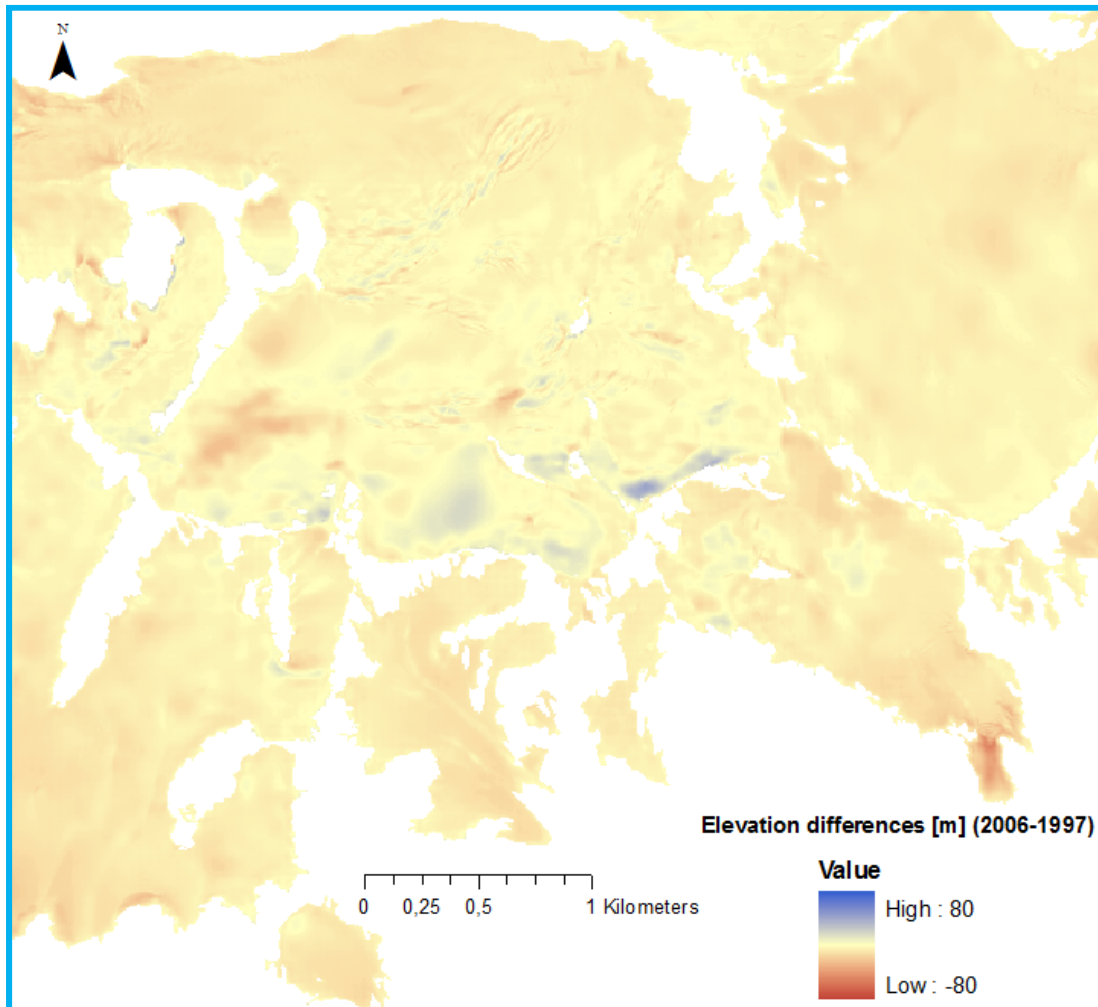


Fig. 4.10b: Illustration of regions including positive elevation changes for the period 1997-2006. Several regions of slight ice thickness increase are observable.

4.3.4.2 Stubai Alps and Übeltalferner

The glaciers of size class 4, which contribute about 55% to the total volume loss, within the Stubai Alps are spatially referenced by the fitting of Fig. 3.3 to topographic maps (Austrian Map Fly, version 4.0). Then the boundaries of the 13 glaciers are digitized and only vertices of a 25 m x 25 m DEM, provided by Ruess (pers. comm., 2011), inside the picked polygons are extracted. For each glacier a mean elevation change

$$\overline{\Delta z} = \frac{\Delta V}{A} \quad (4.11)$$

is calculated for the period 1969-2006. The individual volume differences (ΔV) and glacier areas (A) are extracted from SEISER (2010). The derived mean ice thickness changes and the cell size of the DEM subsets define rectangular prisms. The associated gravity effect is computed using GQuader.

The glacier area of the Übeltalferner from 1996 is extracted from the available DEM (20 m x 20 m resolution). Since no exact information about ablation is available for the whole period 1969-2007 it

4. Gravimetric models and data processing

is assumed to use the mean ice thickness changes determined for the Ötztal Alps. The corresponding gravity effect is determined by applying GQuader.

Size class 2 and 3 glaciers contribute about 27% and 15% respectively to the total volume loss. The gravity effect caused by ablation is estimated based on the results of the sensitivity study (ref. to 4.1). In this context for each size class a distinctive prism basis area is chosen. The individual prism height for each glacier representing the mean ice thickness change is derived from volume loss estimates by SEISER (2010). The horizontal distance to the observation site is determined by using topographic maps (Austrian Map Fly, version 4.0). Glacier size class 1 is neglected due to its minimal contribution to the total volume loss.

4.3.4.3 Missing glaciers

The glacier inventories of the Ötztal Alps are not quite complete, i.e. the areal coverage is not the same in each epoch. Therefore, it can happen, that for some glaciers or for few portions no ice thickness differences can be determined. Fig. 4.11 displays the problem. In yellow colors the coverage of the more recent inventory is shown, while black colors indicate those areas, which could not be taken into account due to incomplete coverage.

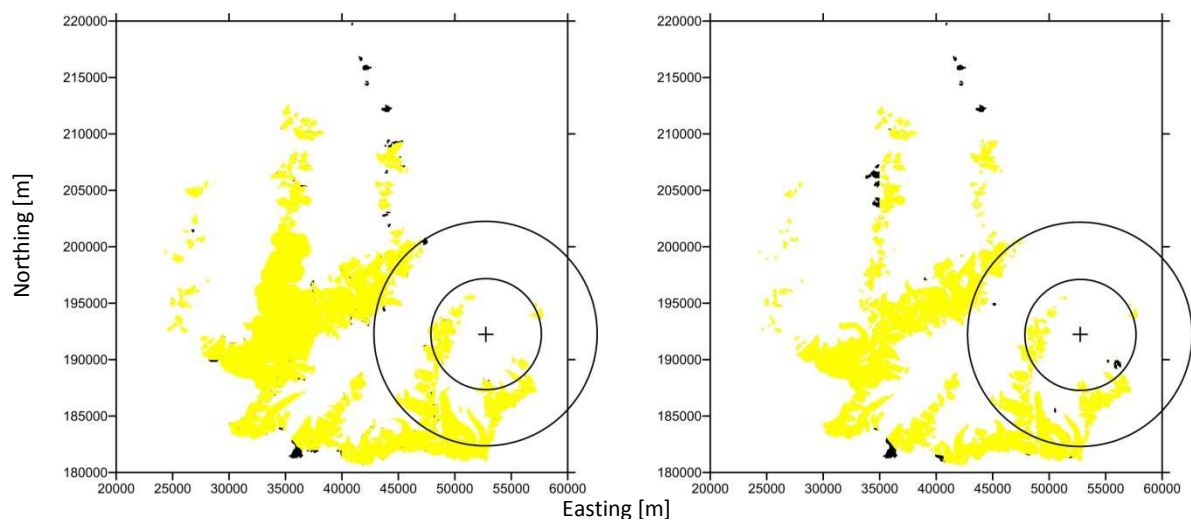


Fig. 4.11: Coverage of the glacier inventories 1969 and 1997 (left) and 1997 and 2006 (right). Black colors indicate areas, where no elevation differences are available and which thus cannot be considered for gravity effect calculation. The two circles give the distance of 5 km and 10 km respectively around Obergurgl (black cross).

Therefore, horizontal distances to Obergurgl and areas of the missing glaciers are extracted from ArcMap. The gravity effect is determined similarly to the sensitivity study (ref. to 4.1), whereby as prism heights the mean ice thickness changes in the Ötztal Alps are used.

Other missing glacier areas are located in South Tyrol close to the Austrian-Italian boarder. Some of them are within a distance of less than 10 km to Obergurgl. The area, the horizontal and the vertical separation with respect to Obergurgl are determined from topographic maps (Austrian Map Fly, version 4.0). The individual lost ice mass geometry is approximated by a rectangular prism with a square as basis area. Its height is defined by the mean ice thickness changes within the Ötztal Alps. The gravity effect of the prism is calculated using Eq. (4.6), whereby depression is considered.

4. Gravimetric models and data processing

5. Results

5.1 Sensitivity study

In this study the ice loss is approximated by one rectangular prism. In order to estimate the gravity effect of ablation at glaciers of size class 2 and 3 within the Stubai Alps (ref. to 4.3.4.2) basis areas of 600 m x 600 m and 1000 m x 1000 m respectively are chosen. For class size 2, prism heights are varied (10, 20, 30, 50 and 100 m) as well as the horizontal ($r_{\text{hor}}=5, 15, 25, 35$ km) and vertical distances ($r_{\text{ver}}=500, 1000, 1500$ m) from the midpoint of the basis area to the reference point. Computations are performed using unit density $\rho=1000$ kg/m³. The results are listed Tabs. 5.1a-d, whereby the negative algebraic sign results from surplus mass above the reference point chosen in this case. However, a mass loss under the same geometrical setting corresponds to a positive gravity effect. Effects of at least 0,5 μGal are given only for a distance of 5 km and a minimum prism height of 20 m (ref. to Tab. 5.1a).

a: $r_{\text{hor}}=5\text{km}$		Prism height [m]				
r_{ver} [m]		10	20	30	50	100
500		-0,10	-0,19	-0,29	-0,50	-1,04
1000		-0,18	-0,37	-0,55	-0,93	-1,90
1500		-0,25	-0,51	-0,77	-1,29	-2,60
b: $r_{\text{hor}}=15\text{km}$		Prism height [m]				
r_{ver} [m]		10	20	30	50	100
500		-0,003	-0,007	-0,011	-0,018	-0,038
1000		-0,007	-0,014	-0,021	-0,036	-0,073
1500		-0,010	-0,021	-0,032	-0,053	-0,107
c: $r_{\text{hor}}=25\text{km}$		Prism height [m]				
r_{ver} [m]		10	20	30	50	100
500		-0,0007	-0,0014	-0,0021	-0,0037	-0,0077
1000		-0,0015	-0,0029	-0,0044	-0,0075	-0,0154
1500		-0,0022	-0,0045	-0,0067	-0,0113	-0,0230
d: $r_{\text{hor}}=35\text{km}$		Prism height [m]				
r_{ver} [m]		10	20	30	50	100
500		-0,0002	-0,0005	-0,0007	-0,0012	-0,0025
1000		-0,0005	-0,0010	-0,0015	-0,0026	-0,0053
1500		-0,0008	-0,0016	-0,0024	-0,0040	-0,0081

Tabs. 5.1a-d: Gravity effect ($\rho=1000$ kg/m³) in μGal of a rectangular prism with a basis area of 600 m x 600 m and different heights (10, 20, 30, 50 and 100 m). r_{hor} and r_{ver} denote the horizontal and vertical distance respectively from the midpoint of the basis area to the reference point.

A similar procedure was used for estimating the effects of glacier size class 3. Here prism height and r_{ver} are set to 20 m and 1000 m respectively. Tab. 5.2 presents the results. Glaciers with a distance of more than 25 km from the observation site do not contribute significantly. Tab. 5.1a and Tab. 5.2 provide the basis for further evaluations performed in chapter 5.5.2.

5. Results

r_{hor} [km]	δg [μGal]
5	-1,028
10	-0,132
15	-0,039
20	-0,016
25	-0,008
30	-0,005
35	-0,003
40	-0,002
50	-0,001

Tab. 5.2: Gravity effect δg ($\rho=1000 \text{ kg/m}^3$) of a 1000 m x 1000 m x 20 m rectangular prism. r_{hor} denotes the horizontal distance to the reference point. The vertical distance is set to 1000 m.

5.2. Man-made gravity effects

5.2.1 DEM modifications

Results for man-made effects (ref. to 4.3.2.1), derived by applying Gravpolysd and using unit density ($\rho=1000 \text{ kg/m}^3$), are presented below. In Tabs. 5.3.-5.5, δg_1 respectively δg_2 stands for the gravity effect of the topography before respectively after man-made mass displacements and the resulting gravity effect is denoted by Δg ($=\delta g_2-\delta g_1$). Mind that the topography model in Gravpolysd extends between surface and a plane area at 0 m. Therefore, the magnitude of δg_1 and δg_2 is dependent on the spatial extent of the DEM used. During the computation process it was noticed that results strongly depend on the DEM data sequence as this influences the geometry of the triangulation mesh. Consequently, gravity effects can vary in the range of a few μGal , which is fatal for the performed evaluations in this thesis. Hence, the sequence of DEM vertices representing the topography before and after the mass displacement is kept constant.

Expansion of the parking area and the building:

The computation results are presented in Tab. 5.3. The triangulation mesh of the topography including the current parking area is shown in Fig. 5.1. Due to the fact that the mass deficit is located below the measuring point, the expansion of the parking area and the building causes a gravity decrease. Values of $-0,52 \mu\text{Gal}$ respectively $-0,12 \mu\text{Gal}$ scaled with an appropriate density value have to be considered for the correction of the gravity time series.

Construction area	δg_1 [mGal] ²	δg_2 [mGal]	Δg [μGal]
Parking area	3,61488	3,61436	-0,52
Building	0,00922	0,00910	-0,12

Tab. 5.3: Computed gravity effects Δg ($\rho=1000 \text{ kg/m}^3$) due to construction work at the parking area and the building next to the absolute gravimeter site.

² 1 mGal = 10^{-5} m/s^2

5. Results

Forest road reconstruction:

A gravity effect of $-0,37 \mu\text{Gal}$ for the broadening of the forest road with associated slope reconstruction is presented in Tab. 5.4 indicating surplus mass above the level of the measuring site. This mass shift is also considered for correcting the observed absolute gravity.

δg_1 [mGal]	δg_2 [mGal]	Δg [μGal]
30,94842	30,94879	-0,37

Tab. 5.4: Computed gravity effect Δg ($\rho=1000 \text{ kg/m}^3$) due to the broadening of the forest road and slope reconstruction.

Avalanche gallery:

Tab. 5.5 represents the gravity effects Δg for different heights (h_{gal}) of the avalanche gallery. An increasing absolute value with increasing construction height is demonstrated. Since all absolute values remain smaller than $0,1 \mu\text{Gal}$ they are not taken into account for corrections.

h_{gal}	δg_1 [mGal]	δg_2 [mGal]	Δg [μGal]
5	8,34498	8,34497	-0,01
10	8,34498	8,34495	-0,03
15	8,34498	8,34494	-0,04
20	8,34498	8,34492	-0,06
25	8,34498	8,34490	-0,08

Tab. 5.5: Gravity effects Δg ($\rho=1000 \text{ kg/m}^3$) for different constant heights (h_{gal}) of the constructed avalanche gallery.

5.2.2 Point sources

Results derived by modeling mass shifts as point sources (ref. to 4.3.2.2) using a density of 1000 kg/m^3 are listed in Tab. 5.6. All gravity effects δg are smaller than $10^{-2} \mu\text{Gal}$ and therefore can be neglected.

Mass displacement	δg [μGal]
Water reservoir	0,0097
Garage 1	-0,0010
Garage 2	-0,0001

Tab. 5.6: Gravity effects δg ($\rho=1000 \text{ kg/m}^3$) of mass displacements approximated by point sources.

5. Results

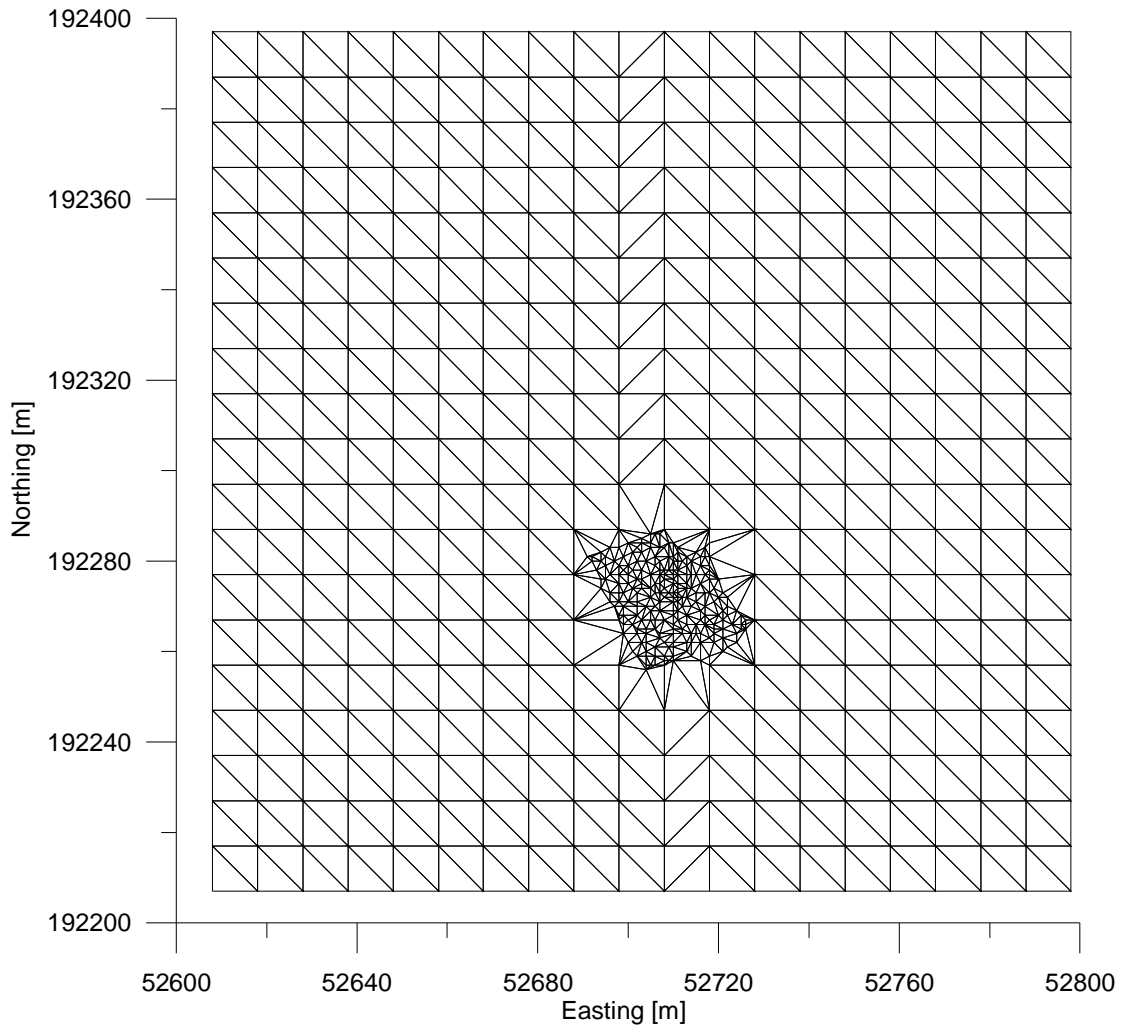


Fig. 5.1: Triangulation mesh used to approximate the topography including the current parking area.

5.2.3 Corrections of the gravity time series

To correct the gravity time series regarding man-made gravity effects a density of 2670 kg/m^3 is chosen to scale above mentioned results of relevant magnitude. This number reflects the average crustal density of the surface rocks in the investigation area. Tab. 5.7 gives an overview of correction values δg_{cor} , which are added to gravity data starting at the indicated time. The date of forest road and building reconstruction is quite exactly known. This is not true for the parking area expansion. It is assumed to have happened in 1995. However, the total correction of $2,7 \mu\text{Gal}$ is small compared to observed gravity changes. It does not reduce the observed gravity increase.

Man-made effect	δg_{cor} [μGal]	Time
Parking area	1,39	autumn 1995
Basement	0,32	autumn 2005
Forest road	0,99	autumn 2008

Tab 5.7: g_{cor} are the values for correcting observed gravity in Obergurgl for the associated man-made effect using a density of 2670 kg/m^3 . The time denotes the moment from which on the measurements are affected by the respective correction value.

5.3 Seasonal gravity variations

RUESS & HÖGGERL (2002) have performed first investigations of the gravity effect of snow cover. They have used a mass layer of a density of 1000 kg/m^3 and 1 m thickness. This mass layer has been put onto the DEM within a radius of 167 km around Obergurgl starting at altitudes varying from 0 to 4000 m representing different snowlines. The results, presented in Fig. 5.2, indicate a dominance of snow masses situated above Obergurgl due to local topography. A mass gain beneath the level of the measurement site, which predominantly is located close to the valley bottom of Ötztal, does not have a great influence, but yields an almost constant gravity effect for the snow cover starting at low altitudes (RUESS, 1995). When approaching the elevation of Obergurgl, a sudden increase of the modulus of the effect is observable reaching its maximum of more than $30 \text{ } \mu\text{Gal}$ at the level of the measurement station due to attraction of only higher situated surplus mass. For a further rising snow line the effect subsides. The presented results overestimate the gravity effect as realistic snow densities are in the range of 250 kg/m^3 to 350 kg/m^3 (RUESS, 1993). Hence, effects of about one third can be assumed leading to a magnitude of about $-10 \text{ } \mu\text{Gal}$ for the maximum effect. Since a layer with constant thickness does not match reality, a height dependent snow thickness given by a 5th degree polynomial (ref. to Fig. 4.9) is used in this study. The results using a layer density of 1000 kg/m^3 are presented in Tab. 5.8. The transition zone contributes a negative gravity effect, as well as the first five far distant zones, which confirms the results obtained by RUESS & HÖGGERL (2002). Scaling the density by 300 kg/m^3 yields a total effect of about $-17 \text{ } \mu\text{Gal}$. It has to be mentioned that the snow situation in the village may differ from the used data due to human influence like the clearance of the parking area next to the Alpine Research Site Obergurgl. Snow on the roof of the building, which would increase the negative gravity effect, is also not considered in the computation. However, in 2004 the difference of gravity measured in autumn and spring shows the same magnitude of about $15 \text{ } \mu\text{Gal}$ (ref. to Fig. 2.2). For the years 1990, 1999 and 2009 differences of approximately 13, 11 and $12 \text{ } \mu\text{Gal}$ are determined. The mean of differences for all years exhibiting measurements in the two seasons is about $5,5 \text{ } \mu\text{Gal}$, whereby three years (1988, 1989 and 2008) show higher spring values than autumn values.

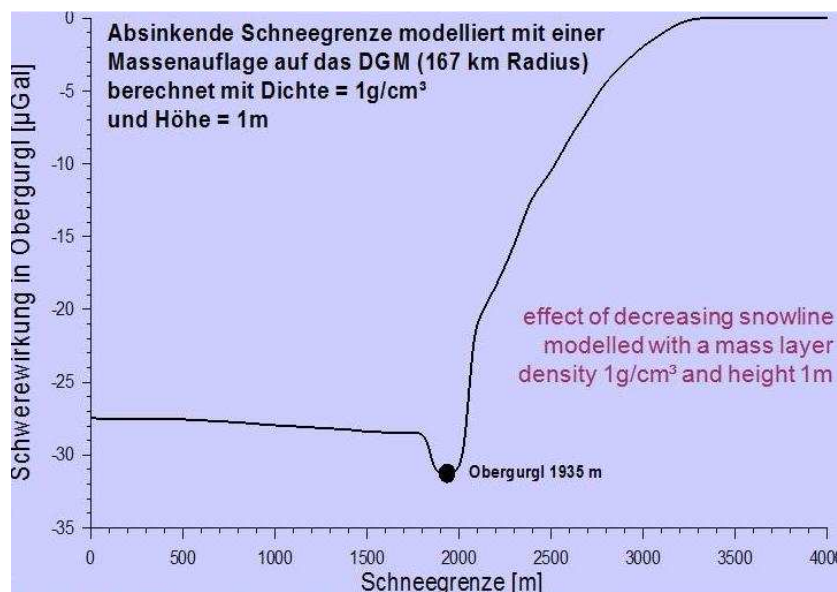


Fig. 5.2: Illustration of the gravity effect of a mass layer with height of 1 m and a density of 1000 kg/m^3 (RUESS & HÖGGERL, 2002). This layer starts at varying altitudes, representing the snow line on the abscissa. On the ordinate the gravity effect is plotted. The maximum absolute effect is reached for a snowline on the same level as the measuring station in Obergurgl.

5. Results

		Transition zone size 3x3 R1	Transition zone size 7x7 R1
Far distant zone	Grid size R	δg [μGal]	δg [μGal]
	1	-30,00	-17,00
	2	-11,00	-11,00
	3	-4,00	-4,00
	4	-2,10	-2,10
	5	-0,09	-0,09
	6	0,10	0,10
	7	0,07	0,07
	Total far distant zone	-47,02	-34,02
Transition zone		-11,96	-23,93
TOTAL		-58,98	-57,95

Tab. 5.8: Results for the computation of the gravity effect of the snow cover with density of 1000 kg/m^3 for two different grid sizes of the transition zone. Detailed information of the contribution of transition and different far distant zones is delivered. The total gravity effects deviate about $1 \mu\text{Gal}$ when using different sizes for the transition zone.

For a qualitative analysis more information about snow distribution is gathered from ZAMG for Obergurgl and weather stations in the surrounding, whereby spatial coverage is extremely scarce and data are not available for each date of measurement. In 1988 a snow cover thickness of 136 cm in Obergurgl fits best to the used model of snow distribution, but measured gravity values for this year do not reflect the seasonal effect (ref. to Fig. 2.2). Another approach is to focus only on gravity values measured in spring ($g_{\text{wm,sp}}$) and to compare the deviation from the overall trend with snow depth determined at the three stations at Pitztal glacier, Obergurgl and Galtür. The locations of these stations are illustrated in Fig. 5.3. As the general gravity increase in Obergurgl is also confirmed by the measurement campaigns in autumn, snow mass cannot be responsible for this trend. However, Fig. 5.4a shows a similarity in the fluctuation of gravity (high frequency gravity variations) and snow thickness at Pitztal glacier (2850 m). In this illustration the reducing effect on gravity of a snow cover situated above the gravity measuring site is indicated. For the other two meteorological stations (Figs. 5.4b-c) similar correlations cannot be derived. Hence, a final clarification for the impact of snow depth is not possible with the available data.

5. Results

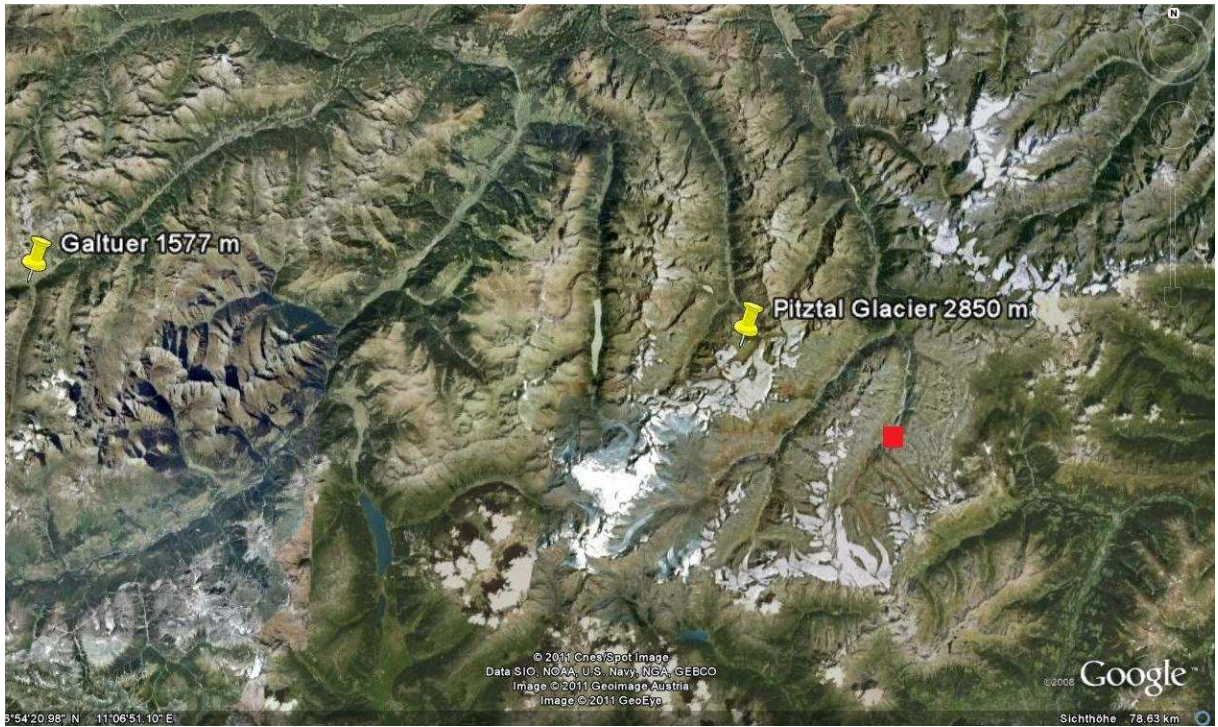


Fig. 5.3: Locations of the weather stations (© 2011 Google). The station in Obergurgl (1942 m) is marked by the red square.

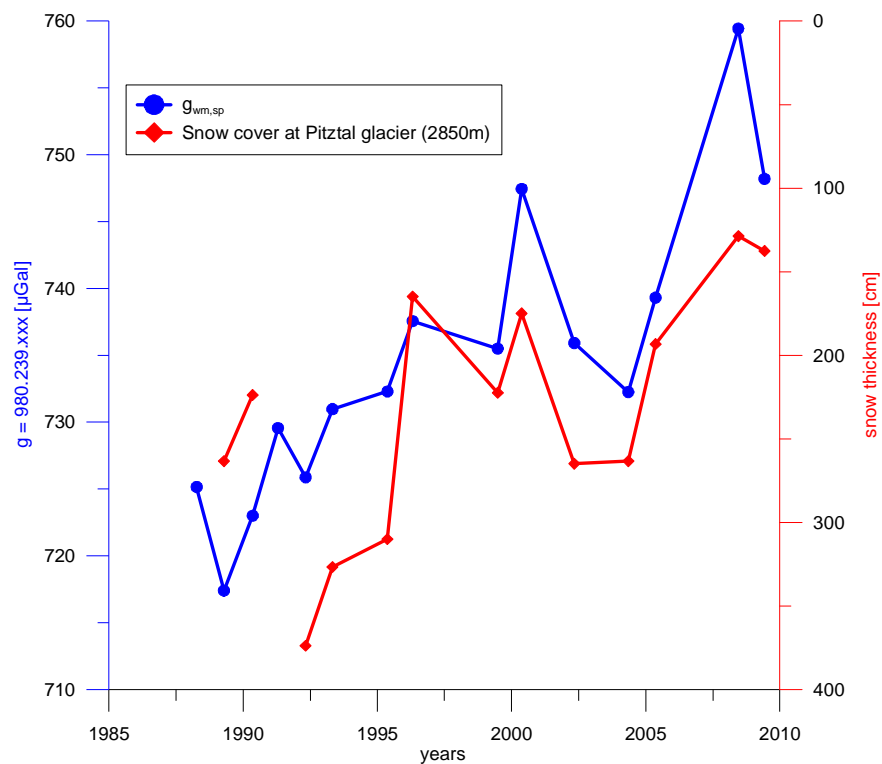


Fig. 5.4a: Observed gravity in spring ($g_{wm,sp}$) and snow thickness (axis increases downwards) at Pitztal glacier at a topographic elevation of 2850 m. A negative correlation is indicated due to surplus mass above the gravity measuring site.

5. Results

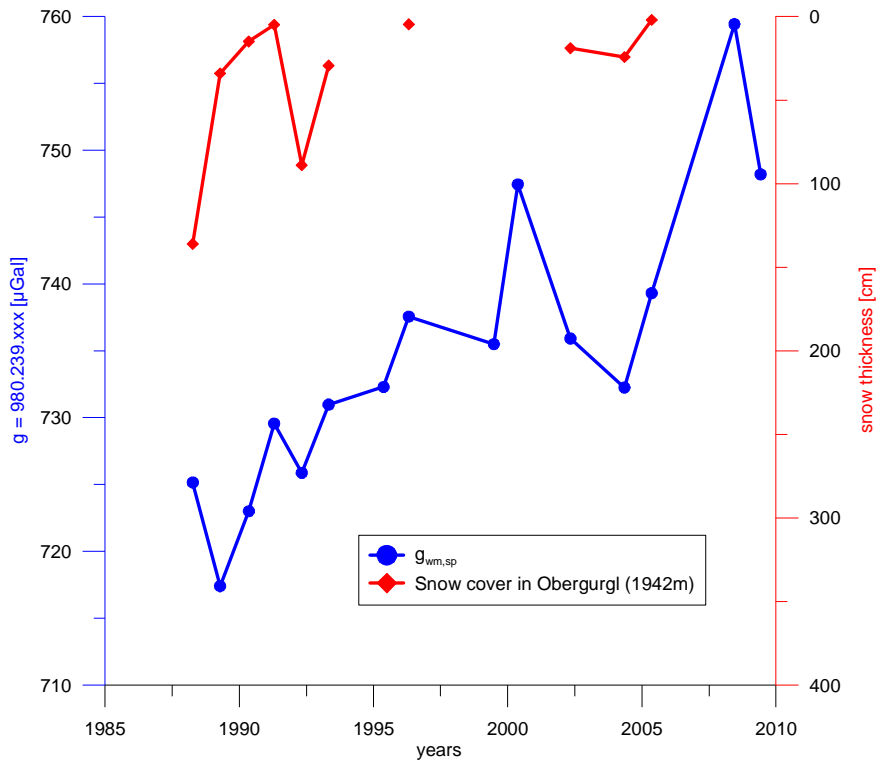


Fig. 5.4b: Observed gravity in spring ($g_{wm,sp}$) and snow thickness (axis increases downwards) in Obergurgl at a topographic elevation of 1942 m.

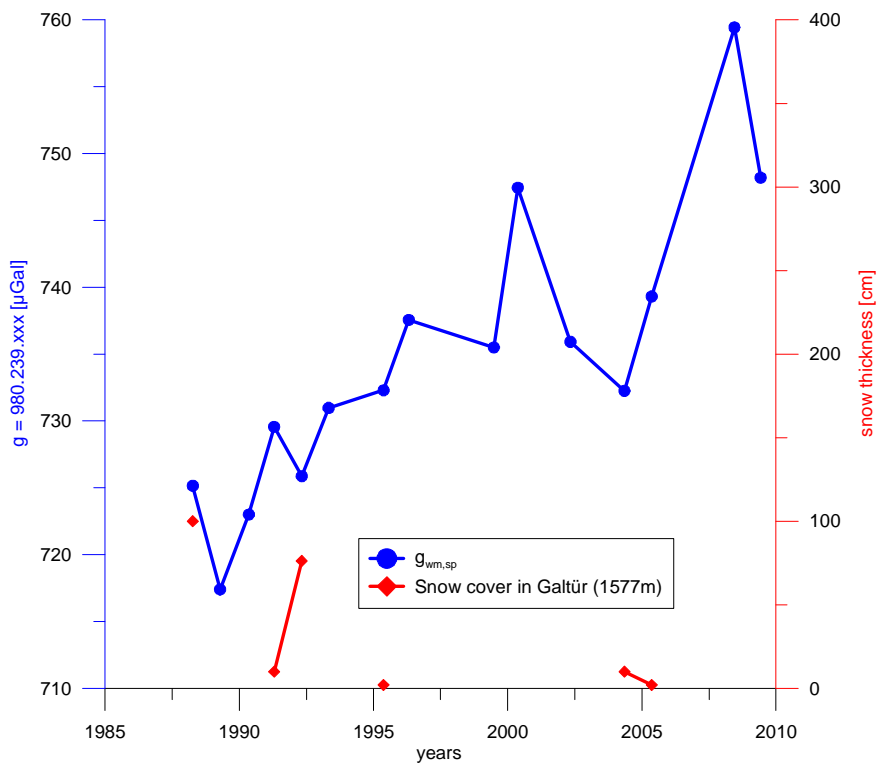


Fig. 5.4c: Observed gravity in spring ($g_{wm,sp}$) and snow thickness in Galtür at a topographic elevation of 1577 m.

5.4 Uplift of the Alps and postglacial deformation

Rates of vertical movements for Austria and especially for the region of the Alps can be found for example at RUESS & HÖGGERL (2002) or at HASLINGER ET AL. (2007). From the latter using GPS permanent stations an uplift of approximately 1-2 mm/a can be assumed for the region of Obergurgl, illustrated in Fig. 5.5a. RUESS & HÖGGERL (2002) present a vertical movement upwards of about 1,5 mm/a from repeated leveling for the same region, shown in Fig. 5.5b. Considering a Free Air gradient of $-0,308 \mu\text{Gal}/\text{mm}$ and the effect of the Bouguer Plate with $+0,111 \mu\text{Gal}/\text{mm}$, the gradient of the uplift amounts to $-0,197 \mu\text{Gal}/\text{mm}$ (e.g. RUESS, 1993). This would signify a gravity decrease between approximately $-4 \mu\text{Gal}$ (1 mm/a uplift) and $-8,5 \mu\text{Gal}$ (2 mm/a uplift) for a period of 22 years (1987-2009).

MEMIN ET AL. 2009 have analyzed ice thinning processes and modeled resulting gravity variations due to deficit mass as well as postglacial rebound for three glaciers in the Mont Blanc massif. For this region two DEMs of the years 1979 and 2003 have been used and ice thickness variations have been computed with a given accuracy of elevation changes of $\pm 2\text{m}$. On average an ice thickness decrease of approximately 2 m/a has been determined causing negative gravity effects of several hundred μGal for this period in the close vicinity of the glaciers. The computation of induced ground deformation rates, with a maximum of 0,38 mm/a 20 m outside the glaciers, leads to the elastic part of gravity variations, which are illustrated in Fig. 5.6. The negative contribution underlines that the Free Air gradient of the uplift dominates the positive mass redistribution effect. In the centre of the Mont Blanc massif a maximum value of about $-2 \mu\text{Gal}$ during 24 years is obtained. At a distance of 4 km from the centre, which is comparable with the distance between the measurement station in Obergurgl and its nearest glaciers, the rebound effect will not exceed $-0,5 \mu\text{Gal}$ within 24 years (cf. MEMIN ET AL., 2009). Since the ice thinning rates in the Ötztal Alps are smaller, a smaller vertical movement compared to the one in Mont Blanc Massif is expected.

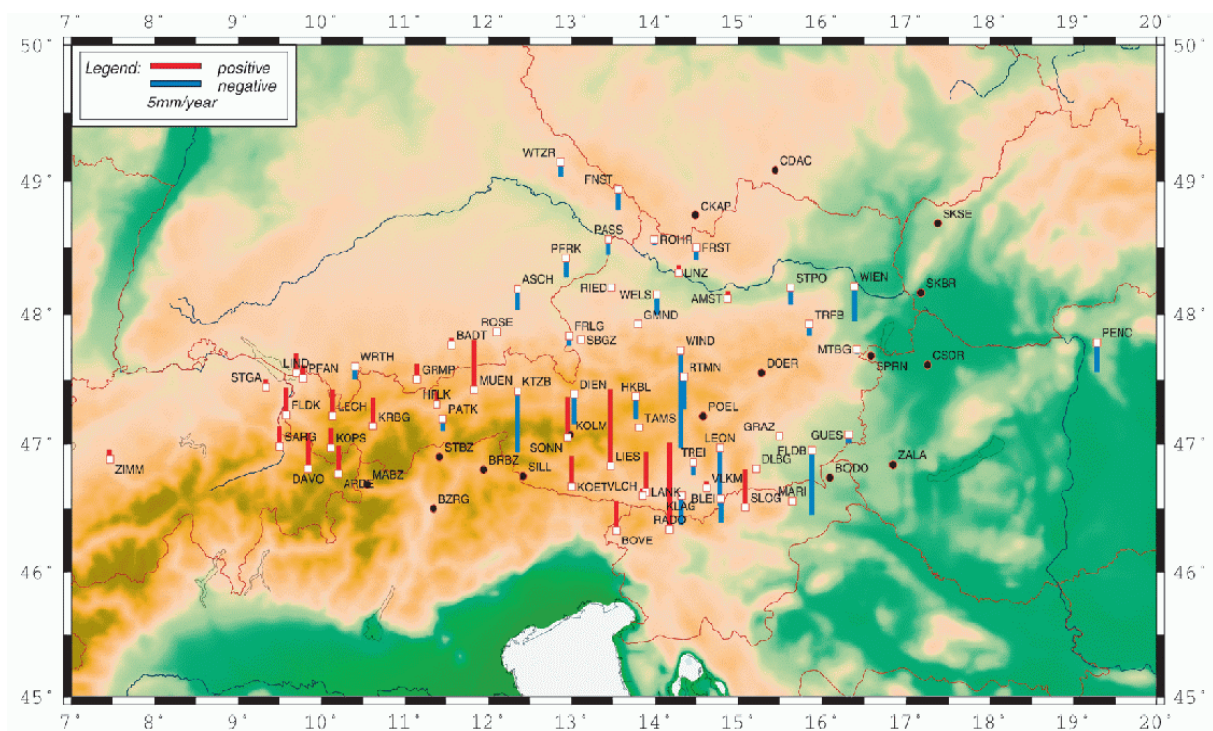


Fig. 5.5a: Vertical velocities with respect to the Eurasian Plate (HASLINGER ET AL., 2007).

5. Results

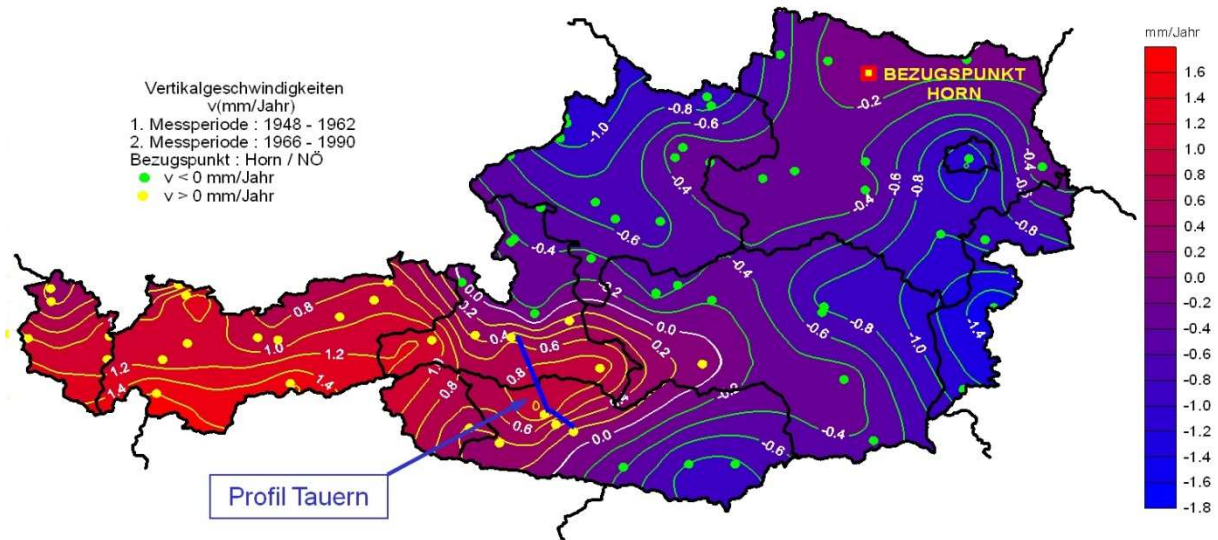


Fig. 5.5b: Vertical velocities (mm/a) within Austria (RUESS & HÖGGERL, 2002).

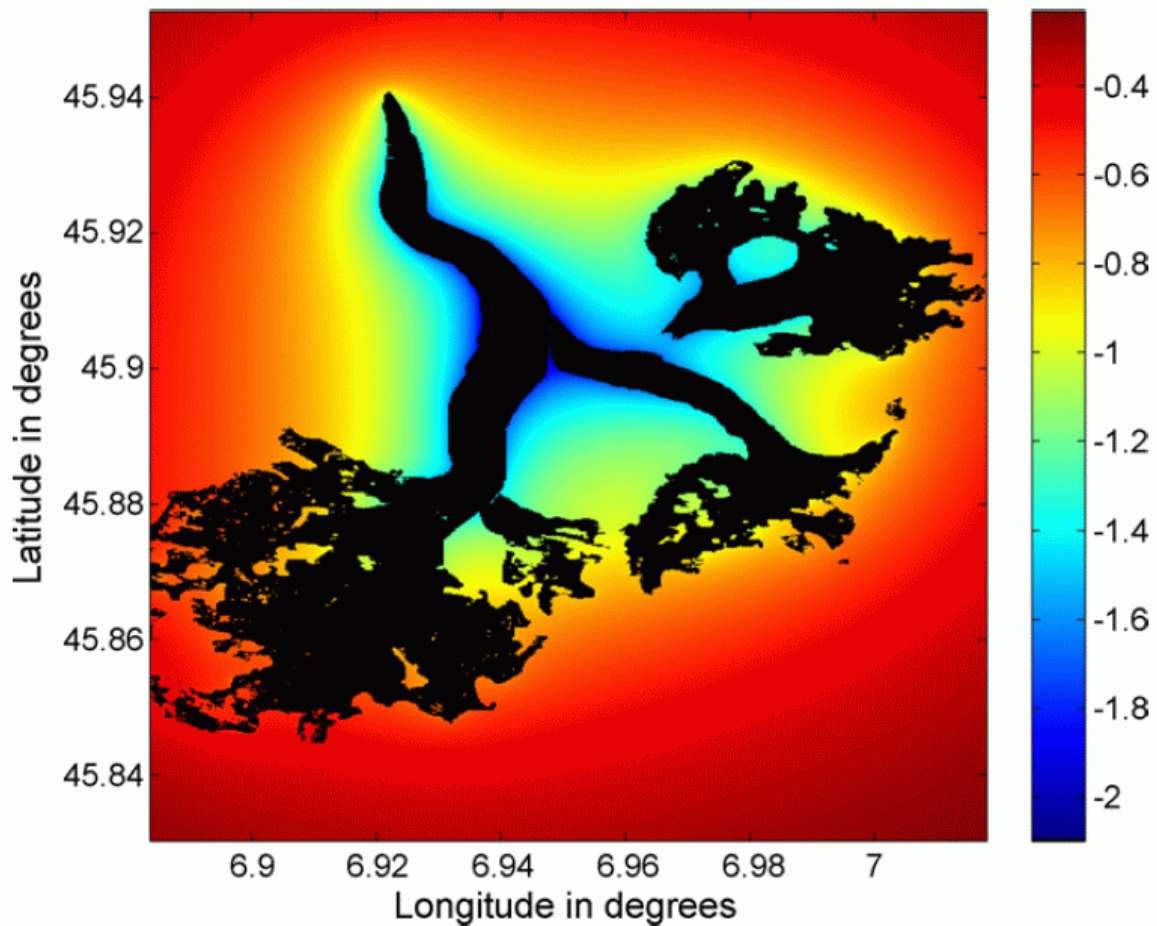


Fig. 5.6: Gravity variations caused by the postglacial rebound effect due to ice thinning in μGal for the three glaciers (black) examined in the Mont Blanc massif (MEMIN ET AL. 2009).

5. Results

This estimate only concerns the local rebound effect. BARLETTA ET AL. (2006) have investigated the glacier shrinkage and its rebound effect for the entire Alps based on glacier inventories of 1996 to 1999. For long wavelength features they predict an uplift rate of about 0,1 mm/a for the whole Alpine chain due to elastic relaxation. A high resolution approach reveals uplift rates of up to 0,9 mm/a, whereby for the western part of Austria including the Ötztal area an estimate of 0,2-0,3 mm/a can be extracted (cf. BARLETTA ET AL., 2006). Using the relation between gravity decrease and uplift of 0,235 $\mu\text{Gal}/\text{mm}$ estimated by MEMIN ET AL. (2009) the corresponding gravity decrease would be $-0,07 \mu\text{Gal}/\text{a}$ to $-0,05 \mu\text{Gal}/\text{a}$ due to elastic rebound. If the extrapolation from the Mont Blanc study is valid, we have to add $-0,02 \mu\text{Gal}/\text{a}$ as maximum estimate, resulting to about $-0,1 \mu\text{Gal}/\text{a}$ in total.

The estimate of the glacier rebound effect alone does not describe the total gravity decrease due to recent crustal movements. Because the observed uplift rates are still under debate, the effects of the observed uplift of the Eastern Alps that includes the elastic rebound are not considered for the correction of the measurement series. However, it should be kept in mind, that uplift can cause gravity decrease in the order of 2 μGal per decade, if 1 mm/a uplift rate is assumed. This number matches the observed elevation changes in the Eastern Alps (RUESS & HÖGGERL, 2002).

5.5 Glaciers

5.5.1 Ötztal Alps

The gravity change due to ablation approximated by rectangular prisms within the Ötztal Alps is calculated in three different ways. Firstly, all changes of glacier thickness are included. Then, only negative thickness changes are considered in order to study the influence of potential mass gain in specified areas. Finally, random errors based on the data acquisition accuracy are added to the elevation.

First the results for period 1997-2006 considering all elevation changes are discussed. As explained in 4.3.4.1 the Ötztal area was divided into 4 subsets. Tabs. 5.9a-d present the gravity effects for each subset using a density of $1000 \text{ kg}/\text{m}^3$. The region around Gurglerferner shows the biggest influence with 7,5 μGal due to most mass loss at short distances (range of 0-10 km) to the reference point in Obergurgl. Both regions of Vernagtferner have a higher ice volume loss in total ($0,66 \text{ km}^3$) than the region of Gurglerferner ($0,43 \text{ km}^3$), but due to greater distances the effect is accordingly minor with 1,35 μGal . With the smallest affected volume ($0,1 \text{ km}^3$) of all areas in a range of 10 to 20 km the influence of ablation in the region of Hochjochferner is as small as 0,18 μGal .

Tab. 5.10 compiles the results for the whole Ötztal area now using an average ice density of $900 \text{ kg}/\text{m}^3$ (e.g. ABERMANN ET AL., 2011). For adding random errors the accuracy estimates of $\pm 0,1 \text{ m}$ for 2006 and $\pm 1,9 \text{ m}$ for 1997 (ref. to 3.1) are used. The results show that positive ice thickness changes, concerning about 7% of glacial area in this period, do not have a severe influence ($-0,17 \mu\text{Gal}$). Random errors added to elevations do not affect the calculations either, delivering almost the same total result ($-0,01 \mu\text{Gal}$).

5. Results

a) Gurglerferner					
Range [km]	δg [μGal]	ΔV [km^3]	# of prisms considered	$\Delta z > 0$	$\Delta z = 0$
0-10	6,78	-0,25	428809	29296	1344
10-20	0,72	-0,18	295598	4893	273
20-30	0	0,00	0	0	0
Total	7,5	-0,43	724407	34189	1617

b) Hochjochferner					
Range [km]	δg [μGal]	ΔV [km^3]	# of prisms considered	$\Delta z > 0$	$\Delta z = 0$
0-10	0	0,00	0	0	0
10-20	0,18	-0,10	148534	2868	100
20-30	0	0,00	0	0	0
Total	0,18	-0,10	148534	2868	100

c) Vernagtferner East					
Range [km]	δg [μGal]	ΔV [km^3]	# of prisms considered	$\Delta z > 0$	$\Delta z = 0$
0-10	0,18	-0,02	56940	2931	166
10-20	0,95	-0,32	608938	36406	1437
20-30	0,02	-0,04	73667	3089	152
Total	1,15	-0,38	739545	42426	1755

d) Vernagtferner West					
Range [km]	δg [μGal]	ΔV [km^3]	# of prisms considered	$\Delta z > 0$	$\Delta z = 0$
0-10	0	0,00	0	0	0
10-20	0,11	-0,13	292102	33300	1545
20-30	0,09	-0,15	404831	45141	2782
Total	0,2	-0,28	696933	78441	4327

Tabs. 5.9a-d: Gravity effect δg ($\rho=1000 \text{ kg/m}^3$) of ablation within the Ötztal Alps, which are divided into 4 regions, for the period 1997-2006 considering both negative and positive ice thickness change. One can also find affected volume (ΔV), the number of rectangular prisms considered for computation as well as the number of prisms representing positive ($\Delta z > 0$) and no elevation changes ($\Delta z = 0$) for the ranges 0-10, 10-20, 20-30 and 0-30 km around Obergurgl.

5. Results

Considered	δg [μGal]	ΔV [km^3]	# of prisms considered	# of prisms omitted	$\Delta z > 0$	$\Delta z = 0$
All ice thickness changes	8,13	-1,20	2309419	0	157924	7799
Negative thickness changes	8,30	-1,22	2151495	157924	157924	7799
All ice thickness changes + random errors	8,14	-1,20	2309419	0	211534	0

Tab. 5.10: Gravity effect δg ($\rho=900 \text{ kg/m}^3$) of ablation for the period 1997-2006 within the Ötztal Alps. Affected volume (ΔV), numbers of considered and omitted prism as well as number of prism representing positive ($\Delta z > 0$) and no elevation changes ($\Delta z = 0$) are listed.

The gravity effect for the period 1969-1997 using a density of 900 kg/m^3 is presented in Tab. 5.11. For adding random errors the accuracy estimates of $\pm 25 \text{ m}$ for 1969 and $\pm 1,9 \text{ m}$ for 1997 (ref. to 3.1) are used. In this time period positive ice thickness changes are greater in number and magnitude. They occur in about 11% of the considered glacier areas. Therefore, they contribute $-0,87 \mu\text{Gal}$. Adding random errors to elevation data causes a difference of $-0,54 \mu\text{Gal}$.

Considered	δg [μGal]	ΔV [km^3]	# of prisms considered	# of prisms omitted	$\Delta z > 0$	$\Delta z = 0$
All ice thickness changes	12,23	-1,52	7060679	0	798889	19121
Negative ice thickness changes	13,10	-1,60	6261845	798889	798889	19121
All ice thickness changes + random errors	12,77	-1,52	7060679	0	2640867	0

Tab. 5.11: Gravity effect δg ($\rho=900 \text{ kg/m}^3$) of ablation for the period 1969-1997 within the Ötztal Alps. Affected volume (ΔV), numbers of considered and omitted prism as well as number of prism representing positive ($\Delta z > 0$) and no elevation changes ($\Delta z = 0$) are listed.

For further evaluation the results taking all both negative and positive thickness changes into account ($12,23 \mu\text{Gal}$ for 1969-1997 and $8,13 \mu\text{Gal}$ for 1997-2006) are considered. Mean ice thickness changes of $-8,6 \text{ m}$ and $-8,1 \text{ m}$ respectively for the two evaluation periods are derived. It has to be mentioned that ABERMANN ET AL. (2009) computed smaller volume losses for both considered time periods (ref. to Tab. 3.1). This originates from the fact that they only considered 81 glaciers in the study area (ref. to Fig. 3.1).

5.5.2 Stubai Alps and Übeltalferner

Gravity effects of size class 4 glaciers are computed using individual mean ice thickness changes ($\overline{\Delta z}$) and individual DEM subsets ($25 \text{ m} \times 25 \text{ m}$ resolution). Calculations have been done for the whole period 1969-2006 considering a density of 900 kg/m^3 by applying GQuader. The results are compiled in Tab. 5.12. For Sulzenaufener and Sulztalferner (No. 1 and 2) indeed the biggest gravity effects are determined, but values of $0,1 \mu\text{Gal}$ respectively $0,07 \mu\text{Gal}$ are much smaller than the magnitude of computed effects in the Ötztal Alps. The affected total volume is about $0,07 \text{ km}^3$ smaller than derived by SEISER (2010). This discrepancy is due to the fact, that the area of the bounding polygons defining each glacier differs from the areas indicated by SEISER (2010). To consider the same ice loss volume as that reported by SEISER (2010), it would be accurate enough to scale the total result in Tab. 5.12 by the volume ratio. This is allowed, as glacier volume is approximated by very small prisms, which can further be treated as point mass considering the large distance of a few km. In this case, the volume enters as a linear quantity. However, such a correction causes a change of the gravity effect from $0,43 \mu\text{Gal}$ to $0,53 \mu\text{Gal}$.

5. Results

No.	δg [μGal]	ΔV [km^3]	$\overline{\Delta z}$ [m]	Range [km]
1	0,10	-0,06	-14,0	10-20
2	0,07	-0,04	-11,5	10-20
3	0,03	-0,03	-13,9	20-30
4	0,02	-0,04	-12,5	20-30
5	0,02	-0,03	-19,5	20-30
6	0,03	-0,02	-14,2	10-20
7	0,05	-0,02	-15,5	10-20
8	0,03	-0,02	-12,9	10-20
9	0,02	-0,02	-12,6	20-30
10	0,03	-0,01	-13,2	10-20
11	0,03	-0,02	-13,1	10-20
12	0,01	-0,01	-10,4	20-30
13	0,02	-0,01	-9,8	10-20
Total	0,43	-0,33	-	-

Tab. 5.12: Gravity effect δg ($\rho=900 \text{ kg/m}^3$) of glacial loss within the Stubai Alps for 1969-2006 for size class 4 glaciers. Glacier numbers correspond with Tab. 3.3. Affected volumes (ΔV), mean ice thickness changes ($\overline{\Delta z}$) and the range, in which masses are located, are listed.

A mean ice thickness change of $-16,7 \text{ m}$, derived from information of the Ötztal Alps glaciers, which show an average loss of this magnitude for the period 1969-2006, is assumed for Übeltalferner. Hence, a gravity effect of $0,34 \mu\text{Gal}$ is computed by applying GQuader and using the available DEM and a density of 900 kg/m^3 .

The size class 2 and 3 glaciers of the Stubai Alps are treated by approximating the lost ice volume by a rectangular prism with its basis area corresponding to its size class ($600 \text{ m} \times 600 \text{ m}$ for size class 2 and $1000 \text{ m} \times 1000 \text{ m}$ for size class 3). The height of the prism is determined using Eq. (4.11) with the distinctive area and individual ice loss extracted from SEISER (2010). As vertical separation between the level of the basis area of the prism and the elevation of the observation site 1 km is chosen which corresponds to the situation of the Stubai glaciers with respect to the elevation of Obergurgl. Then the gravity effect is calculated by using the results of a glacier in a distance of 5 km (ref. to Tab. 5.1a and Tab. 5.2). The horizontal distance and mean ice thickness change of each glacier is considered accordingly by applying a simple correction formula. Tab. 5.13 shows the total results taking into account a realistic glacier ice density of 900 kg/m^3 (ref. to appendix for individual results).

Size class	δg [μGal] 1969-1997	δg [μGal] 1997-2006	δg [μGal] 1969-2006
2	0,20	0,10	0,29
3	0,06	0,03	0,09
2+3	0,26	0,13	0,39

Tab. 5.13: Gravity effect δg ($\rho=900 \text{ kg/m}^3$) of ablation for size class 2 and 3 glaciers within the Stubai Alps for the periods 1969-1997, 1997-2006 and 1969-2006.

5. Results

5.5.3 Missing glaciers

Ablation at glaciers missing in inventories of the Ötztal Alps is evaluated similar to the sensitivity study (ref. to 5.1). Here the prism heights are given by the mean ice thickness changes within the Ötztal Alps (-8,6 m and -8,1 m respectively for the two evaluation periods). The results are scaled with respect to the individual glacier area and horizontal distance to Obergurgl. 1000 m are chosen as vertical distance for each glacier. It becomes apparent that only the two glaciers (Ferwallferner East, Ferwallferner West) within a radius of 5 km around Obergurgl for the period 1997-2006 (ref. to Fig. 4.11) have a relevant contribution to gravity variations. Accordingly, they are considered again in the course of the evaluation of South Tyrolean glaciers to determine their effects more precisely. For ablation at all other glaciers of Ötztal Alps missing in inventories in total a contribution as small as 0,06 μGal is estimated (1969-2006) using a density of 900 kg/m^3 . Therefore, they are not considered in further consequence.

Ferwallferner East (divided into two areas in this study), Ferwallferner West and the glaciers within South Tyrol are treated individually. Their areas, the horizontal and vertical distances to Obergurgl are estimated from topographic maps (Austrian Map Fly, version 4.0) or information is provided by ArcGIS files. Lost ice volume is approximated by one rectangular prism with a square basis area for each glacier using mean ice thickness changes within the Ötztal Alps as prism height. The gravity effects due to ablation are computed using Eq. (4.6) and considering depression. The results are presented in Tab. 5.14. In total the glaciers, which are missing in inventories, contribute 0,9 μGal for the period 1969-2006.

Glacier	r_{hor} [km]	r_{ver} [m]	Prism width [km]	δg [μGal] 1969-1997	δg [μGal] 1997-2006	δg [μGal] 1969-2006
Seewerferner I	6,98	760	1,046	0,13	0,12	0,25
Seewerferner II	6,08	910	0,610	0,08	0,07	0,15
Granatferner	5,20	1020	0,593	0,13	0,12	0,25
Seewerferner III	7,43	890	0,342	0,01	0,01	0,02
Ferwallferner E I	4,57	880	0,385	-	0,06	0,06
Ferwallferner E II	4,48	1030	0,265	-	0,04	0,04
Ferwallferner W	3,62	880	0,192	-	0,03	0,03
Hangenderferner	18,60	860	0,122	0,01	0,01	0,02
Feuersteinferner	20,50	910	0,136	0,01	0,01	0,02
Stubenferner	21,80	830	0,864	0,003	0,003	0,01
Similaun	16,00	1340	1,402	0,03	0,03	0,06
Total				0,4	0,5	0,9

Tab. 5.14: Gravity effect δg ($\rho=900 \text{ kg}/\text{m}^3$) for ablation at glaciers missing in inventories for the periods 1969-1997, 1997-2006 and 1969-2006. Additionally horizontal (r_{hor}) and vertical distance (r_{ver}) with respect to Obergurgl, as well as the individual prism width are presented.

5.5.5 Corrections of the gravity time series

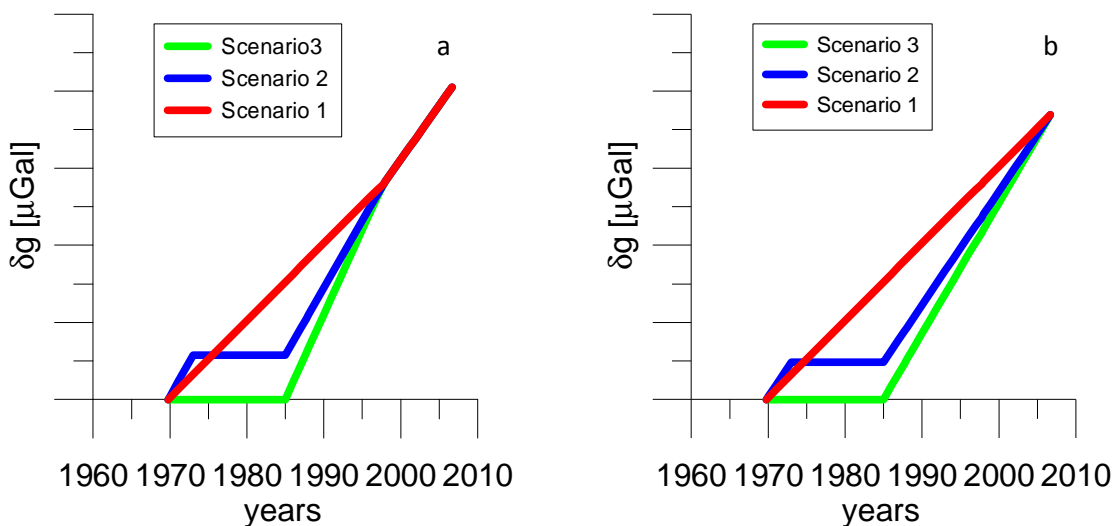
Tab. 5.15 summarizes all gravity effects caused by ice loss during the two evaluation periods. For correcting the gravity time series in general each individual effect is linearly interpolated within the associated time period (scenario 1). In this context for the period 1969-1997 also other scenarios can

5. Results

be assumed. As described in chapter 3.1 three glaciers within the Ötztal Alps showed a mass gain at the beginning of the period between 1973 and 1985, i.e. the ice volume in 1985 was the same as in 1973 (ABERMANN ET AL., 2009). ABERMANN ET AL. (2011) suggest adopting of this behavior on average for all considered glaciers in the Eastern Alps. Hence, steeper slopes are evaluated by consequently eliminating these 12 years (scenario 2). It is also not deceptive to assume that ice loss started only in 1985 looking at Fig. 3.2 (scenario 3). Scenario 3 will present the maximum correction values one can expect for the gravity time series. Figs. 5.7a-b illustrate a scheme for the interpolated gravity effects concerning the three scenarios, whereby it has to be distinguished if gravity effects have been computed for the two evaluation periods or the whole time period 1969-2006.

Glacier area	δg [μGal] 1969-1997	δg [μGal] 1997-2006	δg [μGal] 1969-2006
Ötztal Alps	12,23	8,13	20,36
Stubai Alps size class 2	0,2	0,1	0,29
Stubai Alps size class 3	0,06	0,03	0,09
Stubai Alps size class 4	-	-	0,53
Übeltalferner	-	-	0,34
Missing glaciers	0,4	0,5	0,91
Total			22,52

Tab. 5.15: Computed gravity effects (δg) due to ablation for all considered glacier areas for the periods 1969-1997, 1997-2006 and 1969-2006.



Figs. 5.7a-b: Scheme of gravity effects δg linearly interpolated with time considering three different scenarios for ablation. Scenario 1 assumes a constant ice loss for each year within the period 1969-1997, whereby for scenario 2 and 3 the years 1973-1985 and 1969-1985 respectively are excluded. On the left (a) a gravity effect for each evaluation period is considered, whereas on the right side (b) only one effect for 1969 to 2006 is given.

5. Results

These three scenarios, of course, lead to different total correction values (δg_{cor}), which are illustrated in Fig. 5.8. The curves start at first gravity measurement day (September 29 1987) and end with the last one (September 27 2009). Values from 2007 onwards are extrapolated as no information for ice thinning is available after September 2006. However, for gravity observations performed in October 2006 evaluated correction values are still representative as no major ice mass changes are expected to occur in this small time period. For this date (2006) they amount to about $-13,8 \mu\text{Gal}$ (scenario 1), $-17,5 \mu\text{Gal}$ (scenario 2) and $-19,6 \mu\text{Gal}$ (scenario 3). Extrapolation to 2009 results to corrections of $-20,6 \mu\text{Gal}$ (scenario 2) and $-22,7 \mu\text{Gal}$ (scenario 3) respectively. Scenarios 2 and 3 are used to correct the gravity time series, for which results are presented in the succeeding chapter.

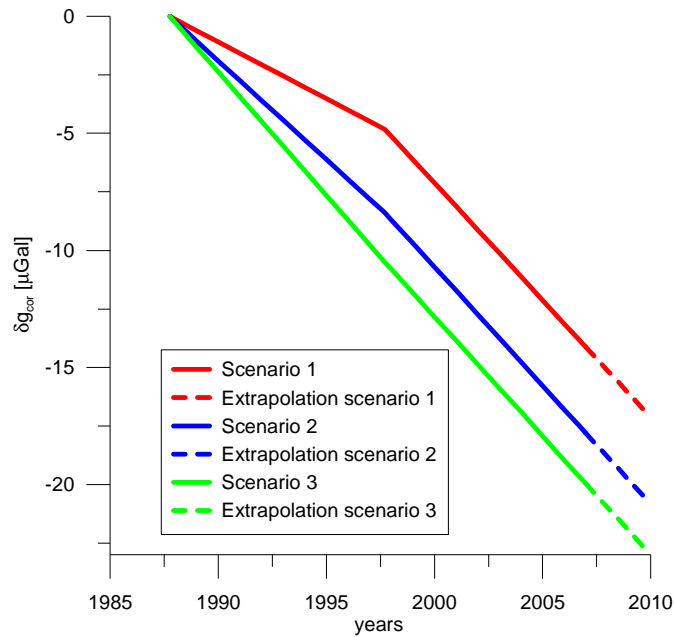


Fig. 5.8: Correction values δg_{cor} concerning glacial ablation for the 3 different scenarios. From 2007 onwards values are extrapolated.

5.6 Analysis

In a statistical analysis the gravity measurement results after correction (g_{cor}) of both the man made effects and glacial ablation including extrapolation (scenario 2 and 3 in chapter 5.5.5) as well as the uncorrected data (g) are adjusted by linear regression. Fitting straight lines to the different datasets is based on the minimization of the chi-square (χ^2) taking the estimated measurement errors into account (PRESS ET AL., 1992). Output parameters of this procedure are the slope b of the straight line, its uncertainty σ_b , χ^2 and the probability Q , which estimates the goodness-of-fit. As another significance criterion the (sample) correlation coefficient (r) and its significance level (sl) are used (e.g. SACHS, 1978). Multiplying b respectively σ_b with the associated time interval the total gravity change Δg for one specific time period and the according total uncertainty σ_{tot} are determined for the linear fits. Furthermore, linear fits were calculated additionally for spring (index sp) and autumn (index au) observations. Beside the whole measurement period (1987-2009) also the period 1997-2006 is evaluated.

For the uncorrected time series the statistical analysis is performed both for the single measurement values (index sm) and the associated weighted means of one campaign (index wm) in order to study the dependence on the datasets used. The achieved results are listed in Tab. 5.16.

5. Results

Dataset	Time period	n	b [$\mu\text{Gal/a}$]	σ_b [$\mu\text{Gal/a}$]	χ^2	Q	r	sl [%]	Δg [μGal]	σ_{tot} [μGal]
$g_{\text{sm,all}}$	87-09	96	1,53	0,09	201	1,E-09	0,77	0,1	33,6	2,0
$g_{\text{sm,sp}}$	87-09	46	1,31	0,14	49	3,E-01	0,80	0,1	27,6	3,0
$g_{\text{sm,au}}$	87-09	50	1,61	0,12	121	4,E-08	0,78	0,1	35,3	2,6
$g_{\text{wm,all}}$	87-09	32	1,40	0,15	57	2,E-03	0,78	0,1	30,8	3,3
$g_{\text{wm,sp}}$	87-09	15	1,30	0,23	13	4,E-01	0,84	0,1	27,5	4,8
$g_{\text{wm,au}}$	87-09	17	1,42	0,20	34	3,E-03	0,77	0,1	31,3	4,4
$g_{\text{sm,all}}$	97-06	38	-1,29	0,34	54	3,E-02	-0,46	1,0	-11,6	3,1
$g_{\text{sm,sp}}$	97-06	18	-0,59	0,60	12	7,E-01	-0,27	-	-3,5	3,5
$g_{\text{sm,au}}$	97-06	20	-1,54	0,42	16	6,E-01	-0,67	1,0	-13,8	3,7
$g_{\text{wm,all}}$	97-06	11	-1,25	0,64	15	1,E-01	-0,46	-	-11,2	5,7
$g_{\text{wm,sp}}$	97-06	5	-0,75	1,20	3	3,E-01	-0,33	-	-4,4	7,0
$g_{\text{wm,au}}$	97-06	6	-1,61	0,75	3	5,E-01	-0,76	-	-14,5	6,8

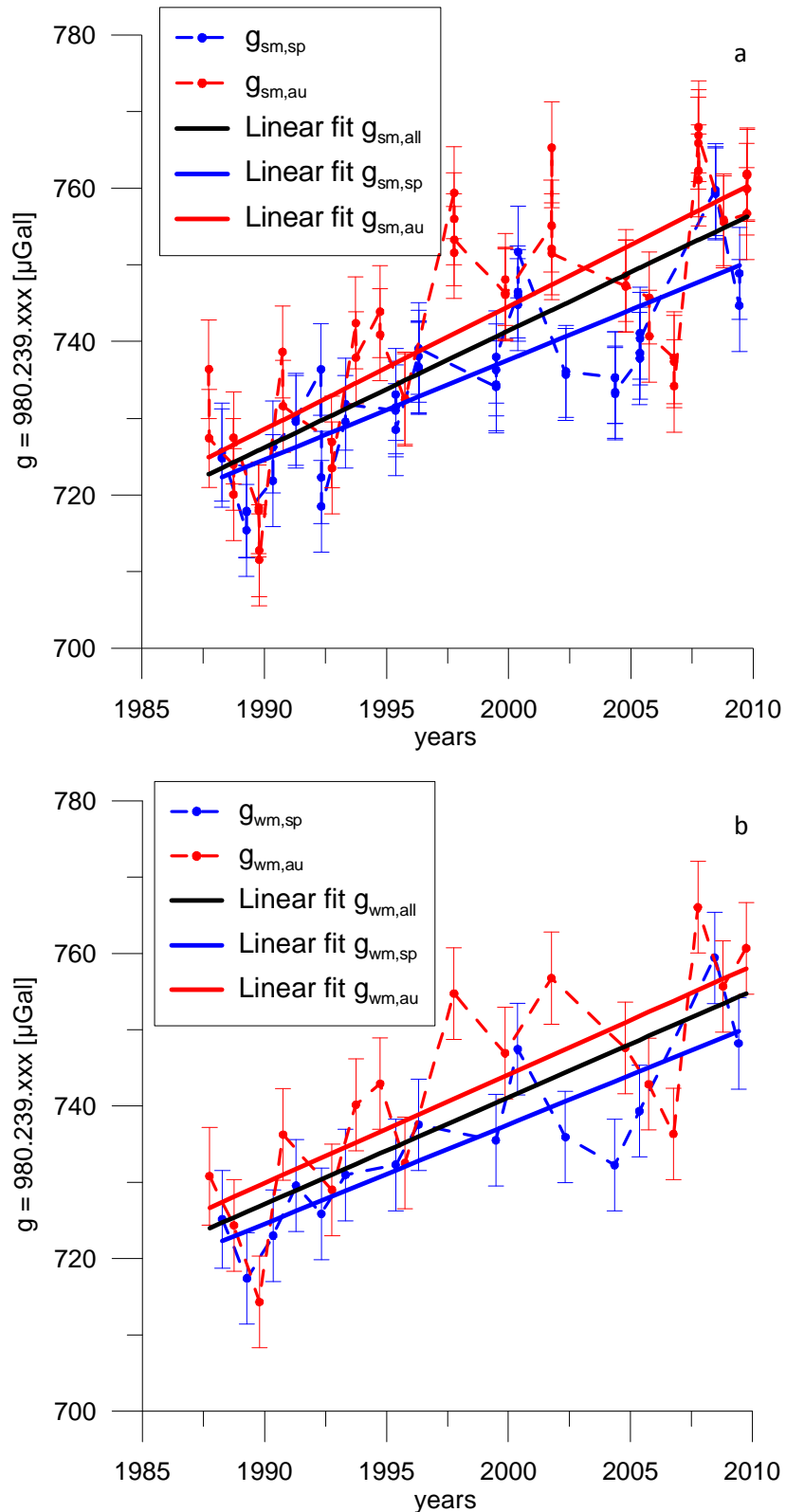
Tab. 5.16: Computation results of linear fits for different data of observed gravity. For a certain time period with n data values the slope of the straight line (b), its uncertainty (σ_b), χ^2 , probability Q, the correlation coefficient (r) and its significance level (sl) are presented. The total gravity change resulting from b is given by Δg and its uncertainty is given by σ_{tot} .

For the whole measurement period the correlation coefficient and its significance level of 0,1% indicate a significant dependency of the variables in each case. This is also confirmed by the values of Q except for $g_{\text{sm,all}}$ and $g_{\text{sm,au}}$ that are too small to award statistical significance for the used model (PRESS ET AL., 1992). The range of the slope varies between 1,30 $\mu\text{Gal/a}$ ($g_{\text{wm,sp}}$) and 1,61 $\mu\text{Gal/a}$ ($g_{\text{sm,au}}$). In contrast, the slope for the period 1997-2006 is always negative. However, its range is rather wide and extends from -0,59 $\mu\text{Gal/a}$ ($g_{\text{sm,sp}}$) to -1,61 $\mu\text{Gal/a}$ ($g_{\text{wm,au}}$). The same holds for the uncertainties σ_b . They can be even larger than the modulus of the slope itself ($g_{\text{sm,sp}}$, $g_{\text{wm,sp}}$). Even though all values of Q are of acceptable magnitude, the correlation coefficient does not indicate significant correlation except for $g_{\text{sm,all}}$ and $g_{\text{sm,au}}$, for which a significance level of 1% is obtained. The adjustment results of the two datasets (g_{sm} and g_{wm} respectively), presented also in Figs 5.9a-d, agree within the error bounds. Therefore, in the following discussion only the dataset containing the weighted means is considered.

For the whole measurement period the slope of the regression line is positive and varies between 1,30 $\mu\text{Gal/a}$ ($g_{\text{wm,sp}}$) and 1,42 $\mu\text{Gal/a}$ ($g_{\text{wm,au}}$). σ_b is of the order 0,20 $\mu\text{Gal/a}$, i.e. the adjustment results do not differ significantly. However, the regression lines valid for observations in spring and autumn respectively plot differently (ref. to Figs. 5.9a-d). For example, an offset of 6,4 μGal can be observed in Fig. 5.9b. As discussed in chapter 5.3, it is not possible to interpret the offset quantitatively. However, the average gravity effect of snow cover in spring can be offered as most probable explanation.

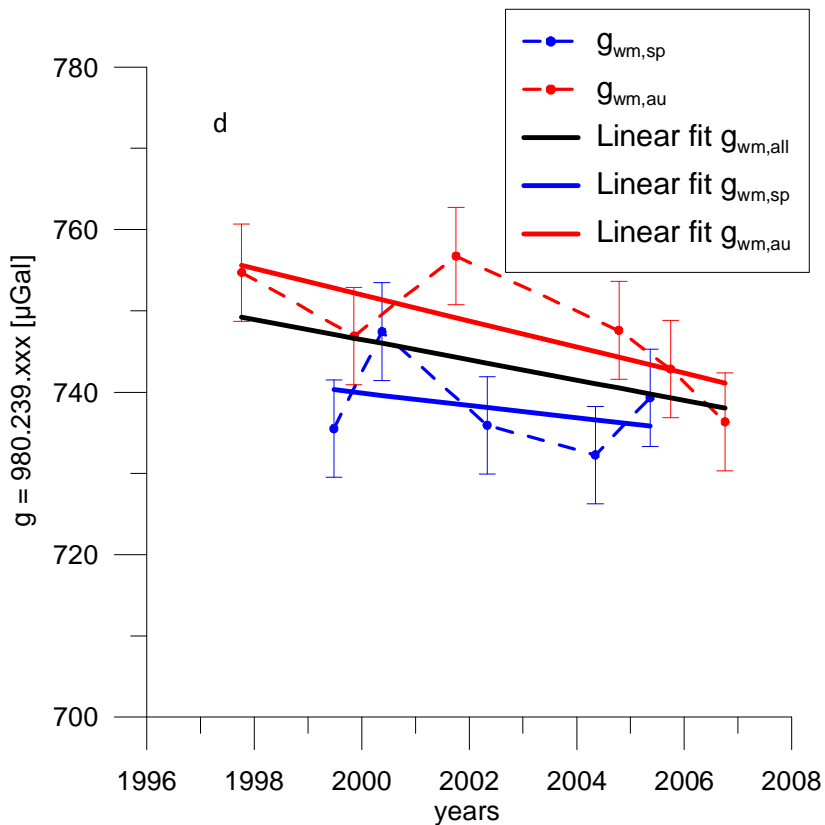
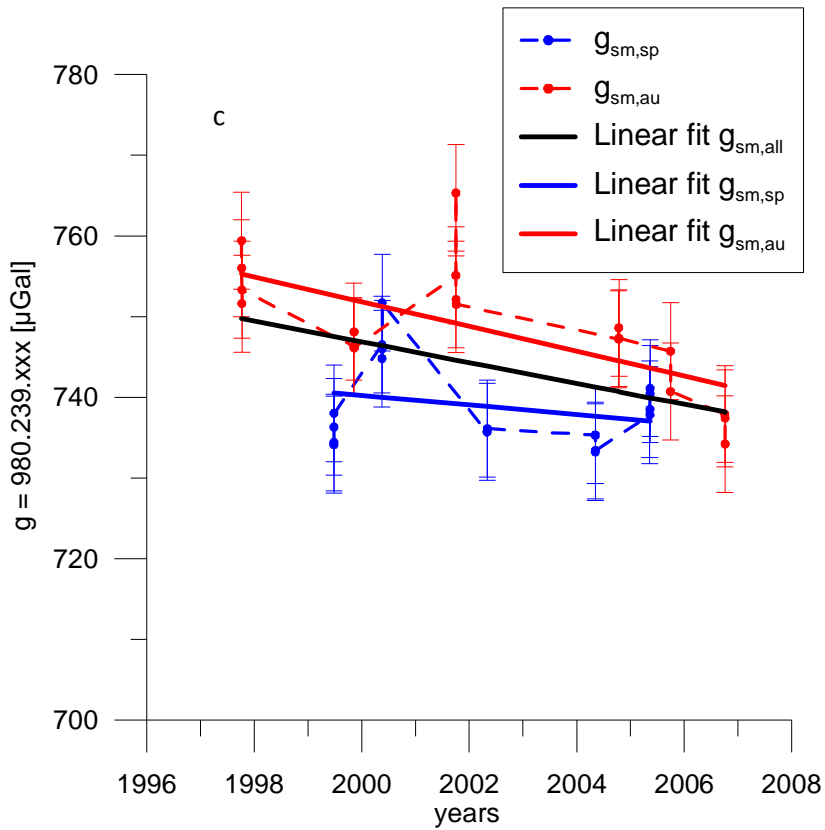
Figs. 5.9c-d show the results for period 1997-2006. As discussed before, it can be doubted if there is a significant gravity decrease. The scatter of measurement results is dominating this time period which is too short to achieve significant trends.

5. Results



Figs. 5.9 a-b: Single measurement values (a) and according weighted means (b) of observed gravity in Obergurgl (1987-2009). Symbols in red and blue refer to autumn and spring data respectively. The solid lines represent the corresponding linear fits, whereby the fit considering all data is shown in black. A gravity increase is indicated by the linear fits. Man-made effects are not corrected yet.

5. Results



Figs. 5.9 c-d: Single measurement values (c) and according weighted means (d) of observed gravity in Obergurgl (1997-2006). Symbols in red and blue refer to autumn and spring data respectively. The solid lines represent the corresponding linear fits, whereby the fit considering all data is shown in black. A gravity decrease is indicated by the linear fits. Man-made effects are not corrected yet.

5. Results

For the corrected gravity time series, the statistical analysis is performed only for the dataset containing the weighted means ($g_{cor,wm,all}$, $g_{cor,wm,sp}$, $g_{cor,wm,au}$). The linear regression results are summarized in Tabs. 5.17a-b considering scenario 2 and 3. Figs. 5.10a-b represent the associated plots for the epoch 1987-2009.

Dataset	Time period	n	b [$\mu\text{Gal/a}$]	σ_b [$\mu\text{Gal/a}$]	χ^2	Q	r	sl [%]	Δg [μGal]	σ_{tot} [μGal]
$g_{cor,wm,all}$	87-09	32	0,58	0,15	58	1,6E-03	0,45	1,00	12,7	3,3
$g_{cor,wm,sp}$	87-09	15	0,48	0,23	14	4,1E-01	0,49	-	10,1	4,8
$g_{cor,wm,au}$	87-09	17	0,60	0,20	35	2,2E-03	0,45	-	13,2	4,4
$g_{cor,wm,all}$	97-06	11	-2,23	0,64	15	1,0E-01	-0,68	5,00	-20,1	5,7
$g_{cor,wm,sp}$	97-06	5	-1,77	1,20	3	3,4E-01	-0,63	-	-10,4	7,0
$g_{cor,wm,au}$	97-06	6	-2,59	0,75	3	5,2E-01	-0,88	5,00	-23,3	6,8

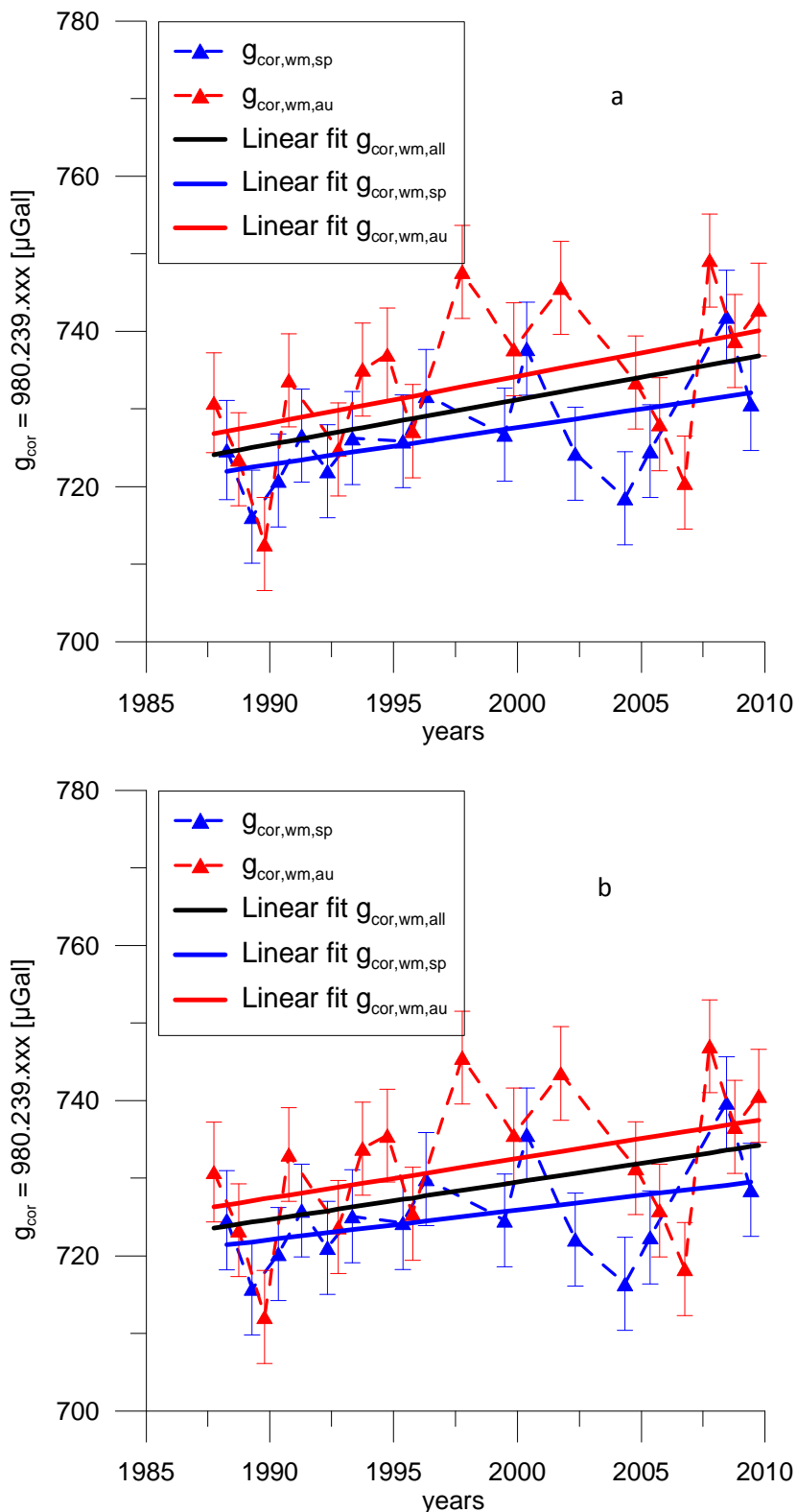
Dataset	Time period	n	b [$\mu\text{Gal/a}$]	σ_b [$\mu\text{Gal/a}$]	χ^2	Q	r	sl [%]	Δg [μGal]	σ_{tot} [μGal]
$g_{cor,wm,all}$	87-09	32	0,48	0,15	57	2,1E-03	0,39	5,00	10,6	3,3
$g_{cor,wm,sp}$	87-09	15	0,38	0,23	13	4,2E-01	0,41	-	8,1	4,8
$g_{cor,wm,au}$	87-09	17	0,51	0,20	34	2,9E-03	0,40	-	11,2	4,4
$g_{cor,wm,all}$	97-06	11	-2,24	0,64	15	1,0E-01	-0,68	5,00	-20,1	5,7
$g_{cor,wm,sp}$	97-06	5	-1,77	1,20	3	3,4E-01	-0,63	-	-10,4	7,0
$g_{cor,wm,au}$	97-06	6	-2,59	0,75	3	5,2E-01	-0,89	5,00	-23,3	6,8

Tabs. 5.17a-b: Computation results of linear fits for corrected observed gravity considering scenario 2 (a; top) and 3 (b; bottom). Presented quantities are the same as in Tab. 5.16.

Results in Tab. 5.17a for the whole gravity measurement period as well as Fig. 5.10a (scenario 2) show that the slope of the regression line decreases by $-0,82 \mu\text{Gal/a}$ due to the applied corrections and varies now from $0,48 \mu\text{Gal/a}$ ($g_{cor,wm,sp}$) to $0,6 \mu\text{Gal/a}$ ($g_{cor,wm,au}$). The uncertainties σ_b do not change because the same errors are assumed as for the uncorrected data. Contrary to the values of Q the regression coefficients do not indicate statistical significance, except for $g_{cor,wm,all}$ (significant level of 1%). Similar results are obtained for scenario 3. Also in this case, the trend remaining after correction is statistically significant only on a low significance level (5%).

For the epoch 1987-2006, for which correction values have not been extrapolated yet, a residual gravity increase ($g_{cor,wm,all}$) of $10,9 \mu\text{Gal}$ can be determined (ref. to Tab. 5.17a). This value is reduced to $9,1 \mu\text{Gal}$ using scenario 3 (Tab. 5.17b) for corrections. For the whole epoch 1987-2009, i.e. including extrapolation, the residual gravity increase ($g_{cor,wm,all}$) amounts to $12,7 \mu\text{Gal}$ (ref. to Tab. 5.17a). For scenario 3 (Tab. 5.17b) this value is reduced to $10,6 \mu\text{Gal}$. The gravity increase observed between 1987 and 2009 is $30,8 \mu\text{Gal}$. Without artificial gravity decrease due to construction work around the station (ref. to 5.2), a total of $33,5 \mu\text{Gal}$ would have been observed by absolute gravity measurements. That means, that 2/3 of the gravity increase observed between 1987 and 2009 can be explained by glacier ablation, 1/3 or about $10 \mu\text{Gal}$ remain unexplained. However, this trend is statistically questionable again, as its significance level is only 5%.

5. Results



Figs. 5.10a-b: Observed gravity (weighted means) for the period 1987-2009 corrected for glacier ablation (scenario 2 in a, scenario 3 in b) and man-made effects. Symbols in red and blue refer to autumn and spring data respectively. The solid lines represent the corresponding linear fits, whereby the fit considering all data is shown in black. A smaller gravity increase is observable due to the applied corrections.

5. Results

The analysis of the period 1997-2006 delivers the same results considering both scenarios. Therefore, only the linear fits of scenario 2 are presented in Fig. 5.10c. Negative values of b ranging from $-1,77 \mu\text{Gal/a}$ ($g_{\text{cor,wm,sp}}$) to $-2,59 \mu\text{Gal/a}$ ($g_{\text{cor,wm,au}}$) are determined. The correlation coefficients (except $g_{\text{cor,wm,sp}}$) are only significant on the 5% level, while the Q values always indicate significance.

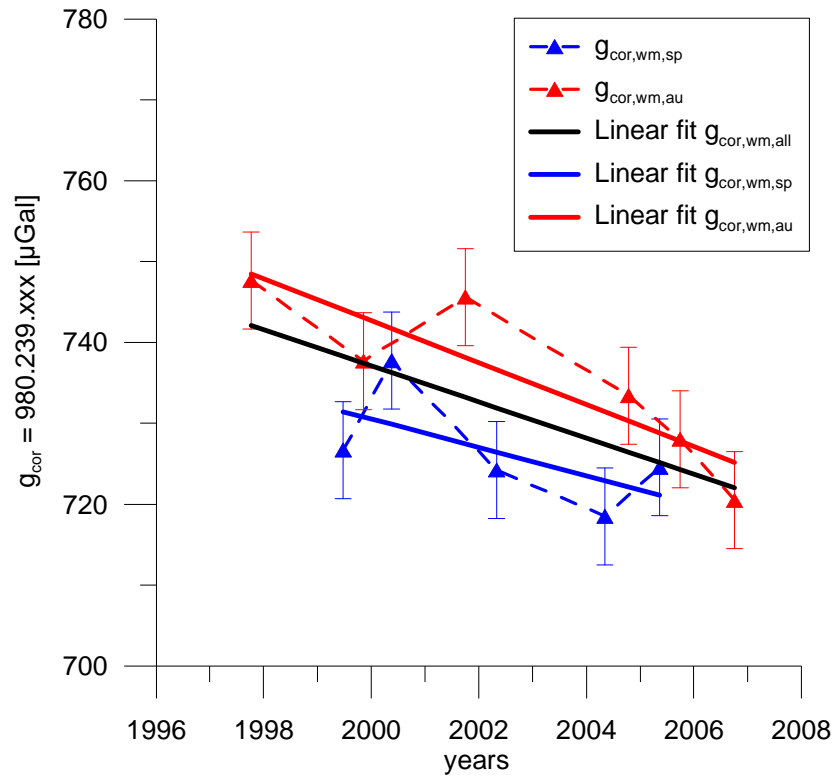


Fig. 5.10c: Observed gravity (weighted means) for the period 1997-2006 corrected for glacier ablation (scenario 2 in a, scenario 3 in b) and man-made effects. Symbols in red and blue refer to autumn and spring data respectively. The solid lines represent the corresponding linear fits, whereby the fit considering all data is shown in black. A greater gravity decrease is observable due to the applied corrections.

5. Results

6. Conclusions

The interpretation of the observed gravity variations in Obergurgl turned out to be a tricky affair. First of all the measurement uncertainty of the observed gravity had to be scrutinized. Taking into account results of ICAGs a value of $\pm 6 \mu\text{Gal}$ was derived for JILAg-6. With respect to the gravity variations in the order of $30 \mu\text{Gal}$, this is a large number. Additional uncertainties could originate from corrections applied to the raw data. Especially the atmospheric pressure correction using a single admittance factor could lead to deviations up to the μGal range in extreme cases. Examining the technical state of the absolute gravimeter, higher accuracies should have been reached for measurements after 1996 due to the purchase of the new laser.

The gravity observations in Obergurgl indicate a gravity increase between 1987 and 2009 which was underlined by the linear regression analysis. The main approach for explaining this gravity increase was the mass deficit above the measurement site caused by glacial ablation. The evaluation of temporal elevation changes in glacial areas based on the analysis of DEMs for the Ötztal Alps constituted an effective tool (ABERMANN ET AL., 2009). First, the terrain elevation acquired in two succeeding glacier inventories was extracted by using ArcGIS software. Then the elevation difference within the glacier areas was determined. However in this context limitations have to be cited. Especially on glacier boundaries unexpected positive elevation changes appeared representing ice thickness gain. A potential reason therefore can be the incorporation of ice-free terrain, for which the acquisition can show high vertical uncertainties. While for the period 1997-2006 ice thickness gain did not seriously affect the computed gravity effects, for the period 1969-1997 higher positive elevation changes contributed about $-0,9 \mu\text{Gal}$. In this context the large vertical uncertainty of 25 m (PATZELT, 1980) for the inventory in 1969 has to be noticed. For glaciers within the Ötztal Alps contained in the inventories, gravity effects of $8,13 \mu\text{Gal}$ (1997-2006) and $12,23 \mu\text{Gal}$ (1969-1997) were determined by approximating the affected ice volume by rectangular prisms with very small basis areas (5 m x 5 m for 1969-1997 and 8 m x 8 m for 1997-2006). The major contribution stems from the range up to 10 km around Obergurgl.

By contrast a total gravity effect of about $2,2 \mu\text{Gal}$ was estimated for ice thinning (1969-2006) within the Stubai Alps, Übeltalferner and other glaciers, which were not contained in inventories. As in these cases no digital elevation changes were available other approaches for the determination of ice volume losses had to be made. Individual ice thickness changes within the Stubai Alps could be derived from SEISER (2010), while for the other glaciers the computed mean thickness changes of the Ötztal Alps ($-8,6 \text{ m}$ for 1969-1997 and $-8,1 \text{ m}$ for 1997-2006) were assumed. Gravity effects were calculated either by approximating the affected ice volume by rectangular prisms with small basis areas (25 m x 25 m for size class 4 glaciers within the Stubai Alps, 20 m x 20 m for Übeltalferner) using DEMs or the lost volume was approximated as a whole by one rectangular prism, for which the basis area was given by the glacier size class (size class 2 and 3 glaciers within the Stubai Alps) or was estimated from topographic maps (glaciers missing in inventories).

Man-made mass displacements were imitated primarily by modifying the DEM of the area around the observation site. Therefore, orientation was ensured by aerial images and topographic maps. This way the modified topography was approximated by polyhedrons with triangle shaped surfaces during the computation process. However, gravity changes due to human interference did not

6. Conclusions

exceed $-3 \mu\text{Gal}$ in total. Hence, they cannot be responsible for greater erratic variations in the measurement series. Their negative contribution does not clarify the observed gravity increase either.

Seasonal gravity variations, which are indicated among others by the linear fits of autumn and spring gravity measurement values (ref. to Figs. 5.9a-b), were tried to be quantified by creating a model for the snow cover varying with topographic elevation. A gravity effect of about $-17 \mu\text{Gal}$ was computed. During the gravity time series only some observations (1990, 1999, 2004 and 2009) exhibited seasonal changes approaching the order of the computed effect. However, it can be assumed that $-17 \mu\text{Gal}$ might be an overestimated value especially as the snow distribution in the village itself cannot be clarified. Additionally, snow mass shifts due to human interference certainly lead to deviations in the near zone. Furthermore, a comparison of the high frequency gravity variations of observations during spring and corresponding measured snow thickness at different elevations was performed. A qualitative correlation could only be seen for the meteorological station at Pitztal glacier (2850 m). Nevertheless, available snow cover data were not sufficient to reach a final clarification for this problem.

For the correction of the observed gravity variations man made effects as well as glacial ablation were considered. A linear relationship between ice mass loss and time was adopted for calculating the gravity effect, whereby the ice thickness gain between 1973 and 1985 (ABERMANN ET AL., 2011) was taken into account. Two scenarios were considered for the correction: no ice loss for 1973-1985 (scenario 2) and 1969-1985 respectively (scenario 3). From 2007 onwards, correction values were extrapolated in each case. Dates for construction works were given quite accurately except for the expansion of the parking area, for which summer 1995 was assumed.

The applied correction for the whole measurement period reduced the gradient by approximately $0,8 \mu\text{Gal/a}$ (scenario 2) and $0,9 \mu\text{Gal/a}$ (scenario 3) respectively. After the correction a positive gravity trend is still visible. However, it shows weak statistical significance. Its origin remains open. Geodynamical processes like the uplift of the Alps or postglacial deformation would contribute to a gravity decrease and its correction would increase the remaining trend. For an appropriate evaluation a precise determination of elevation change at the measuring point itself would be mandatory. Groundwater level variations could be another factor. Groundwater level rise would cause positive gravity changes. Unfortunately, this question cannot be clarified as no hydrological data are available. The corrected observations from 1997 to 2006 suggest a gravity decrease within this period. Although weak statistical significance is given, the low number of performed measurements in this epoch has to be taken into account. Therefore, the idea suggests itself again that the regarded period is too short to deliver a clear trend. Otherwise the behavior would originate from unknown sources as even the assumed effect of vertical uplift rates of 2 mm/a would be dominated by the determined gravity effect of ablation for this period.

To sum up, it can be said, that the impact of ablation on gravity explains most (about $2/3$) of the observed gravity variations. The remaining trend observed in Obergurgl can be seen as due to a mixture of hydrological and geodynamical processes and instrumental uncertainties. In this context further glacier inventories with high spatial resolution would be helpful. Also instrumental improvement is required. With the purchase of the FG5 absolute gravimeter in 2010 by BEV a reduction of measurement uncertainties should be ensured. In this manner the prolongation of the measurement series will also contribute to the clarification of further questions, which comprise the

6. Conclusions

geodynamical as well as the seasonal effects. In this connection additional geodetic, hydrological and meteorological information will be essential.

6. Conclusions

Appendix

Individual gravity effects ($\rho=900 \text{ kg/m}^3$) of ablation for size class 3 glaciers within the Stubai Alps. Numbers and names of glaciers as well as volume losses are adopted from SEISER (2010).

No.	Name	r_{hor} [km]	ΔV 69-97 [km ³] 10 ⁻³	$\overline{\Delta z}$ 69-97 [m]	δg 69-97 [nGal] ³	ΔV 97-06 [km ³] 10 ⁻³	$\overline{\Delta z}$ 97-06 [m]	δg 97-06 [nGal]
14	Berglas Ferner	22,9	-4,22	-4,2	2,0	-2,84	-2,8	1,37
15	Östlicher Grübl Ferner	19,0	-11,33	-11,3	9,6	-6,75	-6,8	5,7
16	Pfaffen Ferner	13,5	-11,01	-11,0	25,9	-4,91	-4,9	11,5
17	Verborgten Berg Ferner	22,1	-5,44	-5,4	2,9	-4,46	-4,5	2,4
18	Sommerwand Ferner	23,3	-7,11	-7,1	3,3	-4,81	-4,8	2,2
19	Grastal Ferner	26,1	-7,26	-7,3	2,4	-2,83	-2,8	0,9
20	Längentaler Ferner	23,2	-5,53	-5,5	2,6	-1,66	-1,7	0,8
21	Simming Ferner W	22,1	-7,61	-7,6	4,1	-2,80	-2,8	1,5
22	Gleirsch Ferner	27,6	-5,17	-5,2	1,4	-3,12	-3,1	0,9
23	Bockkogel Ferner E	18,2	-4,79	-4,8	4,6	-1,14	-1,1	1,1
24	Westlicher Grübl Ferner W	17,7	-3,74	-3,7	3,9	-3,89	-3,9	4,1

Individual gravity effects ($\rho=900 \text{ kg/m}^3$) of ablation for size class 2 glaciers within the Stubai Alps. Numbers and names of glaciers as well as volume losses are adopted from SEISER (2010).

No.	Name	r_{hor} [km]	ΔV 69-97 [km ³] 10 ⁻³	$\overline{\Delta z}$ 69-97 [m]	δg 69-97 [nGal]	ΔV 97-06 [km ³] 10 ⁻³	$\overline{\Delta z}$ 97-06 [m]	δg 97-06 [nGal]
25	Kraspes Ferner	33,2	-6,94	-19,3	1,07	-0,10	-0,3	0,02
26	Bockkogel Ferner W	17,9	-4,48	-12,4	4,39	-1,65	-4,6	1,62
27	Gaisskar Ferner	13,3	-6,95	-19,3	16,62	-4,78	-13,3	11,43
28	Larstig Ferner	26,3	-4,24	-11,8	1,31	-1,35	-3,8	0,42
29	Zwiselbach Ferner	26,5	-5,10	-14,2	1,54	-1,55	-4,3	0,47
30	Warenkar Ferner	13,5	-3,59	-10,0	8,21	-3,44	-9,6	7,86
31	Alpeiner Kräul Ferner	22,4	-3,41	-9,5	1,71	-2,13	-5,9	1,07
32	Griesskogel Ferner	25,8	-2,94	-8,2	0,96	-1,91	-5,3	0,63
34	Grabawand Ferner	20,9	-3,80	-10,6	2,34	-2,30	-6,4	1,42
35	Simming Ferner M	22,2	-6,28	-17,4	3,23	-3,04	-8,4	1,56
36	Falbesoner Knoten Ferner	23,3	-2,41	-6,7	1,07	-2,18	-6,1	0,97
37	Kuhscheiben Ferner	15,7	-1,44	-4,0	2,09	-2,05	-5,7	2,98
53	Windacher Ferner	13,1	-3,81	-10,6	9,53	-1,63	-4,5	4,08

³ 1 nGal = 10⁻¹¹ m/s²

No.	Name	r_{hor} [km]	ΔV 69-97 [km ³] 10 ⁻³	$\overline{\Delta z}$ 69-97 [m]	δg 69-97 [nGal]	ΔV 97-06 [km ³] 10 ⁻³	$\overline{\Delta z}$ 97-06 [m]	δg 97-06 [nGal]
54	Daunkopf Ferner	16,4	-4,62	-12,8	5,89	-1,73	-4,8	2,21
55	Atterkar Ferner	15,1	-1,31	-3,6	2,14	-1,60	-4,4	2,61
56	Kitzkamp Ferner E	10,0	-4,39	-12,2	24,69	-2,35	-6,5	13,22
57	Südlicher Schrankar Ferner	21,7	-2,30	-6,4	1,27	-0,52	-1,4	0,29
58	Östlicher Scheiblehn Ferner E	11,7	-3,56	-9,9	12,50	-1,46	-4,1	5,13
59	Falbesoner Kräul Ferner	22,4	-1,01	-2,8	0,51	-1,55	-4,3	0,78
60	Säuischbach Ferner	23,0	-1,89	-5,3	0,87	-1,12	-3,1	0,52
61	Rotgrat Ferner	25,6	-1,67	-4,6	0,56	-0,76	-2,1	0,25
62	Westlicher Scheiblehn Ferner	10,7	-5,61	-15,6	25,76	-2,02	-5,6	9,28
63	Zischgeles Ferner	28,3	-2,10	-5,8	0,52	-0,50	-1,4	0,12
64	Ochsenkar Ferner	25,4	-1,81	-5,0	0,62	-0,37	-1,0	0,13
65	Hölltal Ferner	19,3	-1,95	-5,4	1,53	-0,94	-2,6	0,74
66	Aperer Freiger Ferner	16,8	-3,40	-9,4	4,03	-0,38	-1,1	0,45
67	Äusserer Mischbach Ferner	27,7	-1,24	-3,4	0,33	0,00	0,0	0,00
38	Rosskar Ferner	16,2	-1,22	-3,4	1,61	-1,39	-3,9	1,84
39	Turm Ferner	22,8	-1,48	-4,1	0,70	-1,04	-2,9	0,49
40	Westlicher Grübl Ferner E	19,0	-5,47	-15,2	4,49	-0,38	-1,1	0,31
41	Seespitz Ferner	21,8	-1,36	-3,8	0,74	-0,35	-1,0	0,19
42	Hangender Ferner	10,4	-1,87	-5,2	9,35	-1,35	-3,8	6,75
43	Östlicher Scheiblehn Ferner E ob.	13,5	-1,33	-3,7	3,04	-0,60	-1,7	1,37
44	Muschen Ferner W	17,9	-1,98	-5,5	1,94	-0,96	-2,7	0,94
45	Östlicher Scheiblehn Ferner W	13,2	-4,17	-11,6	10,20	-0,81	-2,3	1,98
46	Ruderhof Ferner un.	20,3	-0,46	-1,3	0,31	-0,59	-1,6	0,40
47	Grosser See Ferner	18,2	-0,69	-1,9	0,64	-0,57	-1,6	0,53
48	Gamezkogel Ferner	34,1	-1,46	-4,1	0,21	-0,01	-0,03	0,001
49	Kitzkamp Ferner W	9,4	-2,79	-7,8	18,89	-1,07	-3,0	7,25
50	Winnebach Ferner W	25,6	-1,52	-4,2	0,51	-0,42	-1,2	0,14
51	Westlicher Grübl Ferner M	17,4	-3,22	-8,9	3,44	-0,79	-2,2	0,84
52	Aperer Feuerstein Ferner E2	20,1	-2,81	-7,8	1,95	-0,93	-2,6	0,64
68	Gugeliger Ferner	24,6	-1,04	-2,9	0,39	-0,87	-2,4	0,33
69	Nördlicher Sonnenwand Ferner	28,6	-0,96	-2,7	0,23	-0,15	-0,4	0,04
71	Östlicher Grübl Ferner ob.	18,9	-0,83	-2,3	0,69	-0,17	-0,5	0,14

No.	Name	r_{hor} [km]	ΔV 69-97 [km ³] 10 ⁻³	$\overline{\Delta z}$ 69-97 [m]	δg 69-97 [nGal]	ΔV 97-06 [km ³] 10 ⁻³	$\overline{\Delta z}$ 97-06 [m]	δg 97-06 [nGal]
72	Grüne Tatzel Ferner	24,9	-0,38	-1,1	0,14	-0,74	-2,1	0,27
73	Weisskogel Ferner	26,9	-0,70	-1,9	0,20	-0,70	-1,9	0,20
74	Glätte Ferner	26,2	-0,85	-2,4	0,27	0,00	0,0	0,00
75	Südlicher Sonnenwand Ferner	28,0	-1,50	-4,2	0,38	-0,30	-0,8	0,08
76	Fotscher Ferner	28,6	-0,69	-1,9	0,17	-0,57	-1,6	0,14
77	Simming Ferner E	22,2	-1,51	-4,2	0,78	-0,46	-1,3	0,24

Acknowledgements

First of all, I would like to thank my supervisor Prof. Meurers, who devoted a lot of his time to this thesis. His expert knowledge, comments and Fortran codes were a vital contribution.

I am grateful to Dr. Ruess and Mag. Ullrich from the BEV, who supported this thesis with the gravity time series as well as additional information concerning measurements in Obergurgl. Furthermore, I want to thank Mag. Abermann and Prof. Kuhn for providing the DEMs of the Ötztal Alps.

Finally, I am grateful to my family and my girlfriend for their great support during my studies.

References

- ABERMANN J., FISCHER A., LAMBRECHT A., GEIST T. (2010), On the potential of very high-resolution repeat DEMs in glacial and periglacial environments, *The Cryosphere*, 4, 53-65
- ABERMANN J., KUHN M., FISCHER A. (2011), A reconstruction of annual mass balances of Austria's glaciers from 1969 to 1998, *Annals of Glaciology*, 52(59), 127-134
- ABERMANN J., LAMBRECHT A., FISCHER A., KUHN M. (2009), Quantifying changes and trends in glacier area and volume in the Austrian Ötztal Alps (1969-1997-2006), *The Cryosphere*, 3, 205-215
- BÜLLESFELD F.-J. (1985), Ein Beitrag zur harmonischen Darstellung des gezeitenerzeugenden Potentials, Deutsche Geodätische Kommission, Reihe C, Heft Nr. 314, München 1985
- CARTWRIGHT D. E., EDDEN A. C. (1973), Corrected tables of tidal harmonics, *Geophysical Journal of the Royal Astronomical Society*, 33, 253-264, Oxford 1973
- DI LULLO A., DINALE R., SCHROTT D. (2010), Übeltalferner, Haushaltsjahr 2008/2009, Glacierreport, no. 02/2010, Sonderdruck zum Climareport Nr. 178, Hydrographisches Amt Bozen, Lawinenwarndienst – Wetterdienst
- DOODSON A. T. (1921), The harmonic development of the tide generating potential, *Proceedings of the Royal Society (London)*, Series A 100, 306-328, Reprint in *International Hydrographic Review*, 31, no. 1, Monaco 1954
- ETZELMÜLLER B. (2000), On the quantification of surface changes using grid-based digital elevation models (DEMs), *Transactions in GIS*, 4(2), 129-143
- Google Earth, last access: November 23 2011
- GÖTZE H.-J., LAHMEYER B. (1988), Application of three-dimensional interactive modeling in gravity and magnetics, *Geophysics*, 53, no. 8, 1096-1108
- HASLINGER C., KRAUSS S., STANGL G. (2007), The Intra-Plate Velocities of GPS Permanent Stations of the Eastern Alps, *Vermessung & Geoinformation*, 2/2007, 66-72
- JIANG Z. ET AL. (2011), Final report on the Seventh International Comparison of Absolute Gravimeters (ICAG 2005), *Metrologia*, 48, 246–260
- LAMBRECHT A., KUHN M. (2007), Glacier changes in the Austrian Alps during the last three decades, derived from the new Austrian glacier inventory, *Annals of Glaciology*, 46, 177–184
- MEMIN A., REGISTER Y., HINDERER J., LLUBES M., BERTHIER E., BOY J.-P. (2009), Ground deformation and gravity variations modelled from present-day ice thinning in the vicinity of glaciers, *Journal of Geodynamics*, 48, 195-203
- MEURERS B., *Angewandte Gravimetrie*, unpublished lecture notes, University of Vienna, WS 2006/2007
- MILITZER H., WEBER F. (1984), *Angewandte Geophysik, Band 1, Gravimetrie und Magnetik*, Springer Verlag, Akademie Verlag

NIEBAUER T. M. (1989), The Effective Measurement Height of Free-fall Absolute Gravimeters, *Metrologia*, 26, 115-118

NEUMEYER J., PFLUG H. (1997), ADMITT - a Program for Determination of the Atmospheric Pressure Admittance, *Bulletin d'Informations Marées Terrestres*, 127, 9851-9855, Bruxelles 1997

PATZELT G. (1980), The Austrian glacier inventory: status and first results, Riederalp Workshop 1978 - World Glacier Inventory, IAHS-AISH Publ. no. 126

PRESS W. H., TEUKOLSKY S. A., VETTERLING W. T., FLANNERY B. P. (1992), Numerical Recipes in Fortran, The Art of Scientific Computing, Second Edition, Cambridge University Press

RENKA R. J. (1996), ALGORITHM 751, TRIPACK: Constrained two-dimensional Delaunay Triangulation Package, *ACM, Trans Math Software* 22(1), 1-8

RUESS D., Ausgewählte Kapitel gravimetrischer Auswertungen, unpublished lecture notes, University of Vienna, SS 2010

RUESS D. (1993), Schwerevariationen im Alpenen Raum, Tagungsber. 6. int. Alpengravimetrie-Kolloquium Leoben 1993, *Österr. Beitr. zu Meteorol. u. Geophysik*, Heft 8, 113-126

RUESS D. (1995), Die Absolutschwerestation Obergurgl, Institut für Hochgebirgsforschung der Leopold-Franzens-Universität Innsbruck, Jahresbericht 1995, 57-60

RUESS D., HÖGGERL N. (2002), Bestimmung rezenter Höhen- und Schwereänderungen in Österreich, *Pangeo Austria, Programm & Kurzfassungen*, *Österr. Geol. Ges., Inst. f. Geologie und Paläontologie, Univ. Salzburg*, Juni 2002

RUESS D., ULLRICH C. (2011), 20 years of International Comparison of Absolute Gravimeters (ICAG) at the Bureau International des Poids et Mesures (BIPM) in Paris with participation of the BEV, *Vermessung & Geoinformation*, 2/2011, 154-161

SACHS L. (1978), *Angewandte Statistik*, 5. Auflage, Springer Verlag Berlin Heidelberg New York

SCHWIDERSKI E. (1980), Ocean tides, Part I: Global ocean tidal equations, Part II: A hydrodynamical interpolation model, *Marine Geodesy*, 3, 161-255

SEISER B. 2010, Gletscherinventar 2006 der Stubai Alpen, Diploma Thesis, University of Innsbruck

STEIN G. 2006, Interpolation von Schneehöhen im Alpenraum, Diploma Thesis, University of Vienna

STEINHAUSER P., SEIBERL W. (1984), Zur Bedeutung von Absolutschweremessungen für Geowissenschaften und Rohstoffforschung, *Arch. f. Lagerst.forsch. Geol. B.-A.*, Band 5, 167-170, Wien 1984

TAMURA Y. (1987), A harmonic development of the tide-generating potential, *Bulletin d'Informations Marées Terrestres*, 99, 6813-6855, Bruxelles 1987

TELFORD W. M., GELDART L. P., SHERIFF R. E. (1990), *Applied geophysics*, Second edition, Cambridge University Press

tirisMaps, www.tirol.gv.at/tiris, last access: November 24 2011

- TIMMEN L. (2003), Precise definition of the effective measurement height of free-fall absolute gravimeters, *Metrologia*, 40, 62-65
- TIMMEN L., WENZEL H.-G. (1994), Worldwide synthetic gravity tide parameters available on INTERNET, *Bulletin d'Informations Bureau Gravimetrique International*, 75, 32-40, Toulouse 1994
- TORGE W. (1989), *Gravimetry*, Walter de Gruyter
- WAHR J. M. (1985), Deformation Induced by Polar Motion, *Journal of Geophysical Research*, 90, no. B11, 9363-9368
- WARBURTON R. J., GOODKIND J. M. (1977), The influence of barometric-pressure variations on gravity, *Geophysical Journal of the Royal Astronomical Society*, 48, 281-292
- WENZEL H.-G. (1994), Earth tide data processing package ETERNA 3.20, *Bulletin d'Informations Mareés Terrestres*, 120, 9019-9022, Bruxelles 1994
- WENZEL H.-G. (1996), The nanogal software: Earth tide data processing package ETERNA 3.30, *Bulletin d'Informations Marées Terrestres*, 124, 9425-9439, Bruxelles 1996
- ZUMBERGE M. A. (1981), *A Portable Apparatus for Absolute Measurements of the Earth's Gravity*, PhD Thesis, University of Colorado

Curriculum vitae

Persönliche Daten

Name: Arneitz Patrick
Geburtsdatum und -ort: 8. April 1987 in Villach
Nationalität: Österreich
Familienstand: ledig
Email Adresse: Patrick.Arneitz@gmx.at

Schulische Ausbildung

[1993-1997] Khevenhüllerschule Volksschule 1 Villach
[1997-2005] Peraugymnasium BG/BRG Villach

Studium

[2005-2007] Universität Wien: Diplomstudium Meteorologie und Geophysik, erster Abschnitt
[seit 2007] Universität Wien: Diplomstudium Meteorologie und Geophysik, Studienzweig Geophysik

Praktika/Berufserfahrung

[Februar- April 2009] Geologische Bundesanstalt Wien; angestellt als Messhelfer